EFFECTS OF IMPURITIES
ON THE SUPERSATURATION OF NITROGEN
IN A HYPERSONIC WIND TUNNEL

Thesis by

Paul D. Arthur

In Partial Fulfillment of the Requirements

for the Degree of

Doctor of Philosophy

California Institute of Technology

Pasadena, California

1952

ACKNOWLEDGMENT

I would like to express my appreciation to the staff of GALCIT whose help made this work possible. In particular, Dr. Henry T. Nagamatsu provided guidance in the research. Many discussions with Rolf D. Buhler and William Willmarth clarified the problems for me. Paul Jackson assisted with the numerical work. C. A. Bartsch and the shop fabricated the tunnel. Betty Wood, Dorothy Nicholson, and Georgette Pauwels prepared the plots. Charlotte Rade reproduced the thesis. And finally, my thanks to my wife, Mary Arthur, for typing the manuscript.

ABSTRACT

An experimental investigation was conducted to determine the effects of additives on the supersaturation of commercial bottled nitrogen expanded in a hypersonic nozzle. In particular, enough oxygen was added to duplicate air proportions. A stainless steel two-dimensional source-flow nozzle of one-inch width was used to conduct the tests.

Commercially pure nitrogen, expanded from room temperature and 8-1/3 atm. pressure, was found to supersaturate by approximately 18° K or 1.2 Mach number. The supersaturation of the nitrogen was decreased by the addition of impurities, and only a fraction of a percent of carbon dioxide or water vapor was required to eliminate completely all supersaturation. Addition of argon and oxygen was found to be much less effective in decreasing the supersaturation. For the synthetic air, the supersaturation was 16° K or 0.9 Mach number based on air vapor pressure values.

During the collapse of the supersaturated state, the static pressure gradually increased above the isentropic value because of the heat release of the condensing gas. As has been shown before, there was no evidence of condensation shock with nitrogen. The impact pressure was only slightly changed from the isentropic value by the presence of condensation in the flow. After the collapse of the supersaturated state, the flow approximated that of a condensation shock.

From these tests it is concluded that condensation of nitrogen, containing slightly more impurities than present in the commercial nitrogen, and of air of the same purity is principally caused by foreign impurities, not by spontaneous self-nucleation.

TABLE OF CONTENTS

LIST OF FIGURES

SYMBOLS

a	Perfect gas speed of sound, cm/sec
$\tilde{a}$, $\hat{a}$, $\overset{o}{a}$	Speeds of sound in a two-phase fluid defined in Section IV-F
C_L	Specific heat of bulk liquid by volume, cal/cm^3 - deg. K
C_p	Specific heat at constant pressure, Cal/gm - deg. K
C_v	Specific heat at constant volume, Cal/gm - deg. K
d	Liquid phase density, gm/cc
e_L	Bulk liquid energy, cal/gm
g	Fraction of total mass which is in condensed phase
J	Spontaneous nuclei formation rate, number/sec. - cm^3
k	Gas constant, dyne-cm/mol - deg. K
l	Characteristic length, cm.
L	Latent heat of vaporization, cal/gm
M	Mach number, $u/\sqrt{\gamma RT}$
$\mathcal{m}$	Mass flow gm/sec
m	Molecular weight
N	Foreign nuclei concentration, number/gm of carrier gas
N_i	Number of moles of gas i
p	Static pressure, atm.
p_o'	Impact pressure behind a normal shock wave, atm.
r	Drop radius, cm.
r_{cr}	Critical droplet radius by Thompson formula, cm.

r_o	Foreign element nuclei radius, cm.
R	Gas constant
Re	Reynolds number, $\rho ul/\mu$
T	Absolute temperature, degrees K
u	Velocity, cm/sec
V	Total gas volume
W	Droplet surface energy, cal/cm^2
x	Axial distance downstream from throat, inches or cm.
γ	Ratio of specific heats, C_p/C_v
Γ	Mass of molecules striking one cm^2 per sec.
ϵ	Mass ratio of additive
θ	Nozzle expansion angle
λ	Molecular mean free path, cm.
μ	Viscosity, dyne sec/cm^2
ρ	Density of gas liquid mixture, gm/cc
ρ_g	Density of gas, gm/cc
ρ_L	Density of liquid, gm/cc
σ	Surface tension, dynes/cm
ω	Exponent in viscosity approximation

SUBSCRIPTS

$( )_o$	Reservoir conditions
$( )_1$	Reference point of viscosity approximation
$( )_\infty$	Conditions on plane saturation curve
$( )_c$	Conditions at condensation
$( )_D$	Droplet properties
$( )_E$	Equilibrium droplet properties from quasi-steady theory
$( )_s$	Conditions at saturation
$( )_V$	Vapor properties

I. INTRODUCTION

As a perfect gas expands isentropically, the pressure and temperature decrease from their reservoir values in a definite relationship to each other. The pressure and temperature at a point along the expansion depend only on the reservoir conditions and specific heat ratio (γ) of the gas.

Another important pressure-temperature relation is the equilibrium saturation curve - the pressure at which the liquid (or solid for low temperatures) and gas coexist for a given temperature. This relation is theoretically derived as the Clapeyron-Clausius equation (Ref. 1) and is valid for a gas over a large surface of liquid.

On the pressure-temperature plane, it is found that the perfect gas isentrope* will cross the saturation curve if the expansion is continued to a low enough pressure. In a wind tunnel this corresponds to a high Mach number. "Hypersonic" is often used to describe a tunnel expanding above a Mach number of about 5. For equilibrium conditions, the condensed phase (liquid, or solid for low temperatures) will begin to appear in the nozzle at this intersection of isentrope and saturation line. Still postulating equilibrium, the expansion will then follow the vapor pressure curve and become a "saturated" (and isentropic) expansion of gas and liquid (or solid)

---

* Throughout this paper the perfect gas isentropic expansion is referred to as "isentropic expansion", although it is realized that an equilibrium saturated expansion is also isentropic. This notation is usual in wind tunnel work.

instead of the perfect gas isentropic expansion. For the usual hypersonic wind tunnel testing, this departure from the perfect gas isentropic flow is the limit of desired test section operation. Allowance should be made for possible expansion of air around a model before compression. At a Mach number of 10, for instance, one degree further expansion will increase the Mach number by 0.3. Many of the relations used in perfect gas isentropic flow (impact pressure, area ratio, oblique shock angles, etc.) can be computed for a saturated flow (Refs. 2, 3, and 4) with additional difficulty. Some research work is currently being conducted in the GALCIT Hypersonic Wind Tunnel to investigate the possibility of testing in the saturated flow and then correlating the saturated results to the perfect gas isentropic conditions.

Examination of the isentrope-saturation curve intersections shows that, for a given gas, the saturation Mach number can be increased by increasing reservoir temperature or by decreasing reservoir pressure. Decreasing the reservoir pressure has the disadvantage of lower available compression ratio, lower test section pressures, smaller model forces, and lower density. The lower density leads to difficulty in using optical equipment and to the possibility of entering the slip flow regime. For these reasons, heating has been the usual solution. Use of a gas which does not condense until much higher Mach numbers is another possibility, as indicated by the present results with helium.

From experiments in the 1" x 1" tunnel and other work (Cf. Refs. 5, 6, and 7), it is found possible to extend the perfect gas isentropic expansion of a gas beyond the intersection with its saturation curve by using gas sufficiently free of foreign elements. The expansion finally departs from the isentrope and, following a transition path in the p - T plane, establishes itself on the saturation curve. For the tests made with nitrogen, the temperature level of this actual saturation curve seems to be a few degrees lower than that of the usual infinite radius curve.

This "supersaturation" beyond the vapor pressure curve is similar to the "supercooling" of a liquid below the usual crystallization temperature. The addition of foreign substances seems to supply additional nuclei for the gas to condense on, and the supersaturation decreases with additional additive until condensation occurs approximately at the equilibrium saturation point.

This report describes some of the condensation results obtained with commercially pure nitrogen in the 1" x 1" hypersonic wedge nozzle. Also investigated were the effects of addition of carbon dioxide, water, oxygen, and argon in decreasing the supersaturation of nitrogen. Oxygen was added up to air concentration.

II. TEST FACILITY

A. Apparatus

The hypersonic tunnel used for the investigation was a two-dimensional source-flow nozzle expanding from a throat height of 0.010 inch to a final height of approximately one inch with a constant width of one inch. The total expansion angle was 11°. The pressure recovery occurred through a central body diffuser leading through two pipes to the exhaust pumps. Diffuser pressure was maintained by 200 hp rotary vane pumps. Since a large starting compression ratio (1800 to 1) was available, the diffuser efficiency was not critical. The pressure recovery was about 1/5 of normal shock. The tunnel was made of stainless steel using either glass or stainless steel walls. Stainless steel, brass, and bronze were used throughout the supply system to avoid contamination by oxidation. Supply pressure was regulated from commercial nitrogen bottles to maintain constant reservoir pressure during the test. Several mass spectrometer analyses were made of the bottled nitrogen during the test program. The results are presented in Table I. At reservoir conditions of 8-1/3 atm. and 70° F, the tunnel ran for a total time of about 100 minutes on ten bottles in the supply manifold, which was adequate for about five average runs. Later in the research program, an outside dock was constructed to permit a larger number of bottles to be connected. 150 feet of 1/2 inch stainless steel tubing led from the dock along the ceiling of the main hypersonic room to the 1" x 1" tunnel test room. The pressure drop of this line was about 10 psi for the usual tunnel

operating conditions. A schematic drawing of the physical plant is given in Fig. 1, and a photograph of the test equipment is presented in Fig. 2. The construction of the tunnel is described in detail in Ref. 5.

Reservoir pressure upstream of the nozzle was kept constant by a Grove regulator, which was supplied with loading pressure by a commercial hand-operated regulator. This hand regulator alone was inadequate to handle the desired mass flow. During runs, frequent attention was given to this hand adjustment; and the reservoir pressure, which was measured on a 0 to 300 psi Ashcroft gage, was held to ±1/4 psi during the run. Absolute accuracy of the reservoir pressure was probably ± 1%

Nozzle wall static pressures were measured by 0.040-inch diameter taps drilled perpendicular to the diverging walls at 1/4-inch intervals. Plastic tubing led from these taps to a bank of mercury manometer tubes connected in parallel with a bank of silicone manometer tubes. Most static pressure readings were taken on the silicone, as only rarely were the upstream static pressures too large for the full scale of the silicone column. At such times the pressures were measured on the mercury manometer. These 4 mm. manometer tubes were referenced to a Duoseal vacuum pump that maintained a pressure of less than 0.1 mm. mercury absolute. Accuracy of the static pressure ratios was estimated to be ± 1% near the throat and ± 2.5% near the diffuser.

The axial impact pressure* was measured by a 14 mm. diameter mercury manometer, with its reference connected to the same vacuum pump as the other manometers. The .042-inch diameter brass impact tube extended through the center of the wedge diffuser. It could be manually moved along the axis during a run, and its location was indicated by a reference scale on one of the two diffuser pipes. For the high impact pressures reached near the throat the mercury column was by-passed, and a 0-30 psig dial gage used. Impact pressures were not taken within 1/2 inch of the throat, since the pressure gradient there was very steep and made the reading quite sensitive to axial location. Also, any slight displacement of the tip of this cantilever probe off the tunnel center line would put the probe in the boundary layer. The accuracy of the impact pressure measurement was estimated to be ± 0.6% near the throat and ± 1% near the diffuser.

The small amounts of carbon dioxide were added through an orifice, a few thousandths of an inch in diameter, screwed into the elbow of the nitrogen supply line upstream of the steam heater. The carbon dioxide was from a commercial bottle with the pressure controlled by a hand regulator. The resultant carbon dioxide content in the nitrogen was measured by chemical analysis of a continuous sample for runs number 21 and 23. Other carbon dioxide runs were measured through

---

* "Axial impact pressure" was measured by a small brass tube inserted along the center line parallel to the flow direction. This pressure is considered to be the isentropic recovery pressure after a normal shock. The term "impact pressure" is used by Stodola, Ref. 34, although "total head" is also used.

flowmeters or by orifices calibrated by a flowmeter. The accuracy of these larger concentrations was estimated to be plus or minus one part in ten of the resultant concentration. Specifically, the concentration was estimated as ± .001% at the low concentration of .002%, and ± .007% at .07%.

Argon and oxygen were added through flowmeters; no orifice was necessary since the amounts added were larger than the amounts of carbon dioxide. Water was injected under pressure through a small orifice upstream of the heater. The concentration of the water was measured by a dew-point meter that continuously analyzed a sample taken from the elbow downstream of the steam heater. This high pressure continuous reading dew-point meter was developed by the Hypersonic Staff. For low water content, high pressure was needed to bring the saturation temperature up to measurable temperatures. The chrome button on which the "dew" forms was cooled by the expansion of high pressure carbon dioxide. The button temperature was measured by an imbedded thermocouple. From the vapor pressure curve of water the partial pressure of the water content was known. The ratio by volume of water to nitrogen was this partial pressure divided by the total nitrogen pressure.

B. Test Procedure

The nitrogen bottle valves were opened to pressurize the manifold and line from the dock to the basement. After the diffuser pumps were started, the leads to the static holes and nozzle could be connected to their silicone manometer tubes by the valves located above the manometer board. Atmospheric pressure exceeded the range of these silicone tubes, so the tubes were "short circuited" back to their low pressure reservoir except when the tunnel was at a low pressure. The valves used were made of stainless steel, and the manometer fluid returned to a normal level in a few minutes if an accidental over-pressure was applied to it.

A valve bringing the Grove regulator on the line was opened, and the hand regulator was used to build up pressure to a few pounds above the desired reservoir pressure. Finally, the quick acting shutter valve just upstream of the tunnel was opened. After supersonic flow was established, the pressure of the additive was increased until the desired flowmeter reading was obtained.

For the heated runs the steam valve was opened, and the reservoir temperature regulated by this valve.

The axial impact probe was moved along the center line, and the reservoir pressure and temperature were recorded at each station. With the probe withdrawn into the diffuser wedge, the static pressures were read. A thermocouple mounted on the manometer boards was used to obtain the silicone temperature, from which the silicone specific gravity was determined.

C. Unit of Measure of Additive

The unit of measure used for the amount of foreign element added is the volume of foreign element divided by the volume of the nitrogen, each separately expanded to the same pressure and temperature (Cf. Epstein, Ref. 1, p. 7).

$$p_1V_1 = N_1RT_1 \qquad p_2V_2 = N_2RT_2 \tag{2.1}$$

where V_i = total volume, N_i = number mols of the gas. If $p_1 = p_2$ and $T_1 = T_2$, then

$$V_1/V_2 = N_1/N_2 \tag{2.2}$$

showing that the volume ratio is the mole ratio. Since the number of molecules per mole of any gas is the same, the volume ratio is the ratio of the number of molecules. To obtain the ratio by weight from this volume ratio (Eq. 2.2), multiply by the ratio of molecular weights:

$$\text{weight ratio} = \frac{m_1}{m_2}\,\frac{V_1}{V_2} \tag{2.3}$$

For a mixture of two perfect gases in one container, $V_a = V_b = V$ in the above equation. For thermal equilibrium, $T_a = T_b = T$ from which follows $p_a/p_b = N_a/N_b$, i.e., the ratio of partial pressures is the "by volume" ratio. This "ratio by volume" is the one discussed in the previous paragraph, where each gas is expanded separately to the same pressure and temperature. By Dalton's Law, $p = p_a + p_b$.

Thus, for small percentages of foreign gases, the additive p - T isentrope lies below the main isentrope expansion by the ratio by volume, i.e.

$$\frac{p_b}{p_a} = \frac{p_b}{p_a + p_b} \doteq \frac{p_b}{p_a} \quad \text{for} \quad \frac{p_b}{p_a} \ll 1 \tag{2.4}$$

For additives with the same ratio of specific heats as nitrogen, such as oxygen, the additive isentrope is seen to parallel that of the nitrogen (on a log-log plot). But this must also be true for additives of one molecule (argon) or three molecules (carbon dioxide and water), because the partial pressure ratio must remain equal to the ratio by volume. Since the expansion of the additive does not then follow its own isentrope, it is seen that an exchange of energy takes place between the two gases. The specific heats of the mixture are the average by volume of the nitrogen and additive.

D. Waves from the Throat

Throughout the test program slight difficulty was experienced from the symmetrical waves, apparently originating at each end of the throat. At first these waves were shown to be decreased by tighter clamping of the glass or steel walls at the throat, indicating slight leakage of high pressure air from upstream of the throat around the throat to the low pressure region. The two waves intersected on the center line about 1-3/4 inches from the throat (Cf. Fig. 11). Their combined strength at this point was always less than 10%, usually about 5%, and the reflection from the walls could not be detected. Vacuum grease was applied lightly to the sides of the nozzle before clamping the walls on. Later in the test program, the stainless steel nozzle blocks were lapped on both sides, after assembly of the nozzle, and glass walls of selected flatness clamped on.

In an attempt to decrease this wave strength, the throat radius was increased from slightly over 1/16" to 1/8". No measurable improvement was noted by this change. This result was confirmed by tests of R. Mark with a 1" x 1" carbon steel nozzle.

Since mass flow checks have shown the boundary layer at the throat to be quite small, it has been suggested that the build-up of boundary layer on the side walls just downstream of the throat caused a deviation of the main flow inward, resulting in an oblique shock. The strength of these waves seemed to decrease with increasing reservoir pressure (4.15 to 20.72 atm.). As Reynolds number varies

directly as the pressure (Cf. Section III-B), this may substantiate the side wall boundary layer theory. No systematic effect of reservoir temperature could be noted in the range used (290° K to 408° K). As Reynolds number varies inversely as temperature to the 1.26 power, the available variation in Reynolds number due to temperature was only 1.54 to 1 as compared to the 5 to 1 variation due to the available pressure range. This may explain why no temperature effect was noted if the phenomenon was due to side wall boundary layer.

The observed waves did not seem to affect the nozzle static pressures and were thought not to affect seriously the condensation phenomena. It is emphasized that all plotted test data are as read, and waves are not faired out.

This wave problem was noticed in the 5" Hypersonic Tunnel also, and in March 1952 the idea of secondary flow was considered. Work is now being done in the 2-1/2" Supersonic Tunnel on this problem.

E. Absence of Normal Static Pressure Gradients

It has often been suggested that one of the distinguishing features of "hypersonic flow" might be the existence of a static pressure gradient within the boundary layer normal to the flow direction. Fig. 11 shows that this gradient did not exist for the conditions in this nozzle. The static pressures recorded by an axial probe are compared with the nozzle and side wall static pressures. A similar run at 8.33 atmospheres reservoir pressure checked as well.

Two cases of hypersonic boundary layer are to be noted: (1) continuous growth as on a wind tunnel wall and (2) sudden build-up as on a flat plate or body inserted in the flow. In the latter case, a shock wave forms about the body at a small angle with the flow, thus creating the possibility of pressure gradients in the combined viscous-shock layer. This second case is discussed in Ref. 8.

III. DISCUSSION OF EXPERIMENTAL RESULTS

A. Nitrogen Supersaturation

The question of wind tunnel design to avoid water condensation shock in air seems to have been settled to engineering satisfaction by the papers of Ostwatitsch (Ref. 9), Head (Ref. 10), and Burgess and Seashore (Ref. 11).

For the problem of a gas condensing itself, the earliest theoretical work was by Wagner (Ref. 12) and Grunewald (Ref. 13). Subsequent opinions varied from no supersaturation (Ref. 14) to unlimited supersaturation for some reservoir conditions (Refs. 15, 16, and 17). Summaries of the progress in condensation research are given in Refs. 10, 18, and 19.

Bogdonoff and Lees, in their early work with condensation of air in supersonic wind tunnels (Ref. 16), noticed the absence of the violent condensation shock, which was observed when there was sufficient water vapor. They concluded that the supersaturation was so great that no condensation could exist for a considerable range of reservoir conditions and test section Mach numbers. However, the operation of hypersonic wind tunnels (Cf. Refs. 7, 14, 20, and 21) did reveal some non-isentropic effects, principally an increase of the static pressure over the isentropic value corresponding to the impact pressure, as indicated in Fig. 3, Run 23-1. The departure in static pressure from the isentropic value corresponding to the impact pressure was gradual, explaining the conclusion of Bogdonoff and Lees,

mentioned above, as an error in interpretation and not in experimentation. This non-isentropicity can also be seen from the disagreement of the various Mach numbers as computed from the three available pressure ratios as indicated in Fig. 4. It is emphasized that isentropic Mach number has no actual meaning after deviation from isentropic conditions ($M = M_c$ in Fig. 4), but it is one way to indicate condensation. A clearer presentation is to plot the measured pressure ratios against each other as in Fig. 5. This form was suggested by R. Buhler of the Hypersonic Staff. Impact pressure ratio, p_o'/p_o (the ratio least affected by condensation), is plotted against Rayleigh pressure ratio, p/p_o' (the ratio most affected by condensation). Isentropic flows from all reservoir conditions lie on the one isentrope, while curves for the saturated expansions depend on reservoir conditions. These theoretical curves need no experimental assumptions to be plotted, and the measured experimental pressure ratios need no theory to be located on the plot.

Fig. 6 shows that the flow was initially isentropic and that this isentropic expansion could be preserved to a higher Mach number by increasing T_o for a given reservoir pressure. Decreasing p_o also increased the maximum isentropic Mach number, but with the disadvantages mentioned previously. Fig. 6 shows that in this tunnel (until condensation) one-dimensional perfect gas relations with $\gamma = 1.40$ were satisfactory and that frictional effects were not evident on the axis.

Comparison of light scattering data and the pressure data showed this static pressure deviation from the isentrope to be caused by condensation (Cf. Refs. 5, 7, and 21). That it was not due to flow breakdown, separation, etc., was shown by moving the point of pressure rise by adding foreign elements or by changing the stagnation temperature for a given reservoir pressure. The static pressure deviation from isentropic was taken as the criterion of condensation since it was of practical interest to know the limit of isentropic flow.

The rise in static pressure due to condensation can be seen in Fig. 7. Run 23-1 was at $T_o = 293^o$ K, and the flow condensed about 3 inches from the throat. The other two runs were at high enough reservoir temperatures that condensation did not occur in the nozzle. The reservoir pressures were adjusted in an attempt to maintain an approximately constant Reynolds number per unit length and thus give the same boundary layers and effective flow areas in each run. The static pressures near the throat were not the same for each run, indicating changed effective flow areas. Therefore, this attempt at constant effective flow area was not completely successful. This is discussed in the section on Reynolds number effects, III-B. However, the main effect of increased static pressure due to heat release of the condensate can be seen by shifting the heated static pressure curves so they coincide with the unheated curve upstream near the throat.

The properties at the point of condensation were determined in the following manner: the deviation from the isentrope was noted on a

plot of either static pressure vs. x or p/p_o' vs. p_o'/p_o .* Usually it was easier to locate on the latter plot. Mach number, temperature ratio, and saturation pressure (p_∞) for an infinite plane surface at this condensation temperature were then known, and the supersaturation pressure ratio, $p_{condensation}/p_\infty$, was computed. This ratio was unity at the intersection of isentrope and vapor pressure curve (i.e., no supersaturation) and increased with supersaturation.

All computations of the supersaturation pressure ratio ($p_{condensation}/p_\infty$) involved fairing and were somewhat uncertain. The rapid fall-off of saturation pressure (p_∞) at condensation temperatures contributed to the inaccuracy in supersaturation pressure ratio. For the saturation computations, the vapor pressure of nitrogen as shown in Fig. 8 was used, although it was realized that significant percentages of additives would change the saturation curve. The curve in Fig. 8 is from the analytical expressions for vapor pressure recommended in Refs. 22 and 23. Experimental vapor pressure data from Refs. 22, 23, and 24 are noted on the plot. The accuracy of the computed supersaturation parameters was estimated to be +0.5 to -1.0 in $\log_e(p_c/p_\infty)$ and $\pm$ 1.5° K in the supersaturation temperature (saturation temperature minus condensation temperature).

For the nozzle operated with the bottled nitrogen alone (no additive) the average of seven runs listed in Table II shows

---

* As this departure from the isentrope is often quite gradual, a more useful criterion may be the point where the static pressure exceeds the isentropic value by some fixed percentage, say 2% or 5%.

supersaturation of about 18° K and of a Mach number of 1.2 for reservoir conditions of 8.33 atm. and 290° K.

After collapse of the supersaturated state, the flow was approximately that of an equilibrium of saturated vapor (Cf. Refs. 2, 3, and 4) with either liquid or solid nitrogen, depending on the temperature. In the computation of the saturated expansion using Buhler's theory (Figs. 3 and 5) it was not necessary to specify whether the condensed phase was liquid or solid, since the Clapeyron-Clausius approximation to the vapor pressure curve may be fitted within 1% in temperature in the range of interest.

It is emphasized that the gas condensation occurred gradually, whereas water vapor condensation in air was a more severe process. A qualitative explanation may be the lower mass and heat transfer values of the carrier gas at the lower pressure of the gas condensation. The molecular impingement rate is proportional to $p/\sqrt{T}$. Comparing this rate at Mach number 5 (gas condensation) and Mach number 2 (water vapor condensation), we have

$$\frac{p/\sqrt{T}(5)}{p/\sqrt{T}(2)} = \frac{1}{40}$$

This shows the carrier gas impingement rate to be 40 times as great at the water vapor condensation point than at the gas condensation point.

Another item of interest is the relative values of L/C_p , i.e., the temperature rise of the gas due to condensing one gram of the condensate. The approximate figures are:

	L/C_p (° K)
Nitrogen	206
Air	224
Steam	3610
Water in Air	7270

B. Reynolds Number Effects

Flow in the tunnel at all times was in the fluid mechanics regime, well away from slip flow as defined by Tsien (Ref. 25). At M = 4 Reynolds number per centimeter was 3.2×10^5, at M = 6 Reynolds number per centimeter was 1.1×10^5 for 8.3 atm. reservoir pressure and 290° K reservoir temperature. Reynolds number per centimeter is plotted versus Mach number in Fig. 9 for several reservoir conditions. The equation used has been derived as follows:

$$Re/\ell = \frac{\rho u}{\mu} \tag{3.1}$$

For the isentropic expansion,

$$\frac{\rho}{\rho_o} = \left(\frac{T}{T_o}\right)^{\frac{1}{\gamma-1}} = \left(\frac{T}{T_o}\right)^{2.5} \tag{3.2}$$

$$\rho = \frac{\rho}{\rho_o}\frac{P_o}{RT_o} = \left(\frac{T}{T_o}\right)^{2.5}\frac{P_o}{RT_o} \tag{3.3}$$

$$u = Ma = M\sqrt{\gamma RT_o}\left(\frac{T}{T_o}\right)^{1/2} \tag{3.4}$$

$$\mu = \mu_1\left(\frac{T}{T_1}\right)^{\omega} = \mu_1\left(\frac{T}{T_o}\right)^{\omega}\left(\frac{T_o}{T_1}\right)^{\omega} \tag{3.5}$$

$$Re/\ell = \left[M\left(\frac{T}{T_o}\right)^{3-\omega}\right]\left[\frac{P_o}{\mu_1\left(\frac{T_o}{T_1}\right)^{\omega}}\sqrt{\frac{\gamma}{RT_o}}\right] \tag{3.6}$$

For a given slope (ω) of the viscosity approximation, the first bracket is a function of Mach number alone, and the second is a function only of reservoir conditions and viscosity approximation. For $M \ll 1$ this reduces to $Re/l \sim M$, while with the hypersonic approximation $M \gg 1$ (where 1 is neglected in comparison with $0.2\ M^2$).

$$Re/\ell \sim \frac{1}{M^{5-2\omega}} = \frac{1}{M^{3.48}} \qquad \text{for } \omega = 0.76 \qquad (3.7)$$

Viscosity values were obtained from Refs. 26 and 27. Ref. 27 gives experimental values down to 80° K. It was then found that the power law $\mu/\mu_1 = (T/T_1)^{\omega}$ gave a satisfactory fit with $\omega = 0.76$, $T_1 = 200^\circ$ K, $\mu_1 = 1.28 \times 10^{-4}$ dyne sec/cm^2 (Cf. Fig. 10). Changing T_1 and μ_1 would serve to move the region of best fit of this mathematical approximation.

As in the case of air (where $\omega = 0.76$ has been used), an interesting mathematical item occurred for low temperatures, depending on the approximation used for the viscosity. Consider the quantity $\rho\mu$, which is of interest in the laminar boundary layer. The usual assumption of constant pressure across the boundary layer seems valid in the 1" x 1" tunnel, as shown in Fig. 11. For the power approximation of the viscosity relation, $\rho\mu \sim 1/T^{.24}$, indicating unlimited increase in $\rho\mu$ as T approaches zero. On the other hand, the Southerland approximation indicates a maximum in the value of $\rho\mu$ as T decreases, with $\rho\mu$ then decreasing to zero at T = 0. For air,

this maximum occurs at $T = 110^{\circ}$ K. This disagreement at low temperature is indicated in Ref. 28, and it is suggested that hypersonic wind tunnel results ($T < 110^{\circ}$ K) may not have the same boundary layer characteristics as free flight ($T > 110^{\circ}$ K). The experimental values of viscosity used in Ref. 28 are known down to $T = 80^{\circ}$ K.

The difficulty of simulating high flight Reynolds numbers is indicated in Fig. 9 where the Reynolds numbers for given tunnel reservoir conditions decrease with Mach number. Free flight Reynolds number increases as ℓM at hypersonic Mach numbers. The requirements for high model Reynolds number and high tunnel saturation Mach number are in opposition. Heating to avoid condensation decreases Reynolds number, and increasing p_o to increase the Reynolds number decreases the saturation Mach number.

If the Reynolds number is based on nozzle length from the throat, an interesting result is available for the case of a two-dimensional wedge of unit width.

$$Re = \frac{\rho u x}{\mu} \tag{3.8}$$

Continuity requires $\dot{m} = \rho u A$

but $A = x\theta$ for small θ (3.9)

Combining:

$$Re = \frac{\dot{m}}{\mu \theta} \tag{3.10}$$

indicating that for fixed throat and reservoir conditions, Reynolds number increases as

$$Re \sim (1+.2M^2)^{\omega} \qquad \text{based on distance from throat} \qquad (3.11)$$

or $Re \sim M^{2\omega} = M^{1.54}$ in the hypersonic approximation.

This result can be obtained from Eqn. (3.7) by use of the hypersonic area-Mach number relation, $A \sim M^5$. For the wedge nozzle $\ell \sim A$, giving

$$Re = \frac{Re}{\ell}\,\ell \sim \frac{1}{M^{5-2\omega}}\,M^5 = M^{2\omega} \qquad (3.12)$$

as before.

Flow properties can be computed from the static pressures in a condensing flow, if the effective area variation is known. Ref. 14 suggested that this area variation be obtained from a heated, non-condensing run, using the isentropic relations between static pressure and effective area. However, if the effective flow area is assumed given by the impact pressure, and if this impact pressure is assumed unaffected by condensation (Ref. 4 and Section III-E), it can be seen from Fig. 12 that the effective flow area was not constant with a change in reservoir temperature for the present tunnel.* Reservoir pressure was adjusted to maintain constant reservoir

---

* Note that the effective flow areas disagreed ahead of any condensation region (x = 3 inches for run 23-1).

Reynolds number in these runs in an attempt to keep viscous effects the same. Figs. 6, 7, and 12 are for the same set of runs.

The results indicate a thinner boundary layer for the high temperature case, probably due to heat transfer from the flow. For a larger tunnel, where the boundary layer area may not be as large a percent of the total area, the assumption of equivalent flow area, hot or cold, may be valid. Change of throat dimension was not thought to occur, although any throat closure would give changes in the same direction as shown in Fig. 12.

Boundary layer A/A^* was defined as A/A^* geometric minus A/A^* corresponding to center line impact pressure ratio. This assumes a uniform isentropic flow core.

$$Re = \frac{\rho u x}{\mu} \qquad \mu \sim T^{\omega} = \left(\frac{T}{T_o}\right)^{\omega} T_o^{\omega}$$

$$\rho = \frac{\rho}{\rho_o}\rho_o \qquad u = \frac{u}{a^*}a^* \sim \frac{u}{a^*}\sqrt{\frac{T^*}{T_o}}\sqrt{T_o} \tag{3.13}$$

$\frac{T^*}{T_o}$ is a constant of the gas.

$\frac{T}{T_o}, \frac{\rho}{\rho_o}, \frac{u}{a^*}$ are functions of Mach number.

If M is to be the same at the same value of x:

$$Re \sim \rho_o \frac{\sqrt{T_o}}{T_o^{\omega}} \sim \frac{P_o}{T_o^{1.26}} \tag{3.14}$$

if $\omega = 0.76$ is taken for nitrogen.

By constant reservoir Reynolds number, it is meant that $p_o/T_o^{1.26}$ was held constant for the various runs. A secondary effect then was the actual change in Reynolds number due to change in flow channel by the measured change in boundary layer thickness. This amounted to a 5% decrease in Reynolds number for the hot run in one case checked. Were the reservoir pressure increased to keep the test section Reynolds number identical with that of Run 23-1, the boundary layer thickness would decrease even more than indicated in Fig. 12.

That the boundary layer in a two-dimensional wedge tunnel is linear with distance downstream is indicated for laminar flow by Crown (Ref. 29) from Goldstein (Ref. 30). Agreement with this theoretical result is either fortuitous or does indicate that side wall boundary layer is a smaller effect.

The computations of flow properties (Section III-F) were then made using measured impact and static pressures to avoid this uncertainty of boundary layer thickness.

C. Effect of Additives on Nitrogen Supersaturation

The typical effect of added amounts of carbon dioxide is seen in Fig. 3 as an increase of static pressure over the isentropic value corresponding to the impact pressure. The saturated expansion static pressure is shown for comparison. The effect on measured pressure ratios of this carbon dioxide addition is seen in Fig. 5 as causing earlier breakdown of the supersaturated condition, until at 0.26% carbon dioxide condensation may be considered to occur at the saturation point. The computed supersaturation pressure ratios and temperatures are summarized in Table II and plotted in Figs. 13 and 14.

When large amounts of carbon dioxide were added, the flow upstream of the nitrogen condensation was no longer isentropic. The static pressure was higher than the isentropic value corresponding to the impact pressure as shown in Figs. 3 and 5, Run 28-6 for 2% carbon dioxide. This rise in static pressure was caused by the heat release from the condensing carbon dioxide. Saturation and, presumably, condensation of the carbon dioxide occurred well upstream of the nitrogen saturation. If the gradual condensation of carbon dioxide were approximated by the addition of heat at a point, the solution of the continuity, momentum, and energy equations gave the pressure rise across this discontinuity (Ref. 10, and earlier, Ref. 31). The heat added was taken to be the mass of carbon dioxide times its latent heat of vaporization. Using this relation, the

pressure after this carbon dioxide condensation was computed and plotted on Fig. 3. The pressure before the assumed discontinuity was taken as the isentropic value corresponding to the impact pressure at that point. Another run of 1% carbon dioxide checked as well.

The static pressure rise for large amounts of carbon dioxide was not caused by the slight change in the specific heat ratio, as can be seen from Fig. 15. The isentrope of the mixture lay approximately 2% of the way from the $\gamma = 7/5$ to the $\gamma = 9/7$ curve, and this correction was far too small to account for the experimental deviation from the $\gamma = 7/5$ isentrope indicated in Fig. 5.

The effect of the addition of other substances such as water, oxygen, and argon was always to decrease the supersaturation. The computation of supersaturation pressure ratio is discussed in Section III-A and plotted in Fig. 13. Another measure of the supersaturation was the saturation temperature minus condensation temperature. Fig. 14 shows the same trend in this supersaturation temperature, namely, a decrease with more additive. Very small amounts of carbon dioxide and water, approximately 1/4%, added to the nitrogen seemed to provide sufficient nuclei for the nitrogen to condense approximately at the saturation point (Cf. Figs. 13 and 14, which are based on nitrogen saturation values).

The measured pressure ratios for small amounts of carbon dioxide addition are shown in Fig. 16 (Cf. Figs. 3 and 5 for larger amounts of carbon dioxide). The pressure ratios for addition of water,

oxygen, and argon are plotted in Figs. 17 through 22. Pressure data for some "no additive" runs, carbon dioxide runs, and water addition runs are tabulated in Table IV.

Fig. 23 shows the flow Mach number at which various percentages of nucleants saturated themselves when injected into the basic nitrogen flow. The additive saturation Mach number decreased with increased amount of impurity. This plot is in error by two factors:

1. The change in γ of the basic flow due to addition of either one or three atom nucleants (argon and water).*
2. The change in basic nitrogen vapor pressure curve due to the presence of the nucleant.

From this plot it is seen that carbon dioxide and water were probably condensed in the nozzle and in a solid state when the nitrogen saturated. The same concentration of water condensed upstream of carbon dioxide, and this may explain the more severe effect of water on supersaturation. The oxygen and argon were probably still in the gas state. It is believed that this difference in mechanism was responsible for the difference in effect on supersaturation of carbon dioxide and water, and oxygen and argon. No correlation was obtained of time or distance from additive saturation to nitrogen condensation between the water and carbon dioxide runs.

A correction to the supersaturation of the oxygen additive runs was made for the change in the vapor pressure curve of the mixture.

---

* This is discussed in Section II-C.

Addition of oxygen increased the boiling temperature at a given pressure. Wagner's data (Ref. 12) were taken for 20% oxygen (Cf. Fig. 8), and smaller percentages were interpolated. The results of this correction showed practically no effect of oxygen addition on the supersaturation temperature difference of the mixture, but still some decrease of supersaturation pressure ratio with oxygen addition. (Cf. Figs. 13 and 14, dashed lines.) A similar correction could be made for the argon addition runs.

Addition of carbon dioxide to the synthetic air (20% oxygen mixture) was shown to decrease supersaturation in a manner similar to the effect of carbon dioxide on nitrogen alone.

D. Effect of Reservoir Pressure and Temperature on Nitrogen Supersaturation

The range of reservoir pressure available was from 4 atm. (incipient flow breakdown) to 20 atm. (instrumentation and structural limitations). Temperature was varied from ambient (70° F) to 360° F. At the higher temperatures and lower pressures the condensation Mach number was not reached in the tunnel for the 0.010 square inch throat area.

Typical pressure data for the various reservoir conditions are plotted in Fig. 24, showing earlier condensation at higher pressure and lower temperature. The runs are tabulated in Table III, and the saturation and condensation Mach numbers plotted in Figs. 25 and 26. Apparently, an increase in supersaturation at the higher pressure more than offsets the decrease in saturation Mach number. This increase in supersaturation temperature (saturation temperature minus condensation temperature) is shown in Fig. 27. Some of the scatter in the 290° K data is due to reservoir temperatures not exactly at 290°. The range was 284° to 295° K (Cf. Table III). The supersaturation of Run 37-4 is less than that indicated in Table II, but this run was made at the same time as the others in Table III, and the trend with reservoir conditions is considered valid, although the level of supersaturation may be impaired. This may have been due to some contamination in the newly installed supply line. Results of Ref. 6 are shown on Fig. 27 and indicate the same trend with reservoir

conditions, although the supersaturation of the present data is several degrees lower.

Two runs were made with the same percent of carbon dioxide added to each and with the reservoir pressure changed by a factor of two. The results indicate that for 0.03% carbon dioxide (the usual concentration in air) the nitrogen supersaturation temperature at 16.65 atm. reservoir pressure is only 3/4 that at 8.33 atm.

E. Impact Pressure Deficit

From run to run it was noted that the impact pressure at a point in the nozzle was affected by the amount of nucleant, presumably through the change in amount of condensate. Fig. 28 gives the result of varying nucleant with the impact tube at x = 5 inches. It is seen that the impact pressure decreased by as much as 8%. From runs made in the 5" Hypersonic Tunnel it seems that the re-evaporation of the condensed phase occurred within the normal shock which occurred ahead of an impact probe. This test was done with only one amount of condensate, but it seems to indicate that a momentum loss by non-evaporating drops carrying through the shock wave did not occur. A possible explanation may be the entropy rise associated with condensation and the subsequent re-evaporation. This entropy rise will give the proper sign to the change in impact pressure. The entropy rise must be small, for, as shown in Section IV-E, the final state of a condensation shock is close to the equilibrium saturated expansion.

It is of interest to notice that the maximum deficit for argon and oxygen occurred at approximately the same concentration. This concentration was just enough to saturate the nucleant at the Mach number at which nitrogen saturation occurred.

The impact pressure is a function of the effective flow area. This relation for three assumed processes is presented in Fig. 29. The processes are:

1. Perfect gas isentropic expansion

$$\frac{P_o'}{P_o} = f_{cn.}(\gamma, M)$$

2. Perfect gas isentropic expansion to saturation, followed by saturated expansion. Refs. 2, 3, and 4. Discussed in IV-D.

3. Perfect gas isentropic expansion to a supersaturated state, with a sudden collapse. Ref. 18. Discussed in IV-E.

The agreement to first order among the three processes (± 3 %) is the basis for the use of the perfect gas relation for the condensing flow. The computed values are listed in Table V.

F. Integration of Flow Properties

A stepwise integration method has been developed to compute velocity, temperature, density, and percent condensed phase in a one-dimensional flow, knowing static and impact pressures through the nozzle. (Refs. 5 and 14.) Pressure measurements must extend upstream into a region of isentropic flow. The equations are derived in Appendix B. Since the vapor pressure curve for nitrogen is approximated within 1/2% in temperature by $L/R = 844.87^{\circ}$ K (Cf. Fig. 8), this integration and the saturated expansion computations are equally valid for gas-liquid or gas-solid equilibrium. Increase of condensed phase present (percent by mass) is shown in Fig. 30, along with the computed amount for a saturated expansion from Buhler's theory and the amount computed for the condensation shocks.

It will be noted that in the p - T plane (Figs. 31 and 32) the flow, after collapse of the supersaturated state, does not completely return to the infinite plane vapor pressure curve, but remains at a few degrees lower temperature. Two effects seem to be present:

1. The actual saturated vapor consists of a gas in equilibrium with liquid in the form of drops, and the energy of formation of these drops would decrease the vapor temperature.
2. Some change in the infinite plane saturation vapor pressure curve is expected due to the additive.

As shown in the Section III-B and by Fig. 12, the effective area was not the same for hot and cold runs. For this reason the stepwise integration method was developed using impact pressures as a measure of the effective flow area.

G. Air Supersaturation - Scale Effect

Several runs were made in the 1" x 1" tunnel using air from the 5" compressor plant. Comparison of these runs with test data from the 5" tunnel affords some insight into scale effects. For the Mach number 9 nozzle in the 5" tunnel the expansion was so rapid that condensation had begun at the farthest upstream point of measurement. Thus it was impossible to determine the supersaturation, if there were any. For the Mach number 6 nozzle in the 5" tunnel (p_o = 5 atm., T_o = 298° K) the center line air supersaturation was 12.6° K and 0.75 Mach number (Ref. 32) based on Wagner's air vapor pressure curve (Fig. 8). The mean temperature gradient from saturation to condensation was 2.5° K/cm. In the 1" x 1" tunnel (p_o = 8.33 atm., T_o = 298° K) the supersaturation of this same air was 12.3° K and 0.56 Mach number. The mean temperature gradient was 5° K/cm. From the similarity of supersaturation temperature it might be argued that temperature gradients are not a primary parameter in condensation. The data are certainly not conclusive, and a change of 10:1 in gradient would be desired before drawing definite conclusions. The Mach number 9 tunnel had approximately the same temperature gradients as the 1" x 1" tunnel, but as mentioned before, data are lacking on its supersaturation.

By filtering the air through a canister of drierite (water removing chemical) the supersaturation in the 1" x 1" tunnel was increased slightly to 12.9° K and 0.67 Mach number. Addition of a

canister of ascarite (carbon dioxide removing chemical) in the line increased the supersaturation to 14.0° K and 0.74 Mach number. This seemed to indicate that there was considerable carbon dioxide in the 5" air supply.

These data are to be compared with supersaturation of 16.0° K and 0.89 Mach number, still based on Wagner's air vapor pressure data, obtained with synthetic air made up from 20% oxygen in nitrogen (Cf. Table II). This indicates some effect of the impurities in the 5" tunnel air. Addition of 0.09% carbon dioxide to this synthetic air decreased the supersaturation to approximately 6° K.

H. Helium

One run was made in the 1" x 1" tunnel with commercial helium as the working fluid. Isentropic expansion was obtained to M = 7.2, where flow breakdown occurred, as the diffuser and compression ratio were not adequate for the higher Mach numbers obtained in helium. At the same area ratio, a single atom gas (γ = 5/3) is at a higher Mach number than a multi-atom gas. See Fig. 15 for theoretical and experimental expansions at several values of γ . At the station where $M_{HE} = 7.2$, $M_{N_2} = 5.6$, and from Fig. 15 an increase in boundary layer thickness for the helium flow is indicated. Proper diffuser design seems the only obstacle to higher Mach numbers, until saturation conditions are reached ($M_{saturation} \doteq 100$ for helium at p_o = 8.33 atm., $T_o = 294^\circ$ K).

The major objection to use of helium seems to be its cost. Although its mass flow (for same p_o, T_o, and A^*) is only 0.4 times that of nitrogen, cost of equal mass of bottled helium is 187 times nitrogen, resulting in 75 times higher running cost per unit time.

For a 5" x 5" test section at Mach number = 15, p_o = 8.33 atm., $T_o = 294^\circ$ K, $A^* = 0.010$ (assuming approximately 60% boundary layer in the test section). The cost of the helium to make up an estimated 10% loss each cycle amounts to approximately one dollar per minute of running time based on three cents per cubic foot in bulk.

I. Future Experimental Research

The testing reported in this thesis has shown the supersaturation of commercial nitrogen for reservoir pressures to 20.7 atm. and reservoir temperatures to 408° K.* The effects of carbon dioxide, water, argon, and oxygen have been shown at one reservoir condition (8.33 atm. and 290° K). Future work could show the effects of oil, dust, and ions on supersaturation, although the problem of controlled addition of these elements is difficult. Doubling the pressure level has been shown to decrease slightly the supersaturation for significant percentages of carbon dioxide. It would be of interest to check further the effect of additives at other pressure levels.

Probably the most important work yet to be done is an expansion to a slightly supersaturated condition, followed by a constant area section. This would establish the time required at constant vapor properties to collapse the supersaturated state. To do this a contoured section could be faired into the present tunnel. Considerable trouble is expected with this fairing, and the test may be easier in the larger 5" tunnel.

A few axial surveys were made with a thermocouple probe. Some correlation between condensation and a rise in probe recovery factor was indicated at first, but later runs did not seem consistent. The program was abandoned, since considerable time was required for the

---

* Ref. 6 gives the supersaturation to 69 atm. and 590° K.

temperature to stabilize and the consumption of nitrogen was excessive. Now that the outside dock is available, the longer runs are feasible.

Nitrogen and helium have been used, and no merit is seen in using other single gases. Carbon dioxide condenses at low Mach numbers. Argon has a vapor pressure curve very close to oxygen. Pure oxygen is unsuitable from a safety standpoint, because the diffuser pumps are oil-lubricated. Other gases are too dangerous or too expensive.

IV. THEORY

A. Unstable Equilibrium of a Droplet in Supersaturated Vapor

Consider the equilibrium of a supercooled perfect gas and its droplets. By the Thompson-Helmholtz equation:

$$r_{cr} = \frac{2\sigma m}{\rho R T \log_e p_{cr}/p_\infty} \tag{4.1}$$

This relation gives the relation between the thermal equilibrium pressure p_{cr} at temperature T over a drop of radius r and the thermal equilibrium pressure p_∞ for a plane surface of liquid. Several derivations are given by Frenkel (Ref. 33) and Stodola (Ref. 34). For given reservoir conditions, the flow properties can be expressed as a function of temperature only, and the critical radius computed as a function of temperature. The decrease in critical radius with increasing Mach number (from an infinite radius plane surface at saturation) is plotted in Fig. 33. Density and surface tension values are from Stever and Rathbun, Ref. 7, and vapor pressure from Fig. 8. Radius values are probably reliable only above 10^{-7} cm., as pointed out by Gibbs. Mach number is related to nozzle location in Fig. 34.

At constant temperature, the molecular evaporation rate is $\backsim p_{cr}$. The molecular impingement rate $\backsim p_v$ (Refs. 34 or 35). To show that the supersaturated state is unstable, consider a drop of radius r_{cr} and at the same temperature, T, its necessary pressure for

equilibrium $p_{vapor} = p_{cr}$. The evaporation and impingement rates are now equal.

Consider a variation of r_{cr} to some $r_1 > r_{cr}$, keeping the drop at T. For this $r_1 > r_{cr}$ the pressure over the drop is given by the Thompson equation, $p_1 < p_{cr}$. Since $p_{cr} = p_v$, the evaporation rate ($\backsim p_1$) is less than the impingement rate ($\backsim p_{cr}$), causing the drop to grow even larger.

If a variation of drop radius is considered to $r_2 < r_{cr}$, the Helmholtz equation indicates an equilibrium pressure $p_2 > p_{cr} = p_v$. The resultant evaporation rate ($\backsim p_2$) exceeds the impingement rate ($\backsim p_v$), causing the drop to decrease in size. The critical drop size given by the Helmholtz equation is thus seen to be an unstable equilibrium.

As the Thompson formula indicates the radius droplet which is maintained in a given supersaturation, vapor pressure curves for various radii can be drawn. For the 8.33 atm. and 290° K reservoir conditions in the 1" tunnel, Fig. 8 shows the saturation pressure curve for various droplet sizes. From this can be obtained a rough idea of the required droplet growth to give the computed p - T variation, if equilibrium conditions exist.

B. Spontaneous Nuclei Formation

Condensation of a gas in a wind tunnel may occur by at least two phenomena: spontaneous self-nucleation and subsequent growth or condensation on the surface of a foreign particle and subsequent growth. Condensation on the walls of the tunnel or on models is not expected, as the boundary layer wall temperatures which approach stagnation temperatures are much higher than free stream temperatures.

Numerous references have discussed the theory of self-nucleation of a gas. (Cf. Refs. 7, 9, 16, 33, and 36 through 43.) A summary to the present status is given by Stever (Ref.19). As will be discussed, the conclusion of the present thesis is that self-nucleation is not the primary phenomenon occurring in these experiments.

By Boltzman's principle, the rate of spontaneous nuclei formation is

$$J = K e^{-\frac{\Delta W}{kT}} \tag{4.2}$$

$$K \sim \frac{P}{\sqrt{2\pi RT}} 4\pi r_{cr}^2 \qquad \text{(Ref. 38)} \tag{4.3}$$

$$-\frac{\Delta W}{kT} \sim \frac{\sigma^3}{T^3 (\log_e P/P_\infty)^2} \qquad \text{(Ref. 37)} \tag{4.4}$$

The numerical constants are given in Appendix C. The problem then, if condensation is caused by spontaneous nucleation, is to determine

a criterion on J for condensation. It is emphasized that the above relation for J employs values of surface tension, density, and vapor pressure which are not known precisely due to the low temperature and small droplet size. The equation is for droplets, since the formation energy for a crystal would be required for ΔW if the solid state were to be considered.

The nuclei formation equation is exact when applied to a stationary supersaturation as in a cloud chamber, where the expansion is applied and then held constant. Use of the above equation in a continuous expansion like the one which occurs in a wind tunnel is called "quasi-steady" and introduces non-steady errors.

Charyk and Lees (Ref. 40) suggested a tentative criterion on the spontaneous nuclei formation rate (J = nuclei formed per cubic centimeter second). Using their recommendation of $\log_e J = 7.0$ (J = 1100), (Fig. 3, Ref. 40), the predicted supersaturation pressure ratio for the 1" tunnel using nitrogen at reservoir conditions of 8.33 atm. and 290° K is $\log_e (p/p_\infty)_{condensation} = 4.0$ or 14° K supersaturation. Comparison with Figs. 13 and 14 shows this supersaturation was slightly exceeded for commercial nitrogen.

A recent NACA Technical Note (Ref. 43) used $J = 10^{12}$ to define an upper limit of expected supersaturation. The surface tension was decreased for the smaller radii.

Stever and Rathbun (Ref. 7) noted that their experimental condensation occurred where the rates of nuclei formation were very

small. Their approach was to modify the nuclei formation equation for the decrease in surface tension with decrease of droplet size. This gave larger values of nuclei formation rate than before. In addition, the inaccuracies of nitrogen properties should be considered.

As first pointed out by Ostwatitsch (Ref. 38), the nuclei formation rate alone is not the only relevant parameter. Droplets formed just after saturation have a longer time to grow than do those formed farther downstream. The nuclei rate of formation increases downstream, so the total contribution to the condensed phase at a point is a summation of the number of nuclei formed at each previous station times their droplet growth. Since then:

$$g \sim \int_{sat}^{x} J(\xi)\, r^3(\xi, x)\, d\xi \qquad (4.5)$$

where ξ is the point of nuclei formation. (Cf. Bogdonoff and Lees, Ref. 16.)

The conclusion was reached by Bogdonoff and Lees that condensation would not occur along the isentrope for p_o = 860 psia, T_o = 238° K or lower pressures or higher temperatures. This is considered to be in error due to their misinterpreting the experimental data, and the theory developed for this interpretation is in question.

Their further conclusions that carbon dioxide up to 2% did not produce "condensation or any other violent phenomena" is of interest.

The condensation of a gas has been shown to result in a gradual increase of static pressure. Thus, Bogdonoff and Lees probably had condensation with carbon dioxide but did not recognize it. Ref. 43 also reports no change in pressure measurements due to addition of an unspecified amount of carbon dioxide.

An indication that spontaneous condensation did not occur was found in the trend that as purification of the nitrogen increased, supersaturation increased. It is thought that when spontaneous condensation occurs, increased purification will not cause further increase of supersaturation. This limiting of supersaturation did not seem to be reached in the present tests.

It is interesting to note that the arbitrary limit of $(p/p_\infty)_{max} = 1000$, suggested by Charyk and Lees (Ref. 40) as an attempt to indicate the limitation on supersaturation imposed by foreign particles, is quite close to the value obtained for the commercial nitrogen (Fig. 13).

C. Droplet Growth

Buhler (Ref. 18) has presented a theory which equates the difference of energy added by condensing molecules and removed by the re-evaporating molecules to the rate of change of the droplet energy. Buhler's assumptions include:

1. Accomodation coefficient of unity.
2. Droplet vapor pressure given by the Thompson formula.
3. Molecular mean free path much larger than droplet radius.
4. Surface energy term independent of droplet radius and temperature.

The mass of gas striking unit surface in unit time is

$$\Gamma = \frac{P}{\sqrt{2\pi RT}} \qquad \text{(Ref. 35, p. 63)} \qquad (4.6)$$

For the condensing molecules, vapor properties (p_V , T_V) are used, and energy C_pT_V is carried to the droplet.

For the evaporating molecules, droplet properties (p_D, T_D) are used, and energy C_pT_D is carried away from the droplet per unit mass evaporated.

p_D is the pressure over a droplet of radius r and is assumed given by the Thompson formula

$$p_D(T_D) = p_\infty(T_D)\, \exp\left(\frac{2\sigma m}{dRTr}\right) \qquad (4.7)$$

The energy of the droplets is taken as

$$\frac{4\pi}{3} r^3 \rho_L e_L + 4\pi r^2 w \qquad (4.8)$$

e_L , the bulk liquid energy per unit mass, is defined from

$$\rho_L e_L = \rho_L \left[C_p T_D - L(T_D) \right] \tag{4.9}$$

For nitrogen, it happens that

$$\frac{d}{dT_D}(\rho_L e_L) = C_L = 23.9 \times 10^6 \frac{\text{dyne}}{\text{cm}^2\,^\circ\text{K}} = .571 \frac{\text{cal.}}{\text{cm}^3\,^\circ\text{K}} \tag{4.10}$$

where C_L is a constant value, the specific heat of the liquid by volume.

W represents the surface energy term, and is taken by Buhler

$$W = 6.09 \times 10^{-7} \text{ cal/cm}^2$$

The energy equation is then

$$4\pi r^2 (C_p \Gamma_v T_v - C_p \Gamma_D T_D) = \frac{d}{dt}\left(\frac{4\pi}{3} \rho_L e_L + 4\pi r^2 W \right)$$

$$= 4\pi r^2 \left\{ \left[\rho_L (C_p T_D - L) + \frac{2W}{r} \right] \frac{dr}{dt} + \frac{r}{3} C_L \frac{dT_D}{dt} \right\} \tag{4.11}$$

This reduces to:

$$\Gamma_v C_p (T_v - T_D) + (\Gamma_v - \Gamma_D)\left(L - \frac{2W}{\rho_L r} \right) = \frac{r}{3} C_L \frac{dT_D}{dt} \tag{4.12}$$

Droplet growth is given by:

$$4\pi r^2 (\Gamma_v - \Gamma_D) = \frac{d}{dt}\left(\rho_L \frac{4\pi r^3}{3} \right) \qquad \text{or} \tag{4.13}$$

$$\frac{dr}{dt} = \frac{\Gamma_v - \Gamma_D}{\rho_L}$$

The energy equation (4.12) is first solved with the right-hand term set equal to zero. This gives a quasi-steady equilibrium droplet temperature, T_E . Computations for the 1" tunnel at 8.33 atm. and 290° K reservoir conditions have shown that the droplet, if originally at vapor temperature T_V , will increase in temperature toward T_E quite rapidly as compared to the transit time. The droplet will travel only one millimeter for the largest radii considered in the time required to increase its temperature from T_V to T_E - 1/10 $(T_E - T_V)$. The approach to T_E is exponential.

Equations (4.12) and (4.13) are solved with the right-hand term of equation (4.12) set equal to zero and a small correction made for dT_D/dt later. This correction is important only for large droplets, at which time the $2w/\rho_L r$ term may be neglected compared with $L(T_D)$.

These computations were made and are presented in Fig. 35 as dr/dx vs. x. A solution by isoclines will give $r(x, r_o)$ with r_o given by the supersaturation at point in the nozzle where growth of this droplet is considered to start. These drop growth values are good only along the isentrope. When the heat release of condensation increases the vapor temperature and pressure, the previously derived drop growth must be recomputed for the new vapor properties. Rigorously, this would be a stepwise computation of the breakdown of supersaturation.

In Fig. 36 these quasi-steady equilibrium droplet temperatures are compared with the isentropic vapor temperature, saturated expansion temperature, and results of the flow integration.

D. Saturated Expansion

If no supersaturation is realized, a saturated expansion occurs. The problem was discussed by Wagner (Ref. 12). This would require enough nuclei present (foreign impurities) to begin droplet growth at saturation. In a seminar at CalTech in June 1950, R. Buhler developed the equations for this expansion. The experimental results of Bogdonoff and Lees (Ref. 16) seemed to indicate the saturated expansion occurred, as addition of considerable carbon dioxide gave no change in flow properties. The implication is that the flow was already fully saturated. The results of Buhler's derivations are given in Refs. 2, 3, and 4. This theory provides for the expansion along a perfect gas isentrope until the vapor pressure curve is reached. Then the expansion proceeds along this vapor pressure curve. The saturated expansion results are shown in Figs. 3, 5, and 30. and listed in Table IV.

The pressures of the saturated expansion are sensitive to reservoir temperature, but not to reservoir pressure, as shown in Fig. 37. A fixed value of L/R is taken to simplify the numerical work. Accuracy of this value of L/R is shown in Fig. 8.

In Figs. 31 and 32 the saturated expansion is the broken line consisting of the right half of dry isentrope and the lower half of the vapor pressure curve. Experimental results of the 5" hypersonic tunnel also agree approximately with the saturated expansion.

Various speeds of sound have been postulated for the saturated flow. Since agreement is not yet reached, it is important to realize that the usual "Mach number " $M = u/\sqrt{\gamma RT}$ has no significance once the flow departs from the dry gas isentrope. In Refs. 2 and 4, several velocity ratios are defined for the Mach number. These are discussed in the next section.

A recent paper by Ross (Ref. 44) discusses two-dimensional oblique waves with heat addition, creation of some liquid, and change of specific heat ratio across the waves. His conclusion is that the heat addition (by condensation of some of the vapor) in an expansion wave will give a smaller flow deflection than that predicted by the perfect gas relations. This would cause flow disturbances in a hypersonic wind tunnel designed by usual methods.

Ross uses perfect gas relations on both sides of the discontinuity with usual speeds of sound and neglects the thermodynamic energy of the liquid phase created, which is a small term. The flow disturbances discussed by Ross would not appear before the saturation conditions are reached, and thus cannot apply to the throat disturbances found in the 1" x 1" and 5" hypersonic wind tunnels. (Cf. Section II-D.)

For extremely high Mach numbers where the stagnation temperature required for noncondensed flow is unreasonable, it may be necessary to operate with the test section flow fully saturated. A current thesis by Grey (Ref.32) deals with the correlation of test data in a saturated flow with the appropriate values in the dry, perfect gas flow.

E. Condensation Shock

As mentioned in Section III-E, a possible expansion is to follow the perfect gas isentrope to a supersaturated state and follow with a condensation shock to the vapor pressure curve. All flow properties ahead of this shock are known, and the equations of continuity, momentum, energy, and state can be solved graphically with the vapor pressure relation for the five unknowns, p, ρ, T, g, and u.

Computations for the 1" tunnel have shown that the condensation shock results in up to 5% higher pressure and 20% less condensate than the equilibrium saturated expansion at the same effective flow area. The comparison is tabulated in Table V. The pressure and temperature during the shock are approximately linear functions of the amount of condensed phase.

From the experimental data it seems that the shock results are a slightly better approximation to the final state than the saturated expansion. (Cf. Figs. 16, 18, 20, 22, and 30.) It is emphasized that the condensation shock is an end point of a process, and not an equilibrium path to be followed further. From any given shock condition, a new equilibrium saturated expansion would then be established.

F. The Speed of Sound in a Two-Phase Fluid

In order to obtain the appropriate similarity parameter (Mach number) for the flow of a two-phase fluid, it is necessary to know the fluid velocity and the speed of propagation of an infinitesimal disturbance at low frequency. This is discussed in Ref. 4.

1. Several "speeds of sound" have been suggested. If the drops are neither in thermodynamic or mechanical equilibrium with the vapor, the usual perfect gas relations apply.

Momentum

$$u\,du + \frac{dp}{\rho} = 0$$

Continuity

$$\frac{du}{u} + \frac{d\rho}{\rho} = 0$$

Energy (4.14)

$$u\,du + c_p\,dT = 0$$

State

$$p = \rho RT$$

Yielding

$$a^2 = \frac{dp}{d\rho} = \frac{\gamma p}{\rho} = \gamma RT$$

2. If a fraction of the fluid is condensed, one effect is the change in density of the vapor phase. See Appendix B for the approximate density relation. The equation of state is now

$$p = \rho(1-g)RT \qquad (4.15)$$

leading to:

as $g \to 0$ $\quad \tilde{a}^2 \to \gamma RT$

$g \to 1$ $\quad \tilde{a}^2 \to 0$

$$\tilde{a}^2 = \frac{dp}{d\rho} = \gamma(1-g)RT$$

This is derived by Buhler, Ref. 2, and means kinetic but not thermal equilibrium is assumed.

3. Considering a saturated expansion of the vapor and liquid, the Clausius-Clapeyron relation is introduced

$$dp = \frac{L\rho}{R}\,\frac{dT}{T^2} \tag{4.16}$$

Using the Momentum and Continuity equations and neglecting the change in density discussed in the previous paragraph, we have

$$\text{(M)} \qquad u\,du + \frac{dp}{\rho} = 0$$

$$\text{(C)} \qquad \frac{du}{u} + \frac{d\rho}{\rho} = 0 \tag{4.17}$$

$$\text{(S)} \qquad p = \rho RT$$

yielding

$$\hat{a}^2 = \frac{dp}{d\rho} = \frac{RT}{1 - \frac{RT}{L}}$$

independent of g

$\hat{a}^2 = 1.063\ RT$ for $T = 50^\circ$ K

This speed of sound has the effect of the drops following the thermal but not mechanical motion of the vapor.

4. For both mechanical and thermodynamic equilibrium, Buhler (Ref. 4) has derived $\overset{o}{a}$. The equations are

$$(M) \quad u\,du + \frac{dp}{\rho} = 0$$

$$(C) \quad \frac{du}{u} + \frac{d\rho}{\rho} = 0 \qquad (4.18)$$

$$(E) \quad u\,du + c_p\,dT - L\,dq = 0$$

$$(S) \quad p = \rho(1-q)RT$$

$$(CC) \quad dp = \frac{L p}{R}\frac{dT}{T^2}$$

yielding

$$\mathring{a}^2 = \frac{dp}{d\rho} = \frac{(1-q)RT}{1 - 2\frac{RT}{L} + \frac{\gamma}{(\gamma-1)(1-q)}\left(\frac{RT}{L}\right)^2}$$

as $q \to 0$, $\mathring{a}^2 \to 1.12\,RT$ for $T = 50°K$

The last term in the denominator is not numerically significant at low temperatures. A refinement on $\mathring{a}$ using the exact mass equation was computed and was numerically indistinguishable from Buhler's equation.

The above five speeds of sound are plotted in Fig. 38 as functions of g. Although the plot is continued to g = 1, these speed of sound equations are only valid for small values of g. As g $\longrightarrow$ 1.0 these models require droplets to separate from each other, so the vibrations are not transmitted. Thus the speed of sound is decreased. Actually, in bulk liquid the speed of sound is quite large (a = 150,000 cm/sec for water). It is known that a small amount of dissolved gas will decrease the speed of sound in a liquid. Therefore, a sharp increase in a^2 as g $\longrightarrow$ 1.0 would be expected.

From the integrations of the flow properties, it is possible to determine $dp/d\rho$ along the nozzle. This is the square of the speed of sound only when equilibrium conditions are reached, so agreement of $dp/d\rho$ with any of the computed speeds of sound is expected only upstream of condensation and well downstream of the collapse of the supersaturated state. These values are plotted in Fig. 39 along the nozzle and compared with the several computed speeds of sound. The computed speeds of sound use the static temperatures obtained from the integration.

G. Condensation on Foreign Impurities

In an unpublished work on condensation on foreign nuclei, Dr. P. S. Epstein of CalTech concludes that the foreign nuclei are more important than the self-created "germs". For a nucleus concentration of 100 per cubic centimeter of air at S.T.P. he obtains $(p_c/p_\infty)_{max} = 1.1$ and $t = .016$ seconds from saturation to create 1% condensed phase. Dr. Epstein makes the isothermal assumption of equal drop and vapor temperature and thus overestimates the drop growth by a factor of ten or more (see Fig. 36). His computation is for a tunnel which expands to a supersaturated state and maintains this condition for 10^{-3} seconds or more. Other assumptions are that the nuclei are inert, spherical, and of the same size.

An attempt was made to estimate theoretically the effect of foreign impurities on flow parameters. The droplet growth was calculated by Buhler's method (Cf. Section IV-C and Fig. 35) using isentropic flow properties as obtained from impact pressure measurements of Run 23-1. This computation is in error principally in that subsequent heat release will affect the droplet growth.

Then, prescribing the amount of carbon dioxide present, the number of carbon dioxide nuclei available for the nitrogen to condense on is an inverse linear function of the assumed nuclei mass (radius cubed).

No. nuclei x nuclei mass = mass ratio of nucleant

This assumes an average radius of a spherical nuclei, whether in liquid or crystal form.

From the droplet growth curves, the fraction condensed can then be computed for each of the assumed foreign impurity nuclei radii. $r_o = 10^{-7}$ cm. seems reasonable from Run 23-1. The resultant g vs. x is given in Fig. 40 and compared with the values of the experimental integration. Now for addition of 100 times as much carbon dioxide (0.2%), following the above method and using the same nucleus radius would give g values exactly one hundred times as large. That this cannot be indicates that the carbon dioxide nuclei probably grow faster and are much larger at the point of nitrogen saturation for the higher concentrations of carbon dioxide.

If ε is the ratio by mass of impurity,

$$\frac{4\pi}{3} r_o^3 N d_{impurity} = \varepsilon \qquad (4.19)$$

where N is the number of nuclei (of radius r_o) per unit mass of nitrogen. The nuclei are assumed inert, spherical, and of uniform size.

N is assumed constant along the nozzle, so the mass fraction of condensate is:

$$g = \frac{4\pi}{3} r^3 N d_{nitrogen} \qquad (4.20)$$

$$\frac{g}{\varepsilon} = \left(\frac{r}{r_o}\right)^3 \frac{d_{N_2}}{d_i} \qquad (4.21)$$

The density of the foreign substance may differ from that of liquid nitrogen, introducing an error in g of the order of

$$\frac{4\pi}{3} N r_o^3 (d_{N_2} - d_i) \leq \varepsilon \qquad (4.22)$$

This is quite negligible for any appreciable g.

The computation of g is reduced to selecting the appropriate value of r_o for the prescribed ε .

Fig. 35 shows that the foreign nuclei theory gives approximately the correct shape of the g vs. x family for small g at a given concentration of carbon dioxide, but that the values of r_o must be selected to give the proper magnitudes of g. It appears that the following would be reasonable:

% CO_2 by volume	r_o
.002	10^{-7}
.067	2×10^{-7}
.260	4.5×10^{-7}

This indicates larger nuclei for the higher concentrations, rather than just more of the same size.

This is the first approximation of an iteration. The next step would be to compute the change from the isentropic flow properties due to the selected g vs. x schedule. Using the new flow properties, recompute the droplet growth curves. Then from this droplet growth a new g vs. x can be computed, and so forth, until sufficient convergence is reached.

Correcting the drop growth for non-isentropic conditions would decrease the growth until the dg/dx of the saturated expansion is reached. Rather than attempt the tedious stepwise process discussed earlier, Buhler (Ref. 18) has assumed a droplet growth function which matches the isentropic growth for g = 0 and the saturated growth dg_s/dx for $g = g_{sat.}$. With this relation, the g vs. x curves shown in Fig. 40 turn down at the downstream end, due to the decrease in dr/dx there. Later work has shown that the experimental pressure in the breakdown of the supersaturated state can be predicted in shape and within 1/2 centimeter in axial location without the empirical r_o vs. ε schedule indicated above. The radius given by the Thompson formula for the supersaturation existing on the isentrope was taken as the beginning nuclei radius. All radii were considered, and it was shown that a "most effective radius" exists for each concentration of carbon dioxide. This "most effective radius" is quite close to the empirical values given above. Future work will apply this theory to condensation due to water.

V. CONCLUSIONS

The results of this investigation indicate that for impurity concentrations slightly greater than those in commercially pure nitrogen the condensation is caused by foreign impurities and not by the self-nucleation of the gas.

Spontaneous nucleation would seem to require a limit supersaturation ratio, not to be exceeded by further removal of foreign nuclei. In the present investigation, the trend is for increased supersaturation for each lower concentration of impurities. No limit value of supersaturation seems to have been observed within the range of impurities tested. This is taken to mean that spontaneous self-nucleation is not of importance for a gas with slightly more impurities than commercial nitrogen. With the nitrogen alone, it is not known if further removal of impurities would lead to greater supersaturation. For the final decision on just what purity is required for self-nucleation to be of importance, the cloud chamber work with extremely pure nitrogen at Princeton will be of interest.

With relatively pure air, preliminary investigations indicate that air supersaturates slightly less than does nitrogen. The effects of impurities, such as carbon dioxide, water vapor, oil and dust particles, and argon, upon the supersaturation of air must be investigated further.

The experimental results indicate that, commercial nitrogen will supersaturate more than 15° K for the range of reservoir

conditions used. This supersaturation increases slightly with reservoir pressure and decreases with reservoir temperature. The supersaturation is decreased by additives such as carbon dioxide, water vapor, oxygen, and argon. Carbon dioxide and water vapor are extremely powerful nuclei for the condensation of nitrogen, and only a fraction of a percent by volume of either is required to eliminate completely the supersaturation.

During the condensation process of the nitrogen, it has been shown that the condensation is gradual and there is no condensation shock. After collapse of the supersaturated state, the flow properties are approximately those after a condensation shock. As the shock values are not an equilibrium state, a saturated expansion then must follow. It is not known whether the condensed phase is liquid or solid.

It has been shown that the easiest method of detecting the presence of condensation in the nozzle is to measure the static and impact pressures in the flow and determine the ratio of these pressures. The static pressure is sensitive to the condensation, and the impact pressure is least affected by the condensation. The light scattering technique of detecting the onset of condensation is not very convenient.

At extremely high Mach numbers where the stagnation temperature required to eliminate condensation is too high for the structural requirements, it may be necessary to operate with the flow in the test section fully saturated, and it may be possible to correlate the

pressures and forces measured in a saturated flow with those of the dry isentropic flow. A rudimentary theoretical estimate of the amount of condensation to be expected on foreign nuclei has been made.

REFERENCES

1. Epstein, P. S.: "Textbook of Thermodynamics". (1937), John Wiley, New York.

2. Buhler, R.: "Recent Results on the Condensation Investigation". Memorandum to Dr. H. T. Nagamatsu (July 9, 1950), California Institute of Technology.

3. Buhler, R.: "Methods for Determining the Mach Number in Hypersonic Wind Tunnels". Memorandum to Dr. H. T. Nagamatsu (August 21, 1950), California Institute of Technology.

4. Buhler, R., Jackson, P., and Nagamatsu, H. T.: "Oblique Shock Waves with Evaporation; Method of Calculating Free Stream Temperature and Amount of Condensation from Wedge Tests; Remarks on the Pressure Coefficient in Hypersonic Tunnels". Memorandum No. 3 (April 10, 1951), Contract No. DA-04-495-Ord-19, Army Ordnance Department, California Institute of Technology.

5. Nagamatsu, H. T., and Willmarth, W. W.: "Condensation of Nitrogen in a Hypersonic Nozzle". Memorandum No. 6 (January 15, 1952), Contract No. DA-04-495-Ord-19, Army Ordnance Department, California Institute of Technology.

6. Faro, I. D., Small, T. R., and Hill, F. K.: "Supersaturation of Nitrogen in a Hypersonic Wind Tunnel". Journal of Applied Physics (January 1952), Vol. 23, No. 1, p. 40.

7. Stever, H. G., and Rathbun, K. C.: "Theoretical and Experimental Investigation of Condensation of Air in Hypersonic Wind Tunnels". NACA TN 2559 (November 1951).

8. Li, T. Y., and Nagamatsu, H. T.: "Shock Wave Effects on the Laminar Skin Friction of an Insulated Flat Plate at Hypersonic Speeds". GALCIT Hypersonic Wind Tunnel Memorandum No. 11. To be Published.

9. Oswatitsch, K.: "Fog Formation in a Wind Tunnel and Its Influence on Model Tests". Jahrbuch der Luftfahrtforshung (1941), p. 692. Also Translation R. and T. No. 459 and MAPVG 248.

10. Head, Richard M.: "Investigations of Spontaneous Condensation Phenomena". Ph.D. Thesis at California Institute of Technology (1949).

11. Burgess, W. C., and Seashore, F. L.: "Criterions for Condensation-Free Flow in Supersonic Tunnels". NACA TN 2518 (December 1951).

12. Wagner, Carl: "Calculations on the Possibility of Obtaining Higher Mach Numbers in Wind Tunnel Tests". WVA Archive A-3 (1942).

13. Grunewald: "Wind Tunnel Mach Numbers Attainable under Consideration of Supersaturation Phenomena of Air". WVA Archive 204, Kochel (1945).

14. Wegener, P. P., Stollenwerk, E., Reed, S., and Lundquist, G.: "NOL Hyperballistics Tunnel #4 Result I: Air Liquefaction". NAVORD 1742 (January 4, 1951).

15. Puckett, A. E., and Schamberg, R.: "Hypersonic Wind Tunnel Progress Report No. 5"(August 8, 1946), Contract W-04-200 Ord-1463, Ord., Dept. Army, and GALCIT.

16. Bogdonoff, S. M., and Lees, Lester: "Study of the Condensation of the Components of Air in Supersonic Wind Tunnels. Part I: Absence of Condensation and Tentative Explanation". Rep. 146 (May 25, 1949), Contract AF 33 (038)-250, Air Materiel Command, USAF, and Aero. Eng. Lab., Princeton University.

17. Faro, I. D., Small, T. R., and Hill, F. K.: "Hypersonic Flow at a Mach Number of 10". Journal of Applied Physics (February 1951), Vol. 22, No. 2, p. 220.

18. Buhler, Rolf D.: "Theoretical Calculations on the Condensation of Nitrogen and of Air in Hypersonic Nozzles". Ph.D. Thesis at California Institute of Technology (1952).

19. Stever, H. Guyford: "Supersonic Handbook, Vol. III, Section G, Condensation in High Speed Flows". To be Published.

20. Nagamatsu, H. T.: "Results of Recent Hypersonic Flow Research in the Army Ordnance - CIT Hypersonic Wind Tunnel". Phys. Soc. Meeting, Urbana, Ill. (May 1950).

21. Becker, J. V.: "Results of Recent Hypersonic and Unsteady Flow Research at the Langley Aeronautical Laboratory". Journal of Applied Physics (July 1950), Vol. 21, No. 7, pp. 619-628.

22. Aoyama, Shin'ichi, and Kanda, Eizo: "The Vapor Tensions of Oxygen and Nitrogen in the Solid State". Science Reps. (1935), Tohoku Imp. Univ. Sendai, Vol. 24, pp. 107-115.

23. "NBS-NACA Tables of Thermal Properties of Gases". Table 11.50, U.S. Department of Commerce, National Bureau of Standards.

24. "Communications from the Kamerlingh Onnes Laboratory". Univ. of Leiden, 152d, 232b, 245d.

25. Tsien, H. S.: "Superaerodynamics, Mechanics of Rarefied Gases". Journal of the Aeronautical Sciences (December 1946), Vol. 13, No. 12.

26. Tribus, M., and Boelter, L. M. K.: "An Investigation of Aircraft Heaters. II: Properties of Gases". NACA ARR (October 1942), W-9.

27. Landolt-Bornstein: "Physikalisch-Chemische Tabellen". (1923), Vol. I, p. 175, Fifth Edition, Julius Springer , Berlin.

28. Young, G. B. W., and Janssen, Earl: "The Compressible Boundary Layer". Journal of the Aeronautical Sciences (April 1952), Vol. 19, p. 229.

29. Crown, J. C.: "On Boundary Layer Growth in a Compressible Flow between Radial Walls". Journal of the Aeronautical Sciences (October 1950), Vol. 17, p. 667.

30. Goldstein, Sidney: "Modern Developments in Fluid Mechanics". (1938) Oxford, Vol. 1, p. 105.

31. Heybey: "Analytical Treatment of Normal Condensation Shocks". Kochel Report No. 66/72. Available as NACA TM 1174.

32. Grey, Jerry: "The Effects of Air Condensation on Properties of Flow and Their Measurement in Hypersonic Wind Tunnels". Ph.D. Thesis at California Institute of Technology (1952).

33. Frenkel, J.: "Kinetic Theory of Liquids". Clarendon Press, Oxford (1946).

34. Stodola, A.: "Steam and Gas Turbines". McGraw Hill (1927).

35. Kennard, E. H.: "Kinetic Theory of Gases". McGraw Hill (1938).

36. Volmer, M. and Weber, A.: "Germ Formation in Supersaturated Aggregates". Zeitschrift fur Physikalische Chemie (1926), Bd. 119, pp. 277-301.

37. Volmer, Max: "Kinetics of Phase Change". Verlag von Theodor Steinkopff (1939), Dresden and Leipzig.

38. Becker, R., and Doring, W.: "Kinetic Treatment of Germ Formation in Supersaturated Vapor". Annalen der Physik (1936), Folge 5, Bd. 24, pp. 719-752.

39. Oswatitsch, K.: "Condensation Phenomena in Supersonic Nozzles". ZAMM (February 1942), Vol. 22, No. 1, pp. 1-14. Also Translation RTP 1905.

40. Charyk and Lees: "Condensation of the Components of Air in Supersonic Wind Tunnels". Report 127 (March 1, 1948), Aero. Eng. Lab., Princeton University.

41. Probstein: "Time Lag in Self-Nucleation of Supersaturated Vapor". Rpt.168 (November 27, 1950), Princeton University.

42. Gilmore, F.: "The Dynamics of Condensation and Vaporization". Ph.D. Thesis at California Institute of Technology (1951).

43. Hansen, C. F., and Nothwang, G. J.: "Condensation of Air in Supersonic Wind Tunnels and Its Effects on Flow about Models". NACA TN 2690 (April 1952).

44. Ross, F. W.: "The Propagation in a Compressible Fluid of Finite Oblique Disturbances with Energy Exchange and Change of State". Journal of Applied Physics (December 1951), Vol. 22, No. 12, p. 1414.

APPENDIX A

DISCUSSION OF PROBABLE ERRORS

Instrument reading and calibration errors:

Manometer tube	± .1 cm. for small pressures
	± .2 cm. for large pressures
Silicone specific gravity	± .1%
Reservoir pressure gage	± 1/4 psi during a run
	± 1 psi absolute
Reservoir temperature	± 2° F
Impact pressure probe location	± .02 in.
Misalignment of static tap impact tube	x/100" where x is distance from throat

Resultant pressure ratio accuracy: using 8-1/3 atm. and 290° K as the reservoir conditions for these numbers.

p/p_o near diffuser

$$\% \text{ error} = 100 \frac{\pm 0.1 \text{ cm silicone}}{5.0 \text{ cm}} + 100 \frac{\pm 1/4 \text{ psi}}{108 \text{ psi}} + 0.1 = \pm 2.4\%$$

(reading error; p_o error)

p/p_o near throat

$$= 100 \frac{\pm 0.2}{74} + 100 \frac{\pm 1/4}{108} + \pm 0.1 = 0.8\%$$

Similarly:

p_o'/p_o near diffuser = ± 1.0%

p_o'/p_o near throat = ± 0.6%

p/p_o' near diffuser = ± 3.2%

p/p_o' near throat = ± 1.2%

Saturation conditions are presumed accurate to ± .2° K or ± .01 Mach number (same reservoir conditions, no additive).

Due to the fairing of the curves from which the point of departure from the isentrope (condensation) is selected, the absolute value of M_c is probably ± 0.1. This means p_c is accurate to ± .001 atm. and T_c to ± 1.3° K. Saturation pressure p_∞ will be known to ± 5 x 10^{-5} atm. and the resultant accuracy in the supersaturation pressure ratio, p_c/p_∞, is ± 40%, fixing $\log_e p_c/p_\infty$ to +0.5, -1.0. The supersaturation temperature ($T_s - T_c$) will be known to ± 1.5° K. It should be noted that the relative accuracy of several runs made in one day with variation of only one parameter is much better.

The probable errors in the stepwise integration due to fairing of A/A^*, and the area summation of p/p_o A/A^* vs. x plot will give the following accuracy:

u/u^* = ± 1/2%

g = ± .01 in the value of g

T = ± 2° K upstream

± 3° K downstream

APPENDIX B

Stepwise Computation of Flow Properties, Using Measured Static and Impact Pressures

The equations used in the theoretical computation are as derived by Ostwatitsch (Ref. 39).

Assume: A mixture of gas and small liquid drops

The temperature of gas and drops the same*

The velocity of gas and drops the same

Constant value of the latent heat

The gas obeys perfect gas law

Gas density much smaller than liquid density

To develop our equations from those of Ostwatitsch, note that

(volume occupied by unit mass of gas-liquid mixture) =

(volume per mass of gas) x (weight fraction of gas) +

(volume per mass of liquid) x (weight fraction of liquid)

in symbols,

$$\frac{1}{\rho} = \frac{1-g}{\rho_{gas}} + \frac{g}{\rho_{liquid}} \qquad \text{(B-1)}$$

where g is fraction of total weight in liquid form

---

* This implies a slow droplet growth, for, as shown in Fig. 36, droplet and vapor temperatures are not equal for significant growth rates.

Momentum

Ostwatitsch gives $u\,du = -\frac{dp}{\rho_{gas}}$ momentum of gas

$$u\,du = -\frac{dp}{\rho_{liquid}} \quad \text{momentum of liquid} \tag{B-2}$$

Multiply first equation by (1 - g); second by g, and add.

$$u\,du = -dp\left(\frac{1-g}{\rho_{gas}} + \frac{g}{\rho_{liquid}}\right) = -\frac{dp}{\rho} \tag{B-3}$$

Continuity

Ostwatitsch has

$$\frac{d\rho_{gas}}{\rho_{gas}} + \frac{dg}{1-g} + \frac{du}{u} + \frac{dA}{A} = 0 \tag{B-4}$$

for a typical case M = 5

and p_o = 8-1/3 atm., T_o = 290° K., g = 0.10

$$\frac{1-g}{\rho_{gas}} = 8000 \qquad \frac{g}{\rho_{liquid}} = 0.1$$

so it is quite reasonable to use the approximation

$$\frac{1}{\rho} \doteq \frac{1-g}{\rho_{gas}} \tag{B-5}$$

which gives

$$\frac{d\rho_{gas}}{\rho_{gas}} = \frac{dp}{\rho} - \frac{dg}{1-g} \tag{B-6}$$

This leads to the equation in our form

$$\frac{d\rho}{\rho} + \frac{du}{u} + \frac{dA}{A} = 0 \qquad \text{or} \qquad \rho u A = \mathcal{M} = \text{constant} \tag{B-7}$$

Energy

$$d\left(\frac{u^2}{2} + C_p T - L g\right) = 0 \tag{B-8}$$

as Ostwatitsch's $g_1 = 0$, $g_{23} = 1$, $g_3 = $ our g

$$\frac{u^2}{2} + C_p T - Lg = C_p T_o = \frac{u^{*2}}{2} + C_p T^* \tag{B-9}$$

This assumes constant latent heat.

Equation of State

$$p = \rho_{gas}\, RT = \rho(1-g)\, RT \tag{B-10}$$

Using the approximation for gas density discussed before, together with the Clapeyron-Clausius equation, these equations have been used by Buhler (Ref. 3) to develop the functions of a saturated expansion.

For the integration of properties in the nozzle, the Clapeyron-Clausius equation is not assumed, and the measured static pressures permit a solution of the four equations. Area ratios are assumed to be the isentropic values corresponding to the impact pressure, leaving four unknowns, u, ρ , T, and g. The following graphical method of solution is due to Wegener (Ref. 14) and Nagamatsu and Willmarth (Ref. 5).

From continuity and momentum: $$du = -\frac{A}{\mathcal{M}}\,dp$$

$$\int_{\text{throat}}^{x} du = u(x) - u^* = \frac{1}{\mathcal{M}}\int A\,dp \overset{\text{by parts}}{=\!=} -\frac{1}{\mathcal{M}}\left[Ap\Big|_{th}^{x} - \int_{th}^{x} p\,dA \right] \tag{B-11}$$

where x denotes nozzle location.

$$u(x) = u^* - \frac{1}{\mathcal{M}}\left[A(x)\,p(x) - A^*p^* - \int_{th}^{x} p\,dA \right] \tag{B-12}$$

It will be convenient to split this last integral at x_1 and denote

$$\int_{th}^{x_1} p\,dA = K'$$

$$u(x) = u^* - \frac{1}{\mathcal{M}}\left[A(x)\,p(x) - A^*p^* - K' - \int_{x_1}^{x} p\,dA \right] \tag{B-13}$$

where x_1 is downstream of the throat, but upstream of the condensation, so flow is still isentropic there.

As $u(x_1)$ is known from isentropic functions, K' may be evaluated at $x = x_1$:

$$K' = \mathcal{M}\left[u(x_1) - u^*\right] - A(x_1)\,p(x_1) + A^*p^* \tag{B-14}$$

where $\mathcal{M}$ is from reservoir conditions and u, A, and p from measured p and p_o' values.

For computation it is convenient to non-dimensionalize and use:

$$\mathcal{M} = \rho^* u^* A^*$$

$$\frac{u}{u^*}(x) = 1 - \frac{P_o}{\rho^* u^{*2}} \frac{P}{P_o}(x) \frac{A}{A^*}(x) + \frac{P^*}{\rho^* u^{*2}} + \frac{K'}{\rho^* u^* A^*} + \frac{P_o}{\rho^* u^{*2}} \int_{X_1}^{X} \frac{P}{P_o} \, d\left(\frac{A}{A^*}\right) \qquad \text{(B-15)}$$

note

$$\frac{P_o}{\rho^* u^{*2}} = \frac{1}{\gamma \left(\frac{2}{\gamma+1}\right)^{\gamma/\gamma-1}} = 1.35 \qquad \text{for } \gamma = 1.40$$

$$\text{define } K = \frac{K'}{\rho^* u^{*2} A^*} + 1 + \frac{P^*}{\rho^* u^{*2}} = 1.35 \int_{th}^{X_1} \frac{P}{P_o}(x) \frac{d\left(\frac{A}{A^*}\right)}{dx} dx + 1 + \frac{P_o}{\rho^* u^{*2}} \frac{P^*}{P_o}$$

$$= \frac{u}{u^*}(X_1) + 1.35 \frac{P}{P_o}(X_1) \frac{A}{A^*}(X_1) \qquad \text{(B-16)}$$

Then:

$$\frac{u}{u^*}(x) = 1.35 \int_{X_1}^{X} \frac{P}{P_o}(x) \frac{d\left(\frac{A}{A^*}\right)}{dx} dx - \frac{P}{P_o}(x) \frac{A}{A^*}(x) + K \qquad \text{(B-17)}$$

From the equation continuity: $$\frac{\rho}{\rho^*} = \frac{1}{\frac{u}{u^*} \frac{A}{A^*}} \qquad \text{(B-18)}$$

Equation of State

$$\frac{T}{T^*} = \frac{p/p^*}{\rho/\rho^* \quad (1-g)} \qquad \text{(B-19)}$$

Energy Equation $$g = \frac{\frac{\gamma-1}{2}\left(\frac{u}{u^*}\right)^2 + \frac{T}{T^*} - \frac{T_o}{T^*}}{\left(\frac{\gamma-1}{\gamma}\right)\frac{L}{RT}} \qquad \text{(B-20)}$$

The last two are solved by iteration, starting with a g equal to the value at the previous station.

APPENDIX C

SPONTANEOUS NUCLEI FORMATION EQUATION

$$J = K e^{-\Delta W/kT} \qquad \text{by the Boltzmann assumption} \qquad (C\text{-}1)$$

From Volmer and Weber (Ref. 36)

$$-\frac{\Delta W}{kT} = -\frac{4\pi\sigma r_{cr}^2}{3kT} \qquad (C\text{-}2)$$

Using the Thompson formula (4.1) for r_{cr}:

$$-\frac{\Delta W}{kT} = -\frac{16\pi}{3}\left(\frac{\sigma}{T}\right)^3\left(\frac{M}{Rd}\right)^2\frac{1}{\left(\log_e \frac{P}{P_\infty}\right)^2} \qquad (C\text{-}3)$$

The constant of proportionality was taken as:

$$K = 6.08 \times 10^{25}\left(\frac{P_\infty (\text{mm. Hg})}{T}\right)^2 \frac{\sqrt{\sigma m}}{d}\left(\frac{P}{P_\infty}\right)^2 \qquad (C\text{-}4)$$

Using the above constants:

$$\log_e J = \log_e 9.5 \times 10^{25} + \log_e \frac{\sqrt{\sigma m}}{d}\left(\frac{P_\infty (\text{mm. Hg.})}{T}\right)^2 \qquad (C\text{-}5)$$

$$+2\log_e \frac{P}{P_\infty} - 17.49\left(\frac{\sigma}{T}\right)^3 \frac{\left(m/d\right)^2}{\left(\log_e \frac{P}{P_\infty}\right)^2} \qquad \text{(Ref. 37)}$$

APPENDIX D

FREQUENCY OF MOLECULAR COLLISIONS

For M = 5 expanding from p_o = 8.33 atm. and T_o = 290° K, the mean free path (Fig. 33) is 4.2×10^{-5} cm. Mean molecular velocity is 20,800 cm/sec, giving 2×10^{-9} seconds between collisions. Mean tunnel velocity from saturation to condensation (5 cm) is 70,000 cm/sec, giving a transit time of 7.2×10^{-5} seconds. The number of collisions per cm. is 7200, with 36,000 during the transit from saturation to condensation.

EQUIPMENT LIST

Stainless Steel Heater	Heliflow Steam Heater Graham Manufacturing Co.	No. 8CC10
Flowmeter Small	Fischer and Porter Flowrator S7-1186/1	Stainless Steel 1/16" dia. ball float 07-150 tube
Flowmeter Large	Universal Rotameter with Magnesium Bob	No. 44.1.310
1/2" Bronze Lever Quick Acting	Powell Giant Valve No. 360	350 psi max.
Brown Potentiometer Pyrometer	156X15P 325669	-100° F to 500° F
High Pressure Dew Point Meter	Chrome Button Cooled by CO_2	Fogging type
Grove Mity Mite Regulator		
Regulator	Oxweld R-65	0-3000 psig supply 0-400 psig delivery
Regulator	Oxweld R-89	0-3000 psig supply 0-1000 psig delivery
Oxygen Regulator	Victor SR 95	0-3000 psig supply 0-200 psig delivery
Pressure Gage	Ashcroft Laboratory Test Gauge	0-300 psig
Pressure Gage	Ashcroft "Duragage"	0-400 psig
Vacuum Gage	Wallace and Tiernan FA 160	0-20 mm Hg absolute
Vacuum Pump	Welch Duo Seal	Model No. 1405-H

Silicone	DC 200 Dow Corning	10 centistokes viscosity at 25° C. 3 microns vapor pressure at 45° C.
Tubing	Saran Plastic	Joints sealed with Glyptal (G.E.)
Diffuser Vacuum Source	200 HP Fuller Rotary Vane Compressor	No. C-300-300H
Water Removing Chemical	Drierite (Anhydrous $CaSO_4$)	W. A. Hammond Co.
Carbon Dioxide Removing Chemical	Ascarite	Arthur H. Thomas Co.

TABLE I

MASS SPECTROMETER ANALYSIS

Percent by Volume

Linde Air Products Trade Name	"Hi Purity" Nitrogen	"Dry" Nitrogen					
Date of Analysis	Aug. 1950	Aug. 1950	Feb. 1951	Sept. 1951	Sept. 1951	Jan. 1952	Feb. 1952
Run Number			9 - 5	26-6 to - 11	27-1 to -8	34-2 to -6	36-1 to -6
Nitrogen	99.66	99.81	99.82	99.58	99.64	99.78	99.85
Oxygen (±.01)	.24	.12	.09	.18	.17	.09	.06
Argon	.10	.07	.09	.09	.09	.05	.09
CO_2	--	< .007	< .002	< .004	< .004	.007	< .001
H_2O	--	< .0008	< .0021	< .0013	< .0007	< .0006	< .003
Helium	--	< .06	< .01	--	--	.013	< .006
CO	--	--	--	.09	.03	.05	< .001
Hydrogen	--	< .02	< .004	.02	.02	.009	< .002
Hydrocarbons	--	--	< .004	.04	.05	--	--

The water contents are from dew point measurements, which are considered more reliable than the mass spectrometer water contents.

TABLE II

EFFECTS OF IMPURITIES ON THE SUPERSATURATION OF NITROGEN

(Based on Nitrogen Saturation Values)

Estimated Total Per Cent by Volume of Impurity	Reservoir Pressure ATM	Reservoir Temp. ° Kelvin	Condensation Mach Number	$\ln \frac{P}{P_\infty}$ at Condensation	$T_s - T_c$ °Kelvin	$M_c - M_s$	Run Number	How Impurity Was Measured
				No Additives				
.0021 CO_2 .0024 H_2O	8.33	293	5.76	5.58	18.1	1.19	23-1	Chem. Analysis and Dew Point Meter
.42 total .18 O_2 .09A <.004 CO_2 <.0013 H_2O	8.33	295	5.62	4.72	16.1	1.02	26-11	Mass Spectrograph and Dew Pt. Meter
.36 total .17 O_2 .09A <.004 CO_2 <.0007 H_2O	8.33	295	5.74	5.25	17.4	1.14	27-1	Mass Spectrograph and Dew Pt. Meter
---	8.33	290	5.77	5.76	18.7	1.23	34-1	---
.22 total .09 O_2 .05A <.007 CO_2 <.0006 H_2O	8.33	289	5.88	6.41	20.2	1.35	34-5	Mass Spectrograph and Dew Pt. Meter
<.004 H_2O	8.33	296	5.71	5.06	17.0	1.09	22-1	Dew Pt. Meter
---	8.32	297	5.67	4.82	16.3	1.04	27-9	---
Average	8.33	294	5.73	5.37	17.7	1.15		

TABLE II (CONTINUED)

Estimated Total Per Cent by Volume of Impurity	Reservoir Pressure ATM	Reservoir Temp. ° Kelvin	Condensation Mach Number	$\ln \frac{P}{P_\infty}$ at Condensation	$T_s - T_c$ °Kelvin	$M_c - M_s$	Run Number	How Impurity Was Measured
			Adding CO_2					
.0074	8.33	292	5.50	4.28	15.2	.94	23-2	Chem. Analysis
.018	8.33	293	5.44	3.92	14.2	.87	23-4	Chem. Analysis
.018	8.33	299	5.68	4.70	15.9	1.02	21-2	Chem. Analysis
.020	8.32	295	5.60	4.53	15.7	1.00	27-10	Calibrated Orifice
.033	8.33	299	5.54	4.01	14.1	.88	21-1	Chem. Analysis
.043	8.33	293	5.23	2.81	11.3	.66	23-5	Chem. Analysis
.067	8.33	292	4.96	1.61	7.3	.40	23-3	Chem. Analysis
.26	8.32	294	4.59	0	0	0	27-11	Calibrated Orifice
.51	8.32	293	4.57	0	0	0	27-12	Calibrated Orifice
1.11	8.34	293					28-5	Large Flowmeter
2.09	8.34	288					28-6	Large Flowmeter
			Adding H_2O					
.0095	8.34	293	5.45	3.94	14.3	.88	25-4	Dew Point Meter
.026	8.33	293	5.17	2.48	9.3	.60	25-1	Dew Point Meter
.034	8.34	289	4.79	1.01	5.0	.26	25-6	Dew Point Meter
.10	8.34	287	4.50	0	0	0	25-7	Dew Point Meter
.16	8.34	289	4.53	0	0	0	25-5	Dew Point Meter

TABLE II (CONTINUED)

Estimated Total Per Cent by Volume of Impurity	Reservoir Pressure ATM	Reservoir Temp. ° Kelvin	Condensation Mach Number	$\ln \frac{P}{P_\infty}$ at Condensation	$T_s - T_c$ °Kelvin	$M_c - M_s$	Run Number	How Impurity Was Measured
			Adding Argon					
.31	8.33	287	5.49	4.54	16.1	.99	36-2	Small Flowmeter
.43	8.33	295	5.55	4.35	15.1	.95	29-6	Small Flowmeter
.92	8.33	296	5.45	3.72	13.6	.83	29-5	Large Flowmeter
1.2	8.33	286	5.45	4.37	15.6	.96	36-3	Large Flowmeter
2.2	8.34	290	5.51	4.45	15.6	.97	29-4	Large Flowmeter
3.6	8.33	288	5.38	3.94	14.4	.87	33-3	Large Flowmeter
4.3	8.33	285	5.33	3.85	14.3	.86	36-4	Large Flowmeter
			Adding Oxygen					
2.0	8.33	285	5.49	4.66	16.4	1.02	30-1	Large Flowmeter
2.4	8.33	289	5.65	5.20	17.5	1.12	31-3	Large Flowmeter
5.1	8.33	284	5.38	4.11	15.2	.92	30-2	Large Flowmeter
7.3	8.33	290	5.42	3.98	14.4	.88	31-4	Large Flowmeter
10.8	8.33	287	5.18	2.86	11.8	.68	30-3	Large Flowmeter
14.5	8.32	288	5.35	3.78	13.9	.84	31-1	Large Flowmeter
20.2	8.32	285	5.14	2.80	11.7	.67	31-2	Large Flowmeter
19.8	8.33	292	5.28	3.13	12.1	.72	41-2	Large Flowmeter

TABLE II (CONTINUED)

(Supersaturation Based on the Vapor Pressure of Nitrogen-Oxygen Mixture in First Column)

Estimated Total Per Cent by Volume of Impurity	Reservoir Pressure ATM	Reservoir Temp. ° Kelvin	Condensation Mach Number	$\ln \frac{P}{P_\infty}$ at Condensation	$T_s - T_c$ °Kelvin	$M_c - M_s$	Run Number	How Impurity Was Measured
				Adding Oxygen				
2.0	8.33	285	5.49	5.06	16.8	1.04	30-1	Large Flowmeter
2.4	8.33	289	5.65	5.65	18.0	1.15	31-3	Large Flowmeter
5.1	8.33	284	5.38	4.56	16.2	.96	30-2	Large Flowmeter
7.3	8.33	290	5.42	4.49	16.0	.96	31-4	Large Flowmeter
10.8	8.33	287	5.18	3.59	14.0	.86	30-3	Large Flowmeter
14.5	8.32	288	5.35	4.66	16.9	.97	31-1	Large Flowmeter
20.2	8.32	285	5.14	3.77	15.7	.86	31-2	Large Flowmeter
19.8	8.33	292	5.28	4.05	16.3	.92	41-2	Large Flowmeter

TABLE III

EFFECT OF RESERVOIR CONDITIONS
ON SUPERSATURATION OF NITROGEN

(Based on Nitrogen Saturation Values)

Reservoir Pressure ATM	Reservoir Temp. ° Kelvin	Condensation Mach Number	$\ln \frac{P}{P_\infty}$ at Condensation	$T_s - T_c$ ° Kelvin	$M_c - M_s$	Run Number
			No Additives			
4.15	295	5.77	4.71	14.6	1.00	37-5
8.33	294	5.55	4.44	15.4	1.04	37-4
12.55	287	5.25	3.70	15.0	.85	39-2
16.63	285	5.23	3.60	16.8	.93	39-3
20.71	284	5.25	4.42	18.4	1.02	40-1
4.15	330	>6.08				39-7
8.33	330	6.07	4.65	15.2	1.05	39-6
12.55	330	6.00	4.72	16.2	1.08	39-5
16.63	330	5.95	4.76	17.0	1.10	39-4
20.72	330	6.05	5.45	19.2	1.25	40-2

TABLE III (CONTINUED)

Reservoir Pressure ATM	Reservoir Temp. ° Kelvin	Condensation Mach Number	$\ln \frac{P}{P_\infty}$ at Condensation	$T_s - T_c$ ° Kelvin	$M_c - M_s$	Run Number
			No Additives			
8.34	360	>6.40				38-5
10.91	360	>6.41				26-10
12.55	360	>6.47				40-5
16.64	361	6.22	4.25	15.0	1.02	38-4
20.72	360	6.34	5.08	17.6	1.21	40-3
8.34	408	>6.22				38-3
12.56	408	>6.38				38-1
16.65	408	>6.54				38-2
20.72	408	>6.51				40-4
13.73	433	>6.48				26-1

TABLE IV

MEASURED PRESSURE RATIOS

See Table II for reservoir conditions
and supersaturation data

	Run 23-1		Run 27-1		Run 34-1*	
x inches	p_o'/p_o	p/p_o	p_o'/p_o	p/p_o	p_o'/p_o	p/p_o
0.50		.00850		.00852		.00808
0.75	.1161		.1167		.1158	
1.00	.0881	.00338	.0886	.00335	.0900	.00315
1.25	.0754				.0721	
1.50	.0680	.00215	.0677	.00211	.0615	.001913
1.75	.0597				.0554	
2.00	.0510	.001470	.0513	.001455	.0482	.001332
2.25	.0475				.0448	
2.50	.0430	.001097	.0423	.001077	.0410	.001003
2.75	.0382				.0375	
3.00	.0356	.000860	.0358	.000849	.0349	.000815
3.25	.0334				.0326	.000770
3.50	.0315	.000736	.0312	.000714	.0304	.000727
3.75	.0294				.0286	.000706
4.00	.0279	.000678	.0278	.000656	.0267	.000673
4.25	.0264					.000653
4.50	.0254	.000634	.0251	.000618	.0237	.000616
4.75	.0243					
5.00	.0228	.000591	.0226	.000569	.0210	.000564
5.25					.0198	
5.50		.000569		.000558		.000536

* As the nozzle throat radius was increased slightly before Run 34-1, static pressures of Run 34-1 should be compared at the same value of impact pressure, not x.

TABLE IV

CARBON DIOXIDE ADDITION

	Run 23-2 .0074% CO_2		Run 23-4 .018% CO_2		Run 23-5 .043% CO_2		Run 23-3 .067% CO_2	
x inches	p_o'/p_o	p/p_o	p_o'/p_o	p/p_o	p_o'/p_o	p/p_o	p_o'/p_o	p/p_o
0.50		.00853		.00860		.00849		.00848
0.75	.1157							
1.00	.0880	.00336	.0878	.00336	.0876	.00336	.0879	.00337
1.50	.0680	.00214	.0680	.00213	.0681	.00213	.0679	.00215
2.00	.0511	.00147	.0519	.00146	.0516	.00145	.0516	.00150
2.50	.0432	.00109	.0425	.00112	.0426	.00116	.0431	.00121
3.00	.0351	.000902	.0352	.000962	.0351	.000994	.0349	.00102
3.50	.0318	.000812	.0308	.000853	.0302	.000861	.0303	.000873
4.00	.0275	.000740	.0270	.000761	.0266	.000754	.0267	.000766
4.50	.0243	.000670	.0237	.000677	.0235	.000666	.0234	.000672
5.00	.0217	.000608	.0211	.000612	.0210	.000599	.0215	.000606
5.50		.000583		.000564		.000551		.000557

TABLE IV

WATER ADDITION

	Run 25-4 .0095% H_2O		Run 25-1 .026% H_2O		Run 25-6 .034% H_2O	
x inches	p_o'/p_o	p/p_o	p_o'/p_o	p/p_o	p_o'/p_o	p/p_o
0.50		.00856		.00861		.00855
0.75	.1174					
1.00	.0892	.00337	.0888	.00340	.0832	.00328
1.25	.0749					
1.50	.0681	.00213	.0758	.00215	.0669	.00213
2.00	.0511	.001474	.0515	.001493	.0504	.001535
2.50	.0424	.001092	.0429	.001176	.0437	.001193
3.00	.0361	.000906	.0363	.000989	.0360	.000995
3.50	.0317	.000811	.0312	.000858	.0308	.000858
4.00	.0278	.000731	.0272	.000773	.0268	.000746
4.50	.0248	.000655	.0240	.000662	.0240	.000658
5.00	.0218	.000595	.0216	.000596	.0214	.000582
5.50		.000579				.000566

TABLE V

COMPARISON OF ISENTROPIC, SATURATED EXPANSION,
AND CONDENSATION SHOCK PROPERTIES AT CONSTANT AREA RATIO

Area Ratio	Isentropic Flow				Saturated Expansion				Condensation Shock		
A/A^*	p/p_o	$T\ ^oK$	p_o'/p_o	x Run 23-1	p/p_o	$T\ ^oK$	p_o'/p_o	g	p/p_o	$T\ ^oK$	g
	$T_o = 290^oK$				$p_o = 8.30$ atm. $T_o = 290^o$ K				$p_o = 8.30$ atm. $T_o = 290^o$ K		
					L/R = 844.87°K $T_s = 56.7^o$ K				L/R = 844.87°K $T_s = 56.7^oK$		
24.1	.00199	49.1	.0639	1.52	.00213	55.0	.0641	.023	.00219	55.1	.019
30.7	.00140	44.4	.0506	2.04	.00160	54.0	.0507	.036	.00166	54.1	.030
39.6	.000970	39.9	.0395	2.68	.00119	53.0	.0397	.050	.00125	53.2	.042
51.6	.000660	35.8	.0305	3.60	.000877	52.0	.0307	.064	.000919	52.2	.051
68.1	.000443	31.9	.0233	4.94	.000637	51.0	.0235	.077	.000677	51.2	.061
90.8	.000294	28.4	.0176	--	.000457	50.0	.0177	.091	.000490	50.2	.066

FIG. I

SCHEMATIC OF PLANT

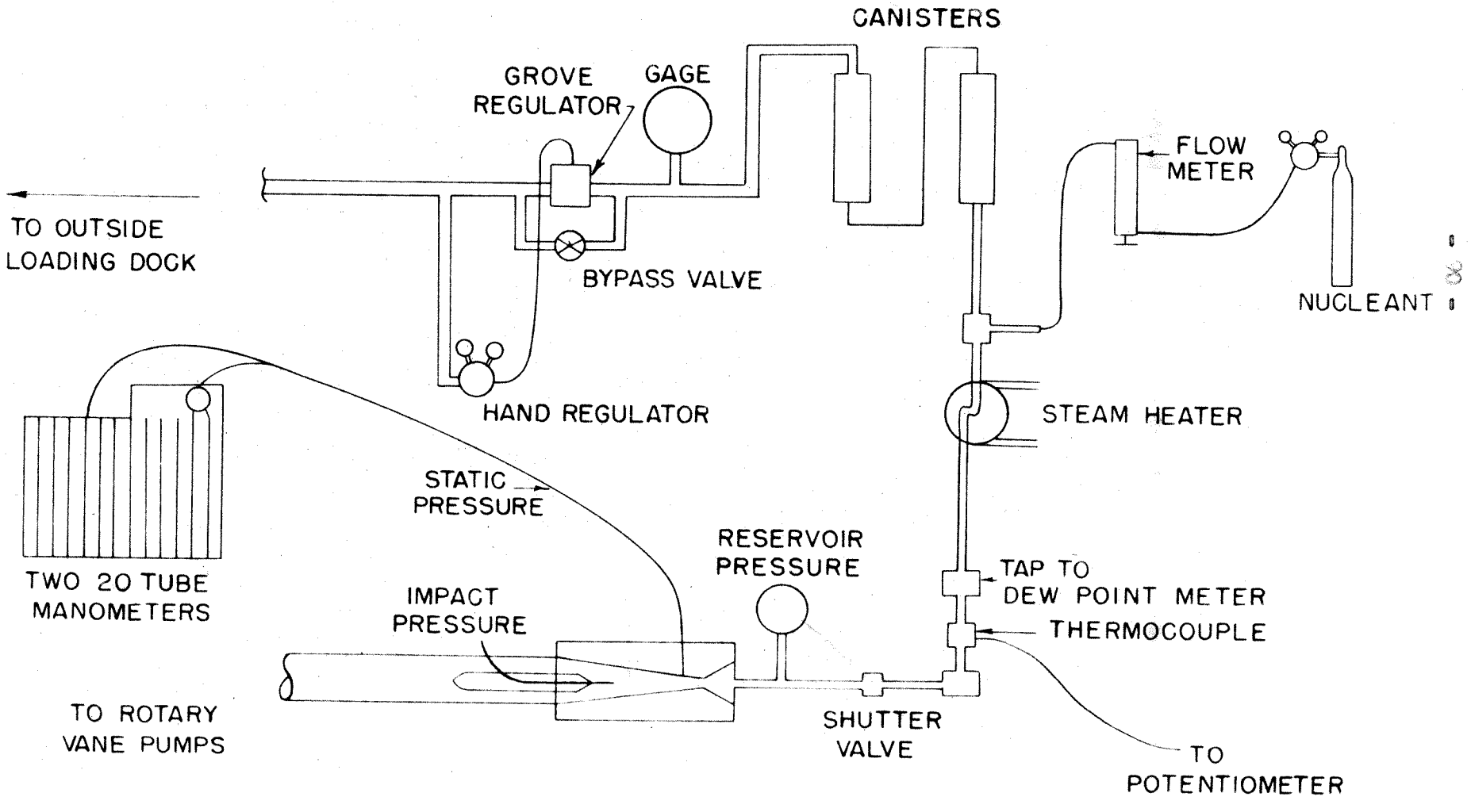

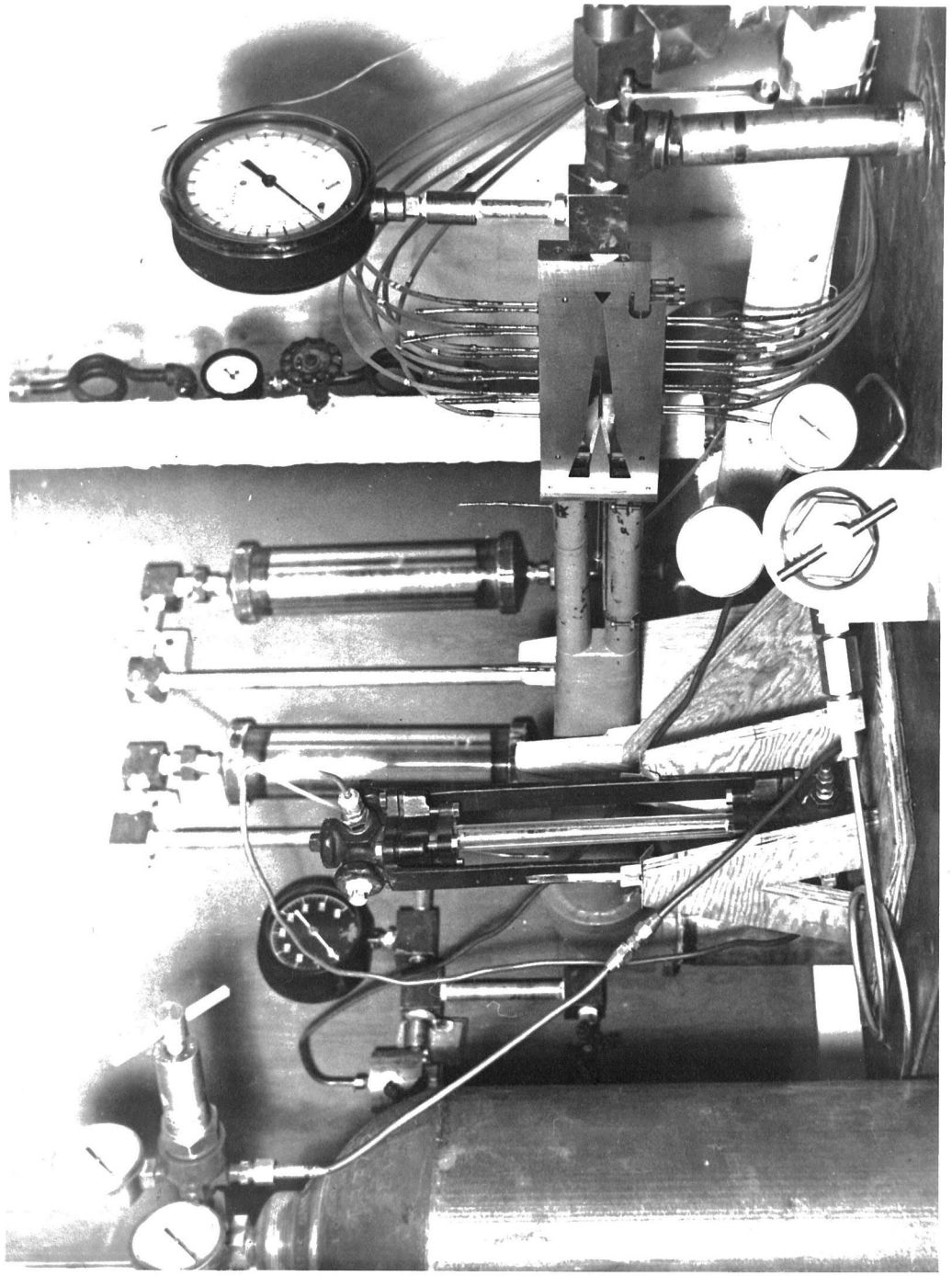

FIG. 2 - PHOTOGRAPH OF TEST EQUIPMENT

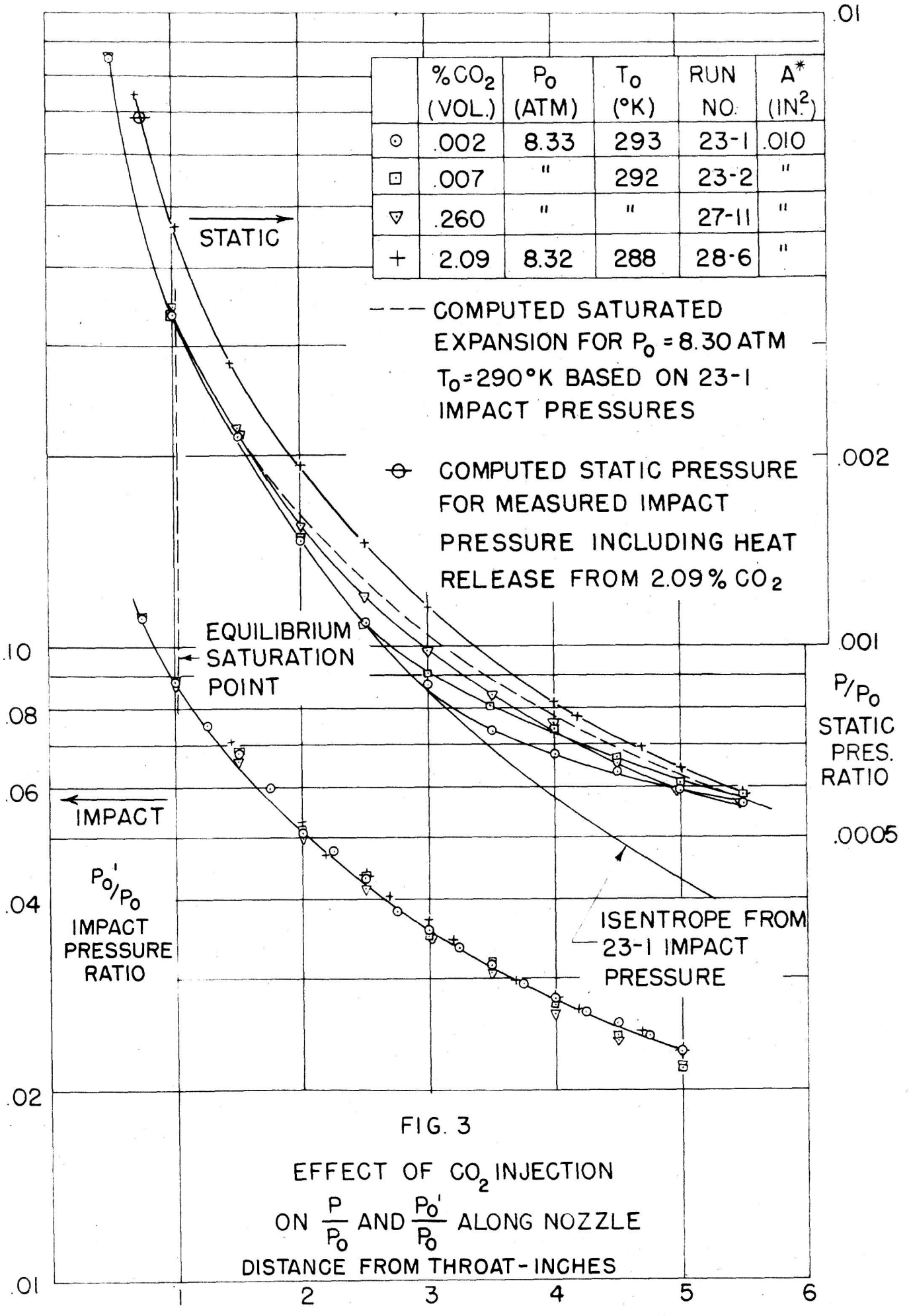

FIG. 3

EFFECT OF CO_2 INJECTION ON $\frac{P}{P_0}$ AND $\frac{P_0'}{P_0}$ ALONG NOZZLE

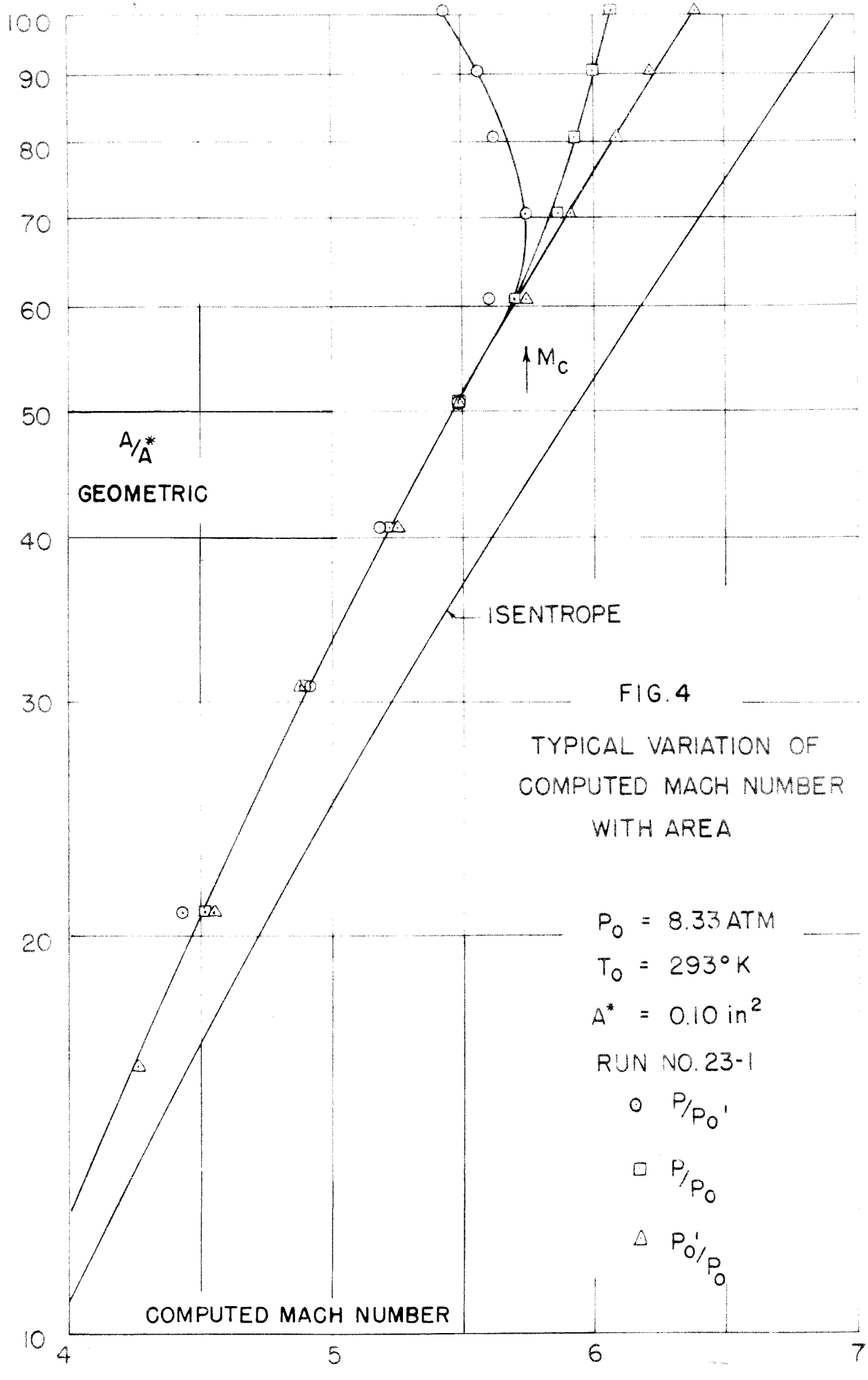

FIG. 4

TYPICAL VARIATION OF COMPUTED MACH NUMBER WITH AREA

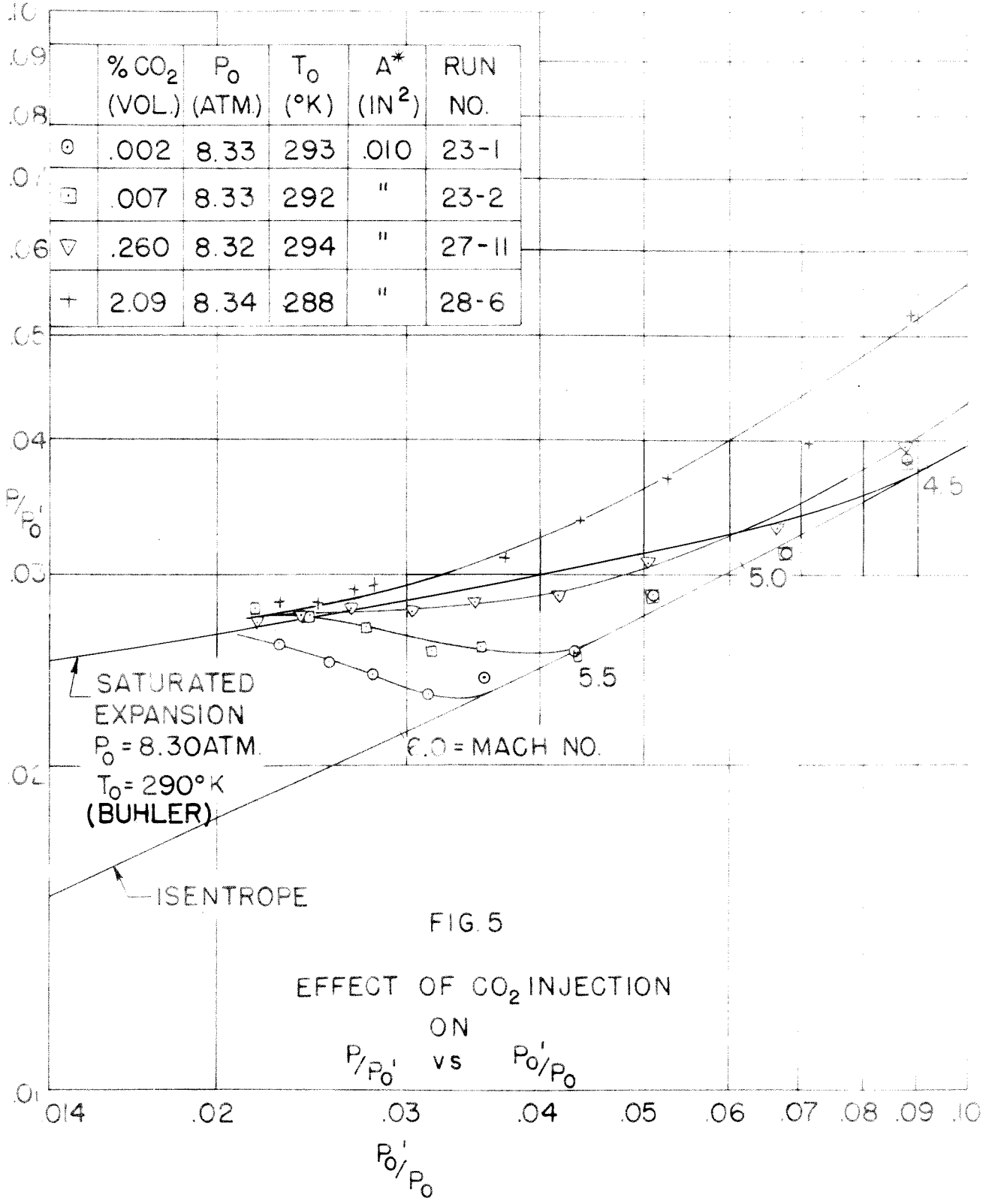

FIG. 5

EFFECT OF CO_2 INJECTION ON P/P_o' vs P_o'/P_o

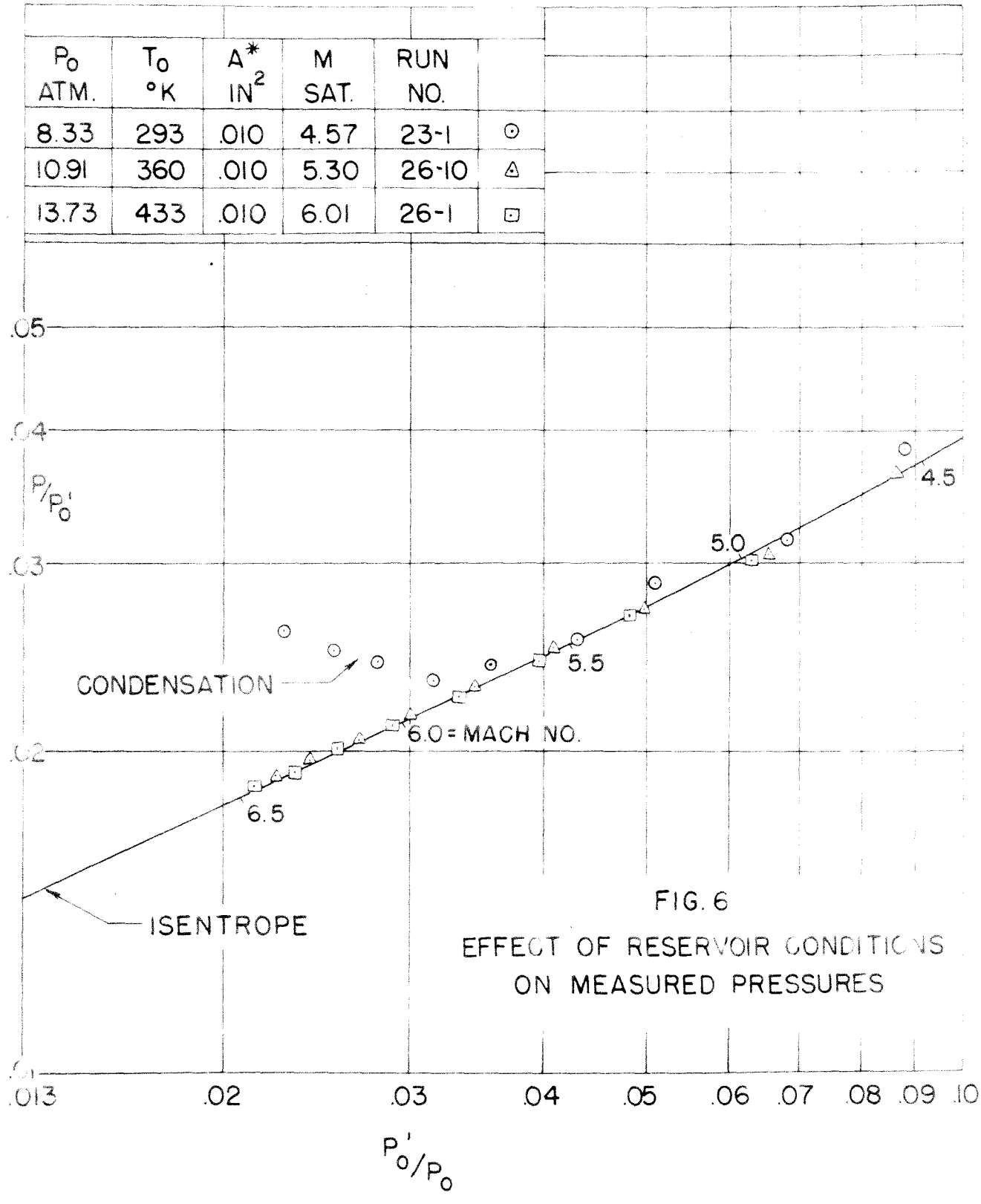

FIG. 6

EFFECT OF RESERVOIR CONDITIONS ON MEASURED PRESSURES

FIG 7

EFFECT OF RESERVOIR CONDITIONS

AT CONSTANT RESERVOIR REYNOLDS NUMBER

	P_o (ATM)	T_o (°K)	A^* $(IN.)^2$	RUN NO.
○	8.33	293	.010	23-1
△	10.91	360	"	26-10
□	13.73	433	"	26-1

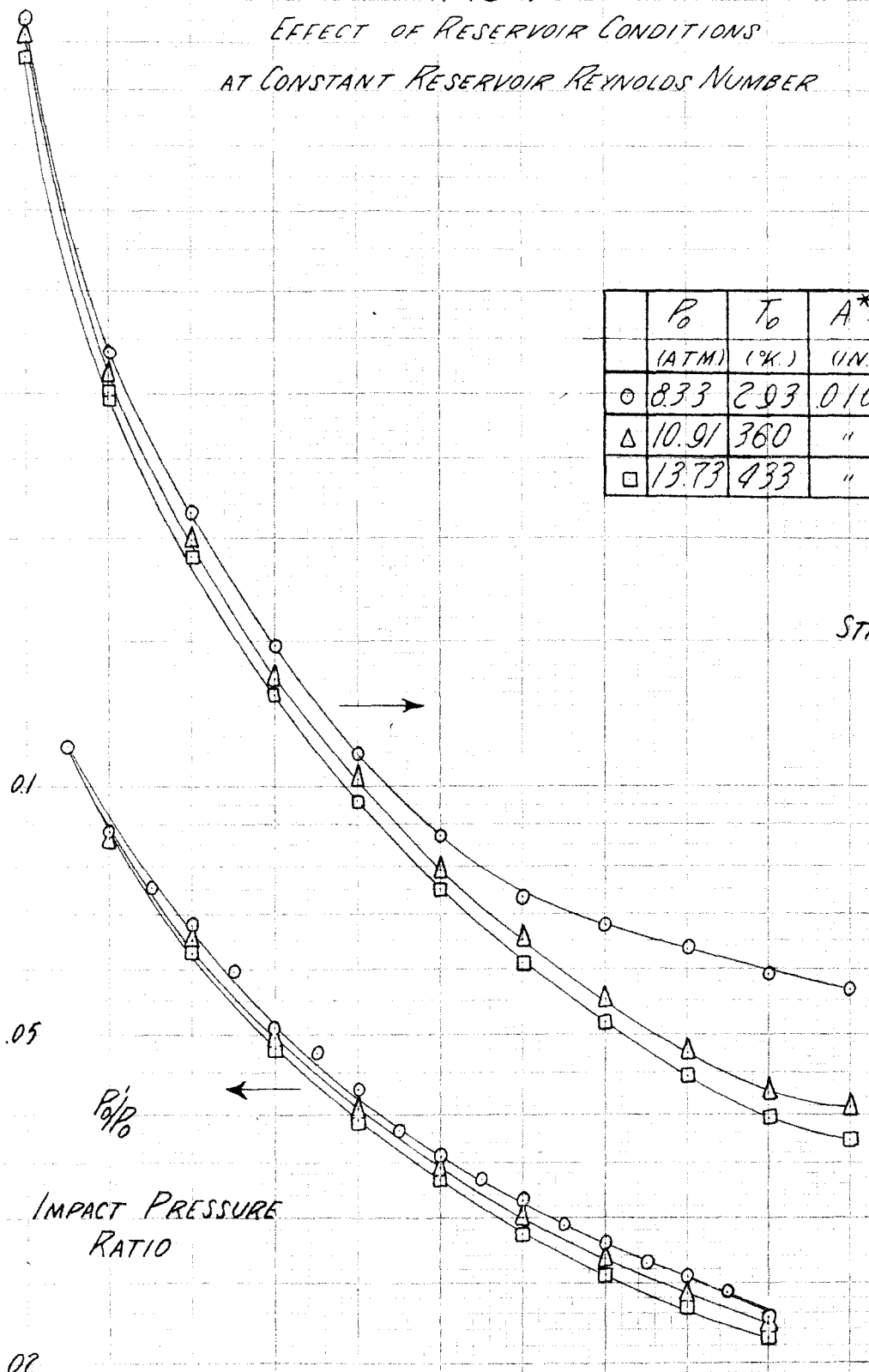

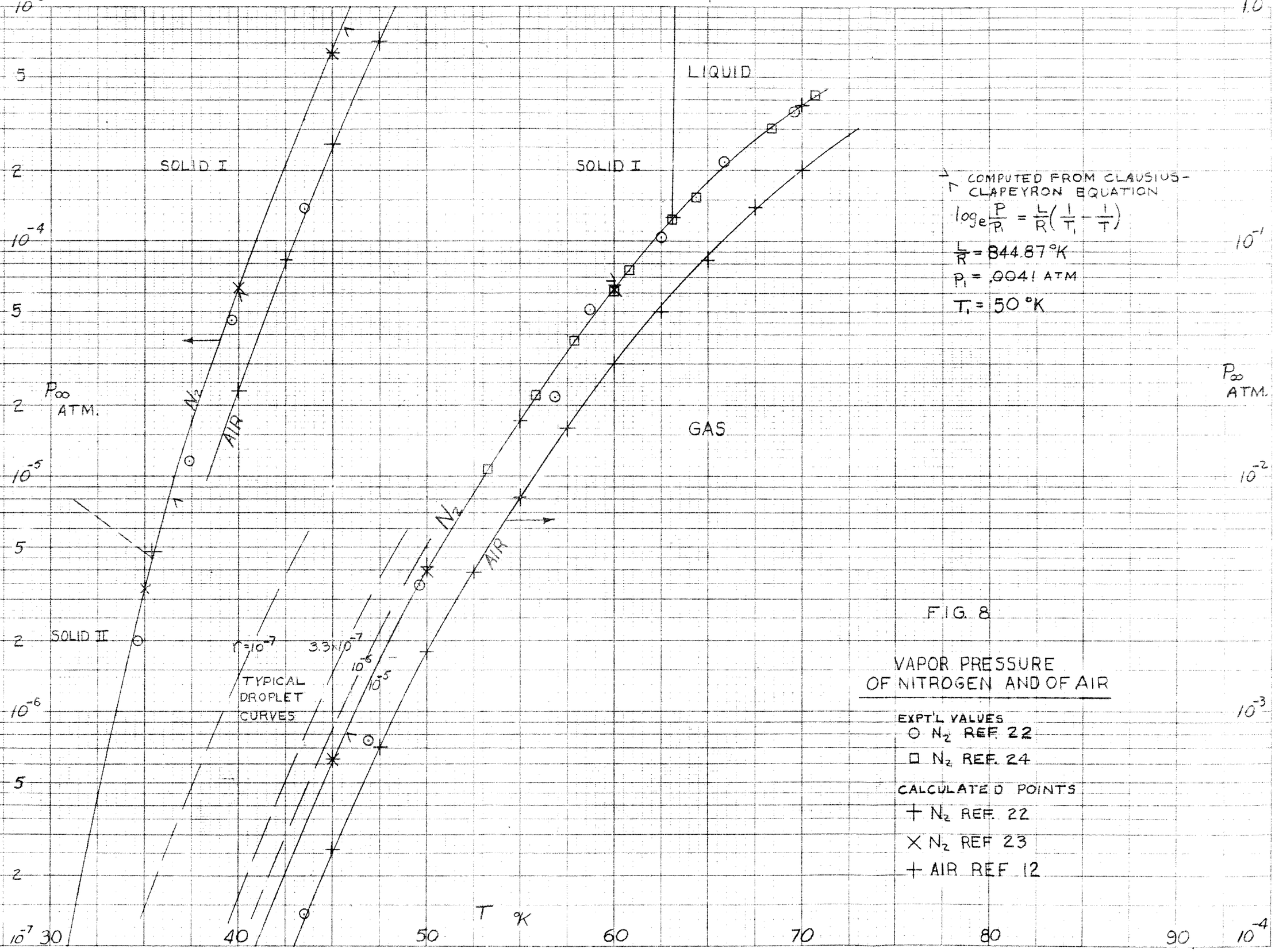

FIG. 8

VAPOR PRESSURE
OF NITROGEN AND OF AIR

EXPT'L VALUES
○ N_2 REF. 22
□ N_2 REF. 24

CALCULATED POINTS
+ N_2 REF. 22
× N_2 REF 23
+ AIR REF 12

FIG. 9
REYNOLDS NUMBER PER CENTIMETER
VS. MACH NUMBER

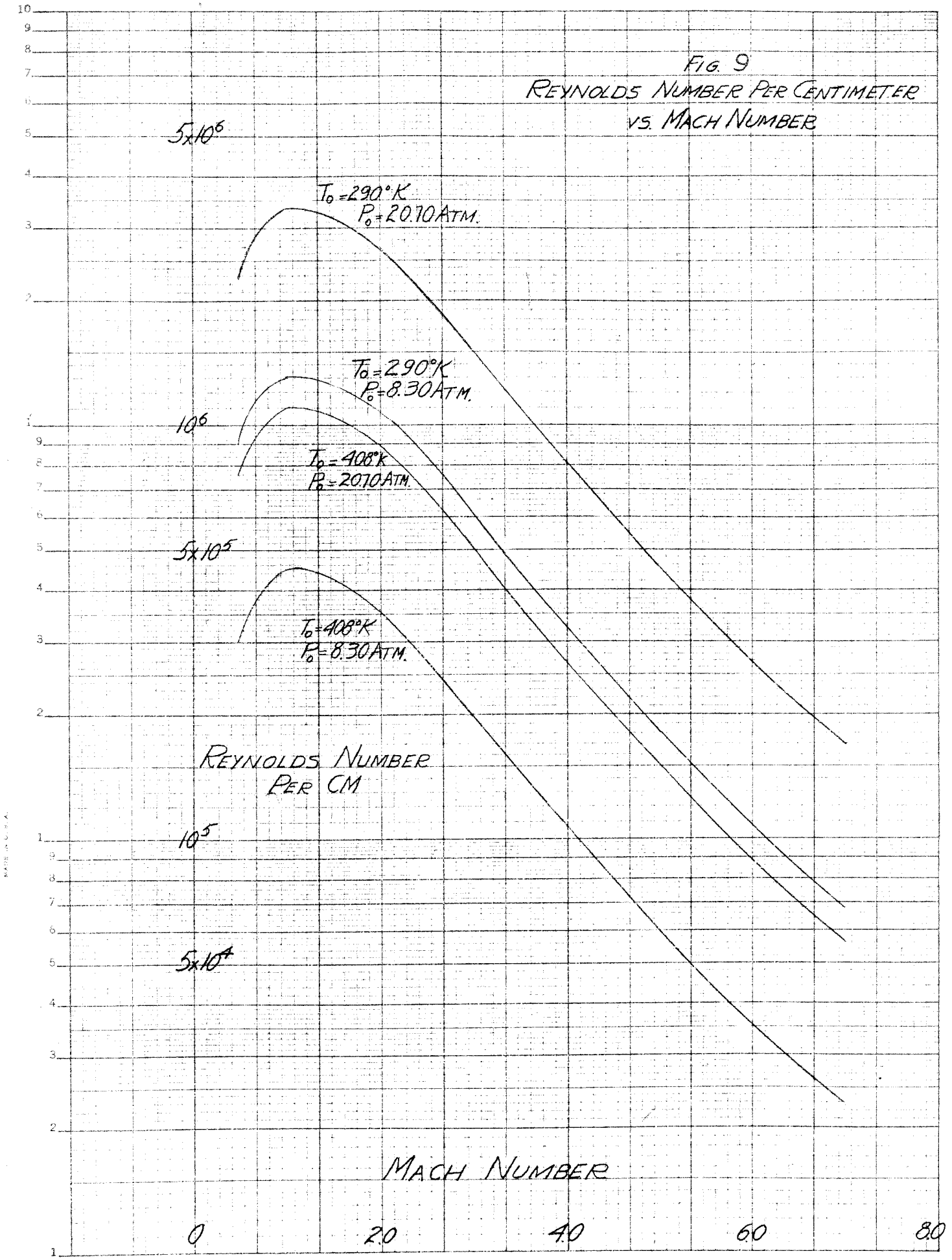

VALIDITY OF A POWER LAW APPROXIMATION FOR THE VISCOSITY OF NITROGEN

FIG 10

SOLID LINE COMPUTED FROM $\frac{\mu}{\mu_1} = \left(\frac{T}{T_1}\right)^{\omega}$

$\omega = 0.76$, $\mu_1 = 1.28 \times 10^{-4} \frac{\text{dyne sec}}{\text{cm}^2}$, $T_1 = 200°K$

o VALUES TABULATED IN TRIBUS AND BOELTER REF. 26

Δ LANDHOLT - BÖRNSTEIN REF. 27

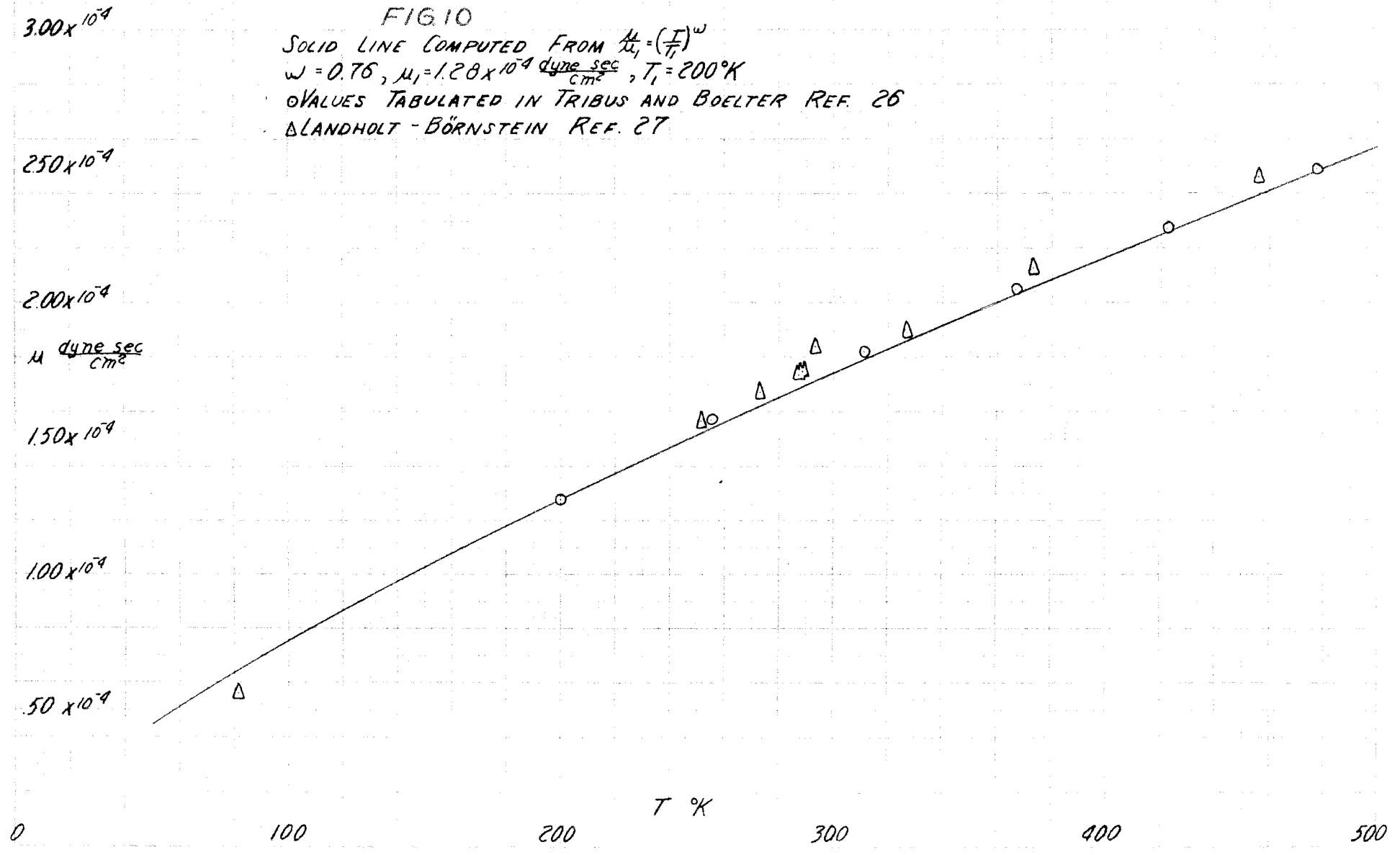

AGREEMENT BETWEEN CENTERLINE AND WALL STATIC PRESSURES

FIG. 11

P_0-ATM.	T_0-°K	A^*-IN.^{2}	RUN No.
4.14	289	.010	28-23

○ STATIC PROBE ON CENTERLINE

□ ORIFICES ON DIVERGING WALLS

△ ORIFICES ON SIDE WALL

NOTE - FLOW BREAKDOWN FELT FURTHER UPSTREAM ON PROBE

STATIC PRESSURE RATIO P/P_0

.010
.009
.008
.007
.006
.005
.004
.003
.002
.001
.0009
.0008
.0007
.0006
.0005
.0004
.0003
.0002
.0001

○ PROBE

△ WALLS

STATIC PRESSURE PROBE DIMENSIONS

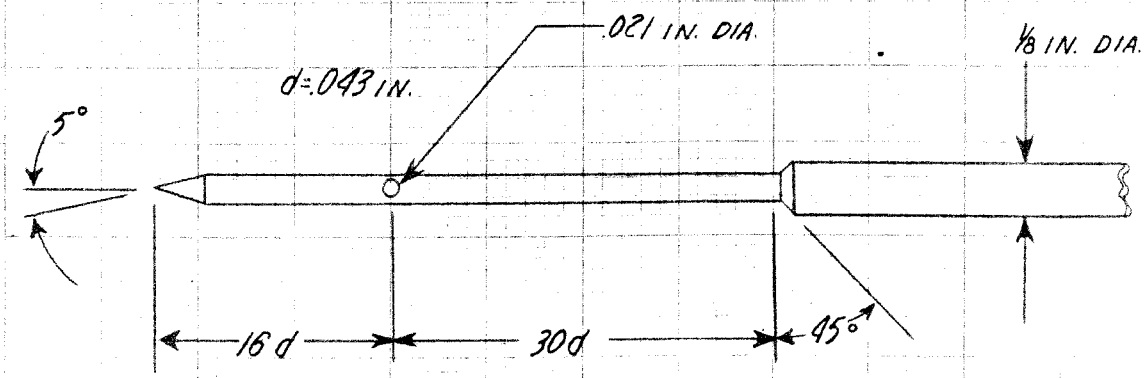

X (INCHES FROM THROAT)

0 1 2 3 4 5 6

BOUNDARY LAYER GROWTH IN THE 1" TUNNEL
AT EQUAL RESERVOIR REYNOLDS NUMBERS.
THE NOZZLE IS A TWO-DIMENSIONAL WEDGE
EXPANDING LINEARLY TO $\left[\frac{A}{A^*}\right]_{GEOM.} = 100.6$ AT X=5"

FIG. 12

$$\left[\frac{A}{A^*}\right]_{BOUNDARY\ LAYER} = \left[\frac{A}{A^*}\right]_{GEOM.} - \frac{A}{A^*}\left(\frac{P_0'}{P_0}\right)$$

	P_0 (ATM.)	T_0 (°K.)	A^* (IN.)^2	RUN NO.
○	8.33	293	.010	23-1
△	10.91	360	"	26-10
□	13.73	433	"	26-1

30
20
10

DISTANCE FROM THROAT, INCHES

½ 1 2 3 4 5 5½

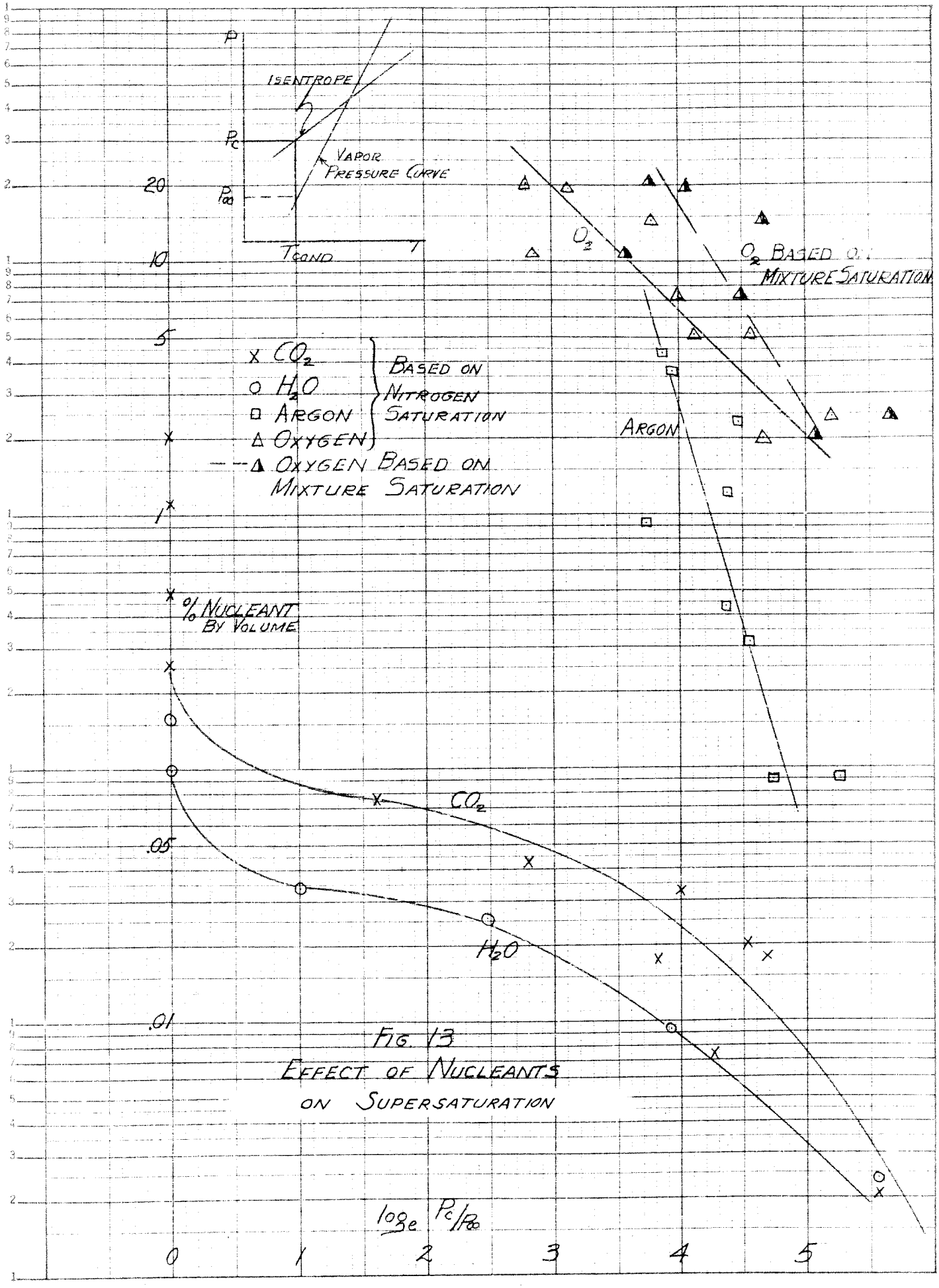

FIG. 13

EFFECT OF NUCLEANTS ON SUPERSATURATION

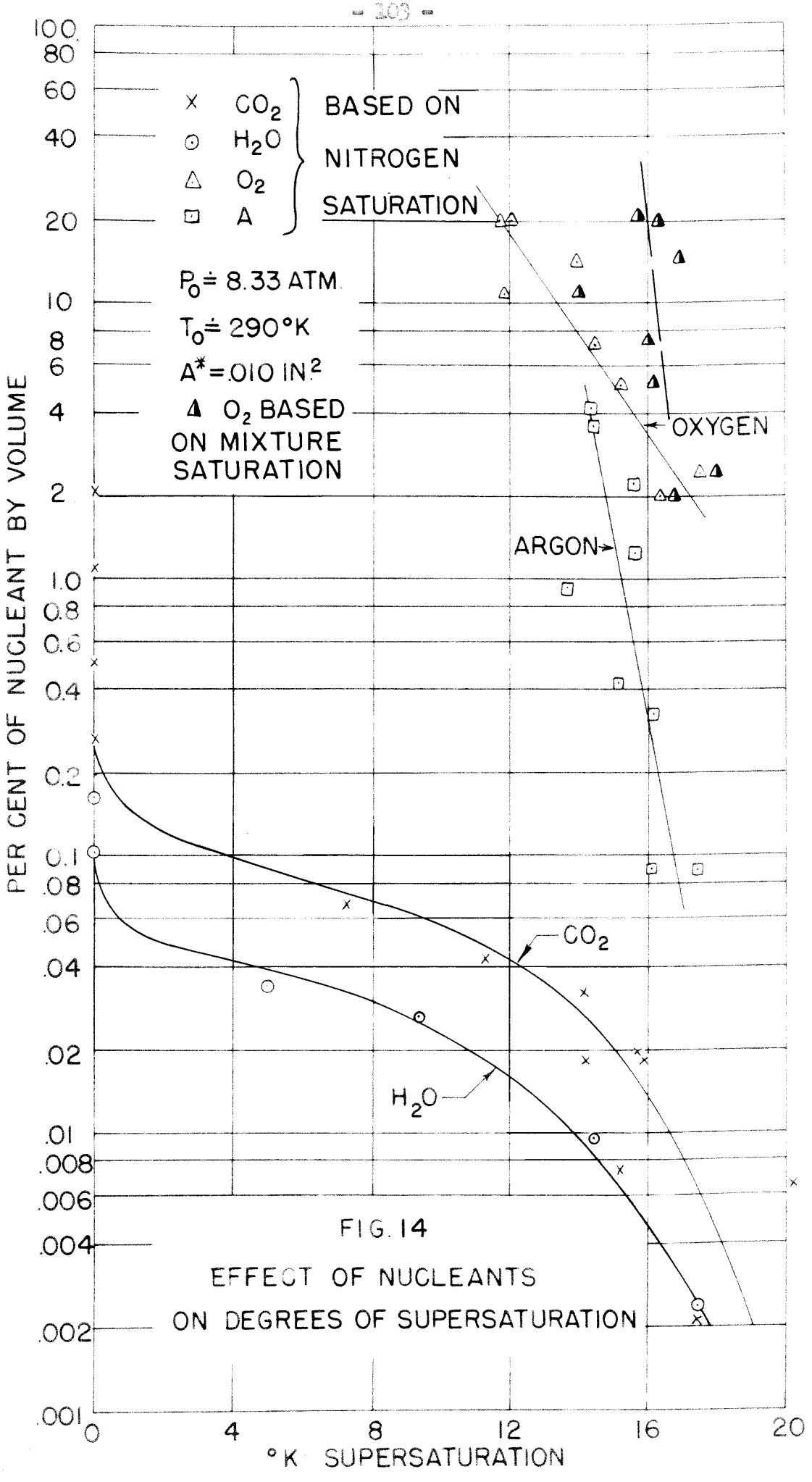

FIG. 14

EFFECT OF NUCLEANTS ON DEGREES OF SUPERSATURATION

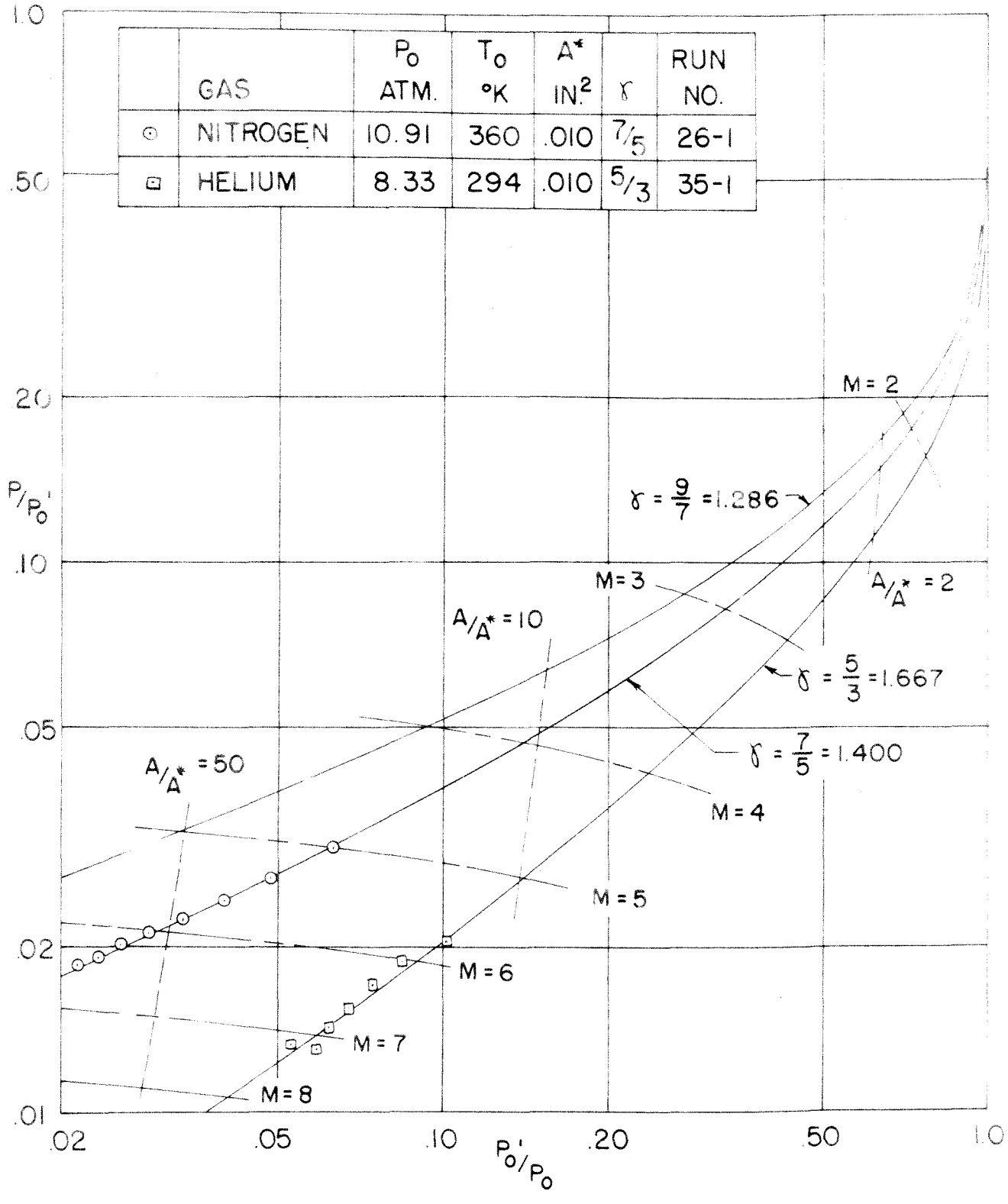

FIG. 15

ISENTROPES FOR VARIOUS VALUES OF SPECIFIC HEAT RATIO $\gamma = \frac{C_p}{C_v}$

FIG. 16

EFFECT OF CO_2 ADDITION ON MEASURED PRESSURE

	% CO_2 VOLUME	P_o ATM.	T_o °K	RUN No.
⊙	—	8.33	290	34-1
Q	4.004	8.33	295	27-1
○	.002	8.33	293	23-1
□	.007	8.33	293	23-2
△	.018	8.33	293	23-4
▽	.043	8.33	293	23-5
+	.067	8.33	293	23-3

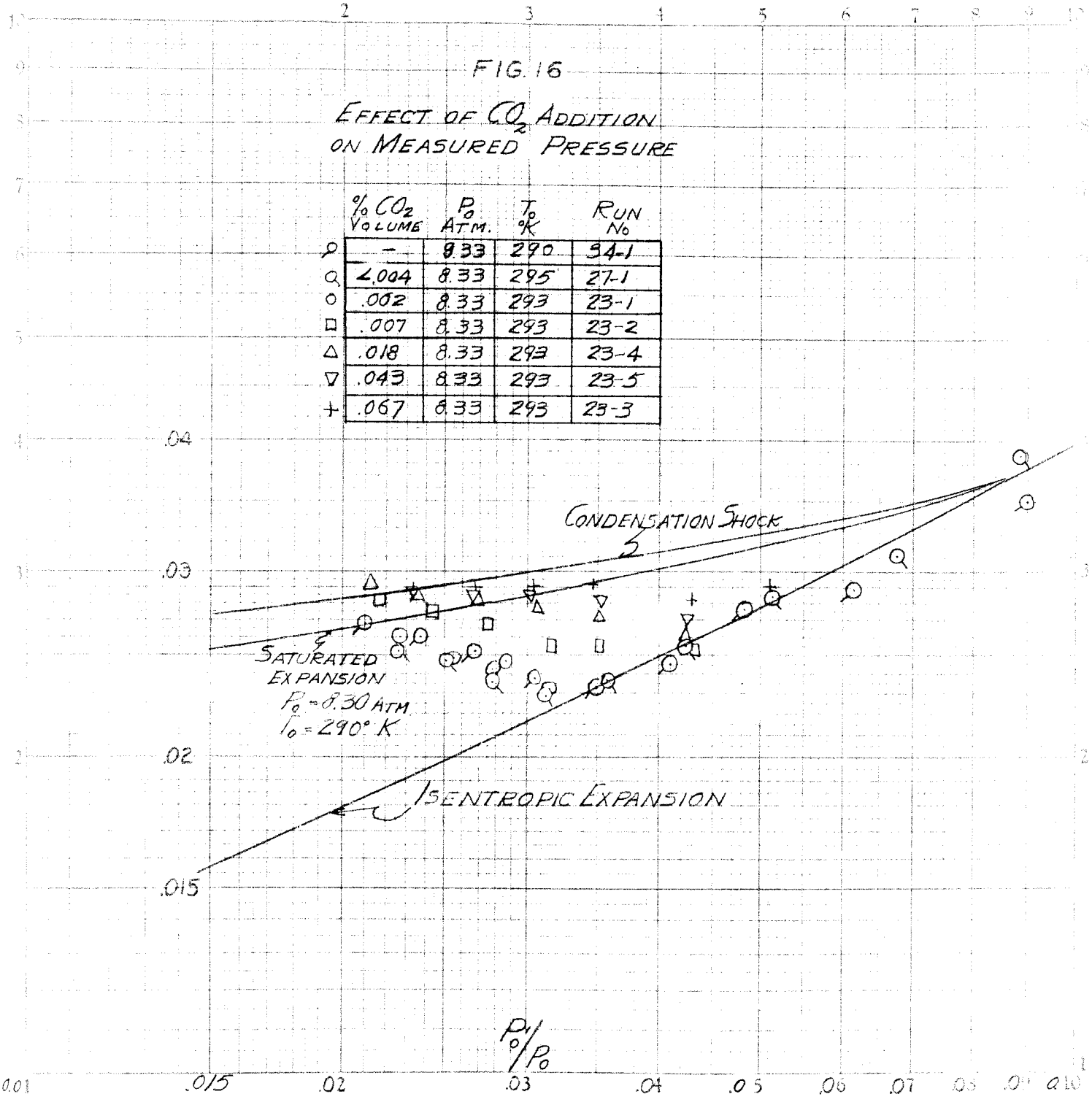

EFFECT OF WATER ADDITION ON IMPACT AND STATIC PRESSURES

FIG. 17

P_o''/P_o & P/P_o vs X

	% Water Volume	P_o Atm.	T_o °K	A^* In.²	Run No.
⊙	.002	8.35	293	.010	23-1
⊡	.009	8.34	293	.010	25-4
▽	.026	8.32	293	.010	25-1
+	.16	8.34	289	.010	25-5

STATIC PRESSURE RATIO P/P_o

IMPACT PRESSURE RATIO P_o'/P_o

DISTANCE FROM THROAT - INCHES

.5 1 2 3 4 5 6 7

.01 .005 .002 .001 .0005

.10 .05 .02

10 9 8 7 6 5 4 3 2 1

FIG. 18
EFFECT OF WATER ADDITION ON MEASURED PRESSURES
P_0'/P_0 VS. P/P_0'

	% WATER VOLUME	P_0 ATM.	T_0 °K	A^* IN.^{2}	RUN NO.
○	.002	8.35	293	.010	23-1
□	.009	8.34	293	.010	25-4
▽	.026	8.32	293	.010	25-1
+	.16	8.34	289	.010	25-5

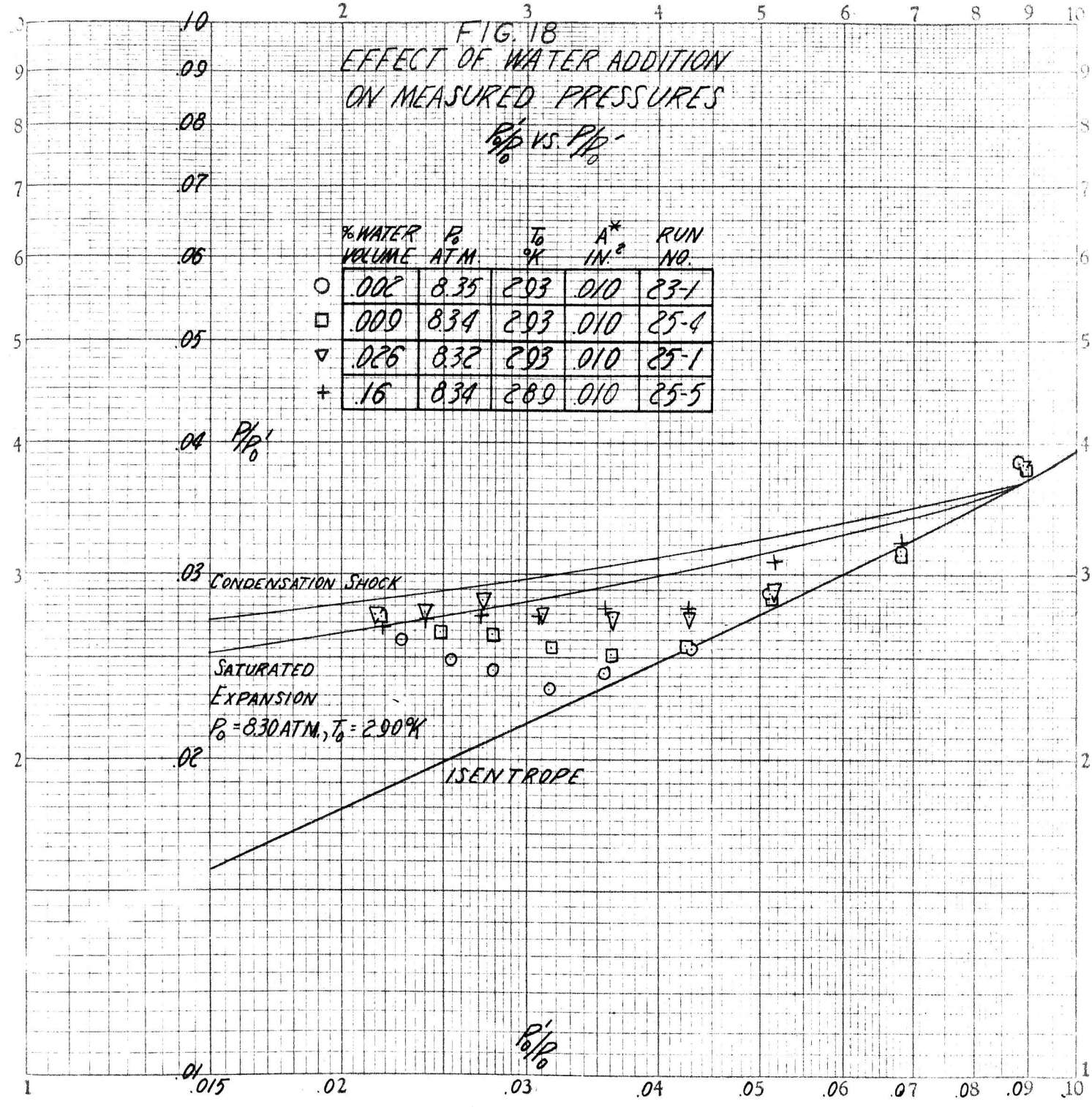

FIG. 19
EFFECT OF O_2 INJECTION
P_0'/P_0, P/P_0 ALONG NOZZLE

	$\%O_2$ VOLUME	P_0 ATM.	T_0 °K	A^* IN^2	RUN NO.
○	2.45	8.33	289	.010	31-3
□	7.35	"	290	"	31-4
△	14.6	8.32	288	"	31-1
▽	20.3	"	285	"	31-2

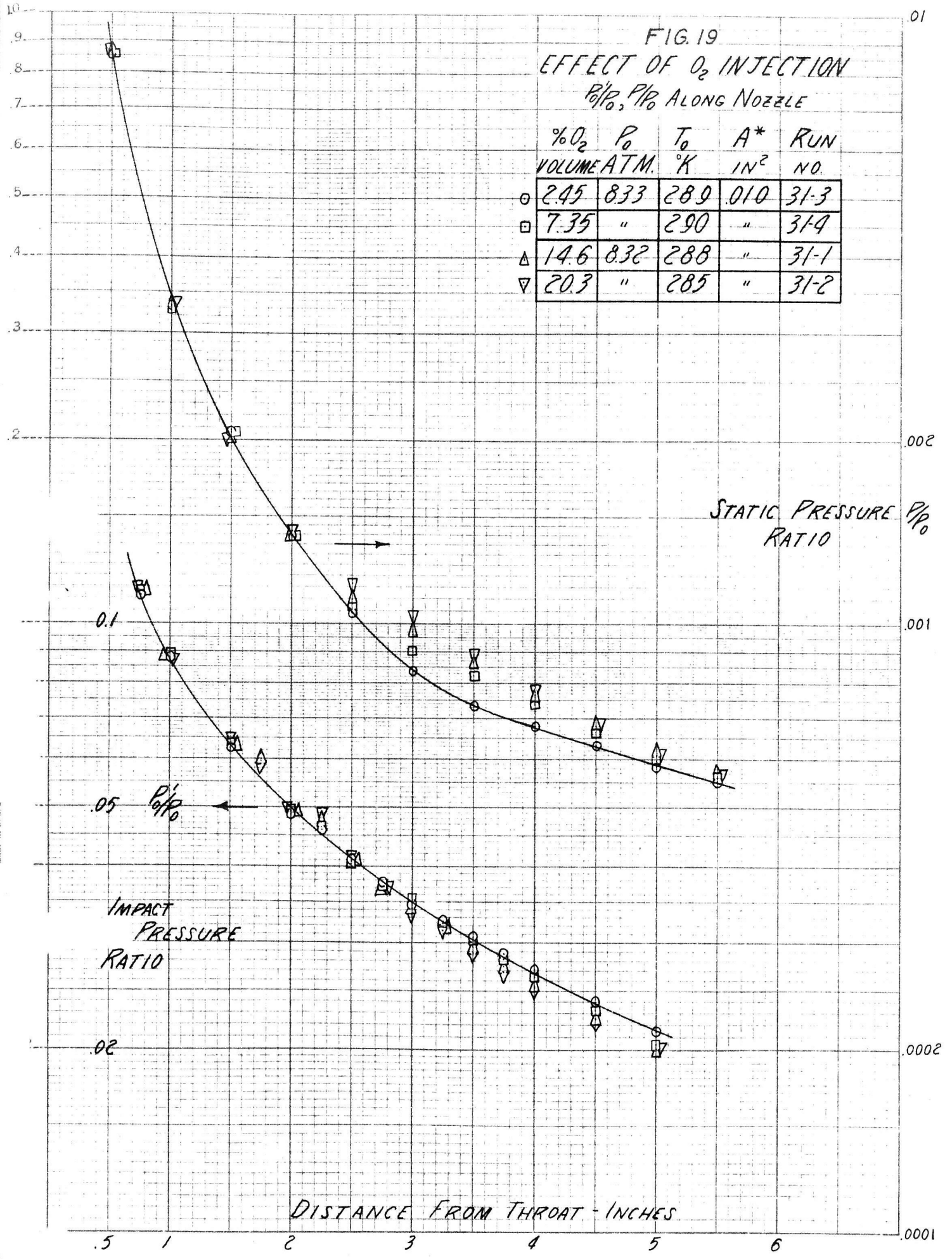

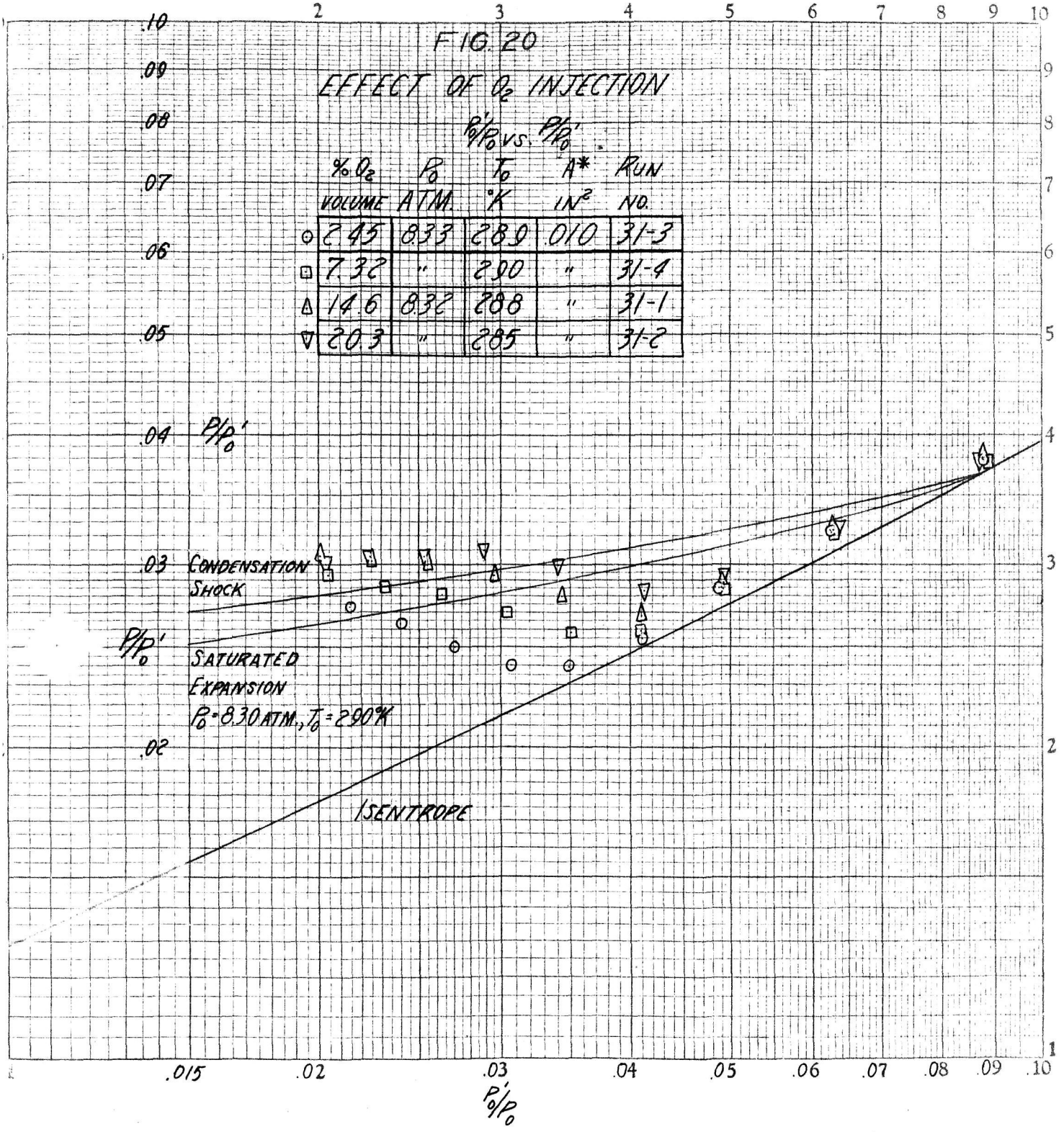
FIG. 20
EFFECT OF O_2 INJECTION
P_0'/P_0 VS. P/P_0'
% O_2 VOLUME
P_0 ATM.
T_0 °K
A^* IN²
RUN NO.
2.45 | 8.33 | 289 | .010 | 31-3
7.32 | " | 290 | " | 31-4
14.6 | 8.32 | 288 | " | 31-1
20.3 | " | 285 | " | 31-2
P/P_0'
CONDENSATION SHOCK
P/P_0'
SATURATED EXPANSION
P_0=8.30 ATM., T_0=290°K
ISENTROPE
P_0'/P_0

FIG. 21

EFFECT OF ARGON INJECTION

P_0'/P_0, P/P_0 ALONG NOZZLE

	%A VOLUME	P_0 ATM.	T_0 °K	A^* IN^2	RUN NO.
⊙	.09	8.33	292	.010	36-1
□	.31	"	287	"	36-2
△	1.2	"	286	"	36-3
▽	4.3	"	285	"	36-4

STATIC PRESSURE RATIO P/P_0

IMPACT PRESSURE RATIO P_0'/P_0

DISTANCE FROM THROAT - INCHES

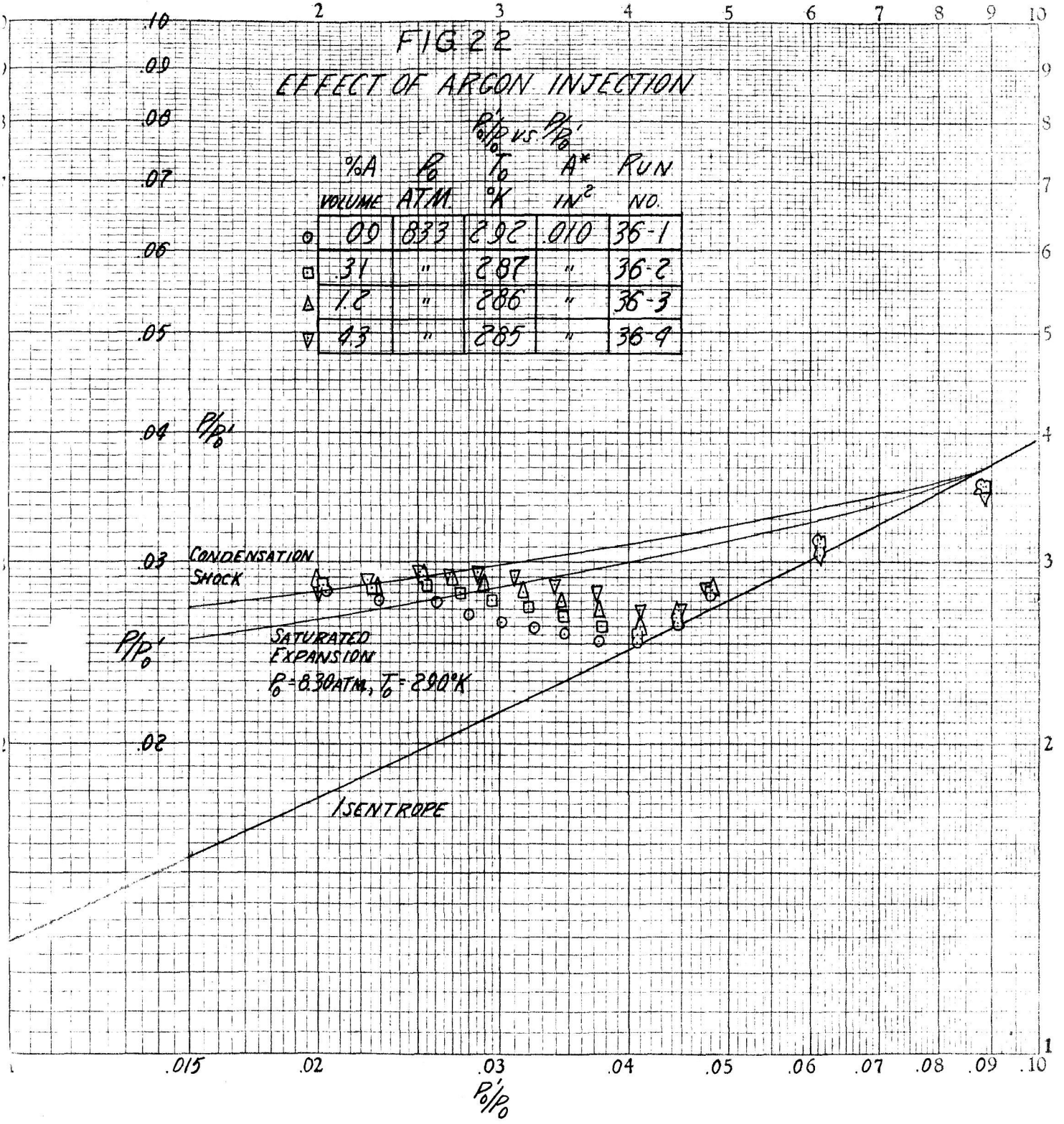
FIG 22
EFFECT OF ARGON INJECTION
P_0'/P_0 vs. P/P_0'
%A VOLUME
P_0 ATM.
T_0 °K
A* IN²
RUN NO.
○ 09 833 292 .010 36-1
□ .31 " 287 " 36-2
△ 1.2 " 286 " 36-3
▽ 4.3 " 285 " 36-4
P/P_0'
CONDENSATION SHOCK
SATURATED EXPANSION
P_0=8.30ATM, T_0=290°K
ISENTROPE
P_0'/P_0

FLOW MACH NUMBER FOR ADDITIVE SATURATION

FIG. 23

$P_0 = 8.33$ ATM.
$T_0 = 290$ °K
$A^* = .010$ IN.^{2}

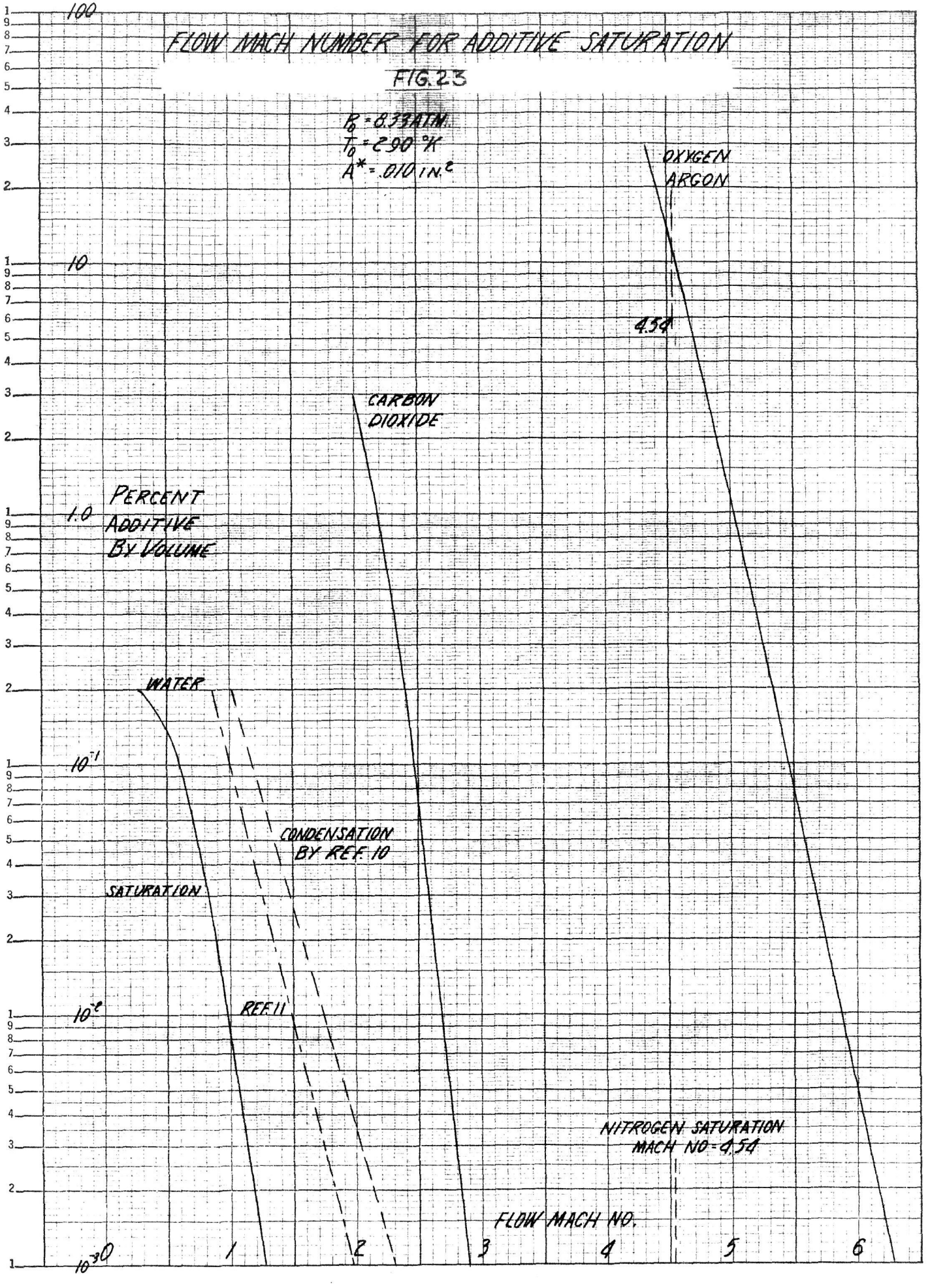

FIG. 24

EFFECTS OF RESERVOIR CONDITIONS ON $P/P_{0'}$ VS. $P_{0'}/P_0$

	T_0 °K	P_0 ATM.	RUN No.
○	295	4.15	37-5
□	285	16.63	39-3
△	284	20.71	40-1
▽	330	20.72	40-2

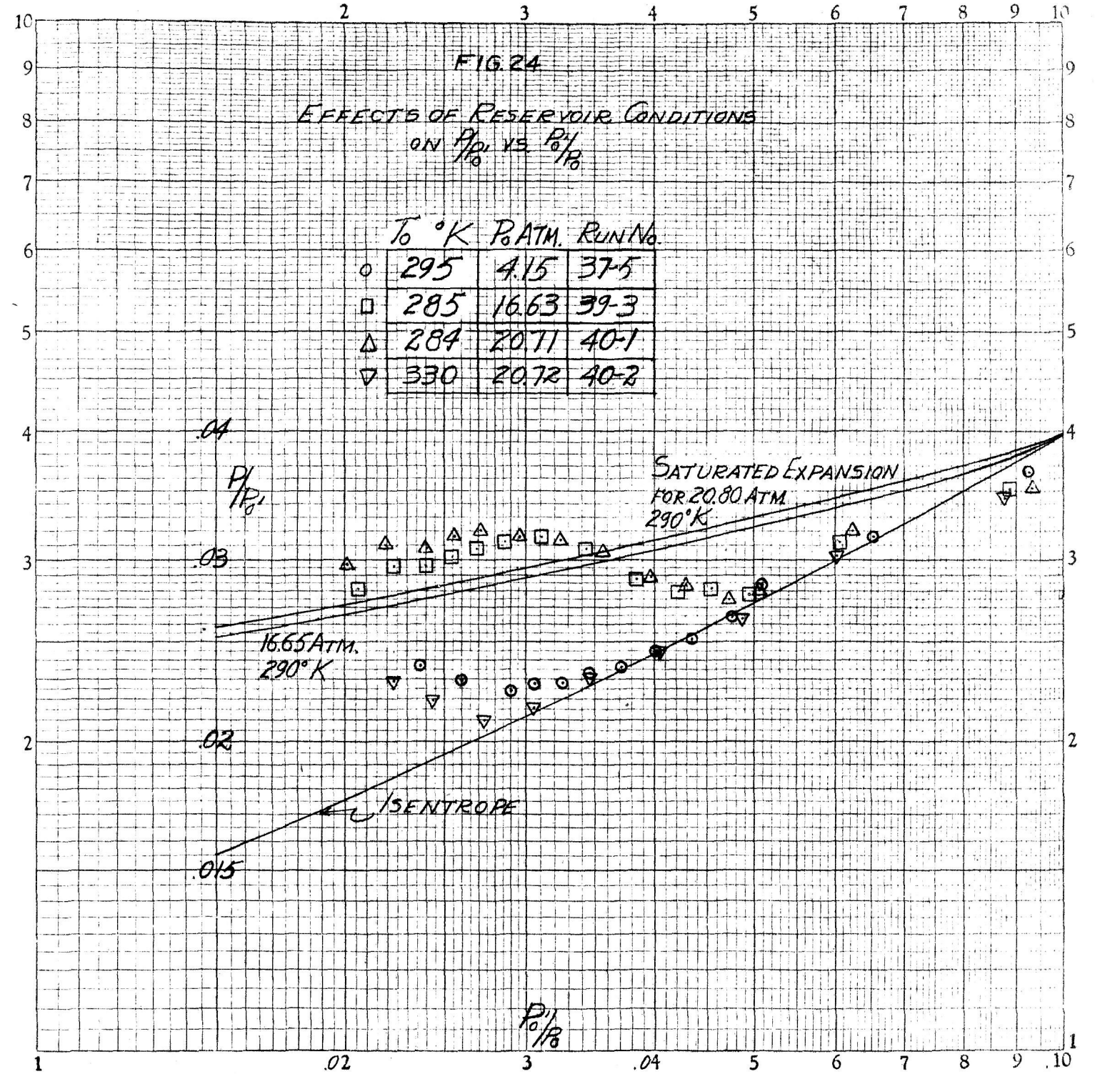

FIG. 25
EFFECTS OF RESERVOIR PRESSURE AND TEMPERATURE ON SATURATION MACH NUMBER OF NITROGEN
(REF. 23, 24 & 25)

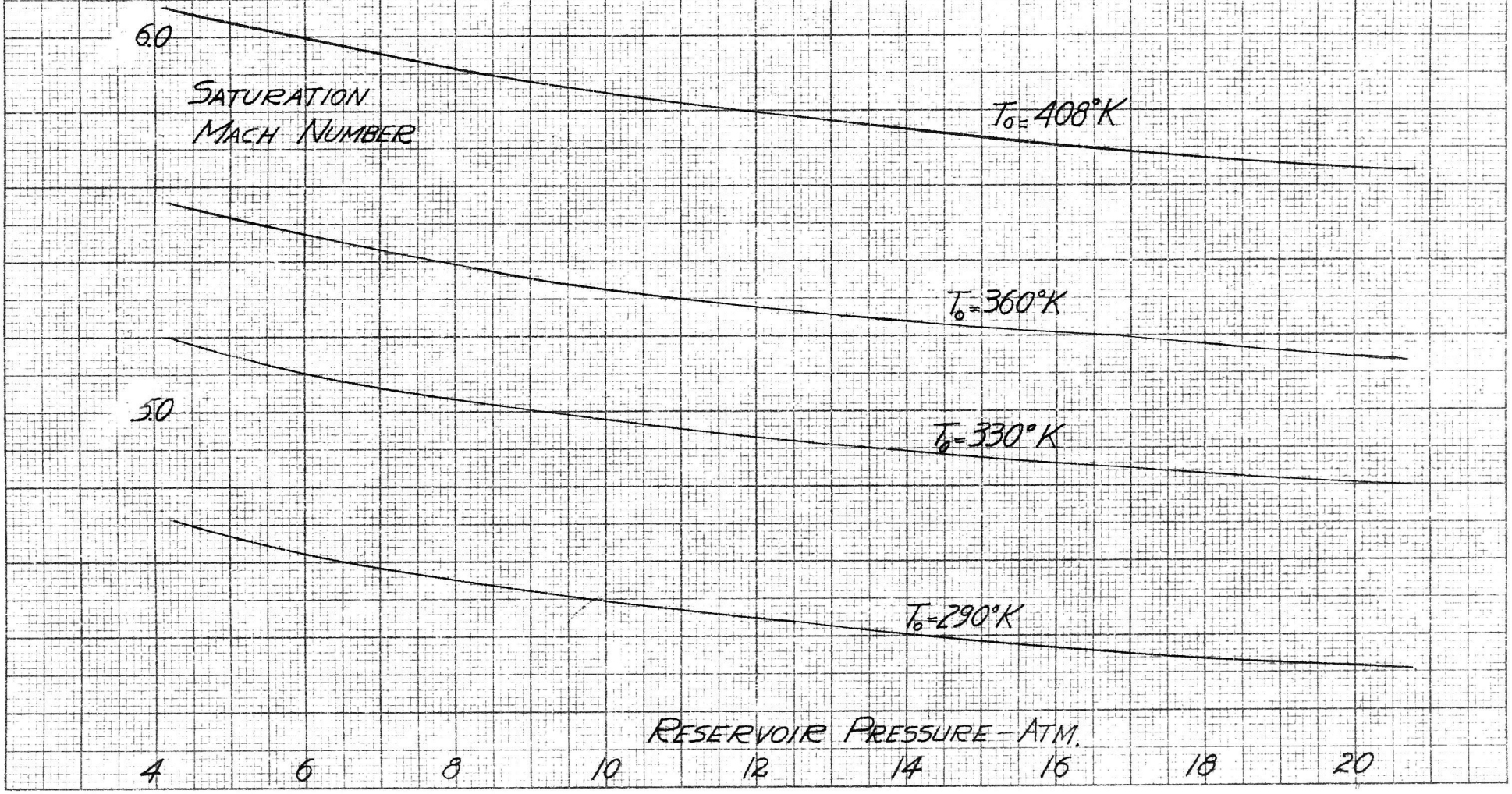

FIG. 26

EFFECTS OF RESERVOIR PRESSURE AND TEMPERATURE ON CONDENSATION MACH NUMBER OF NITROGEN

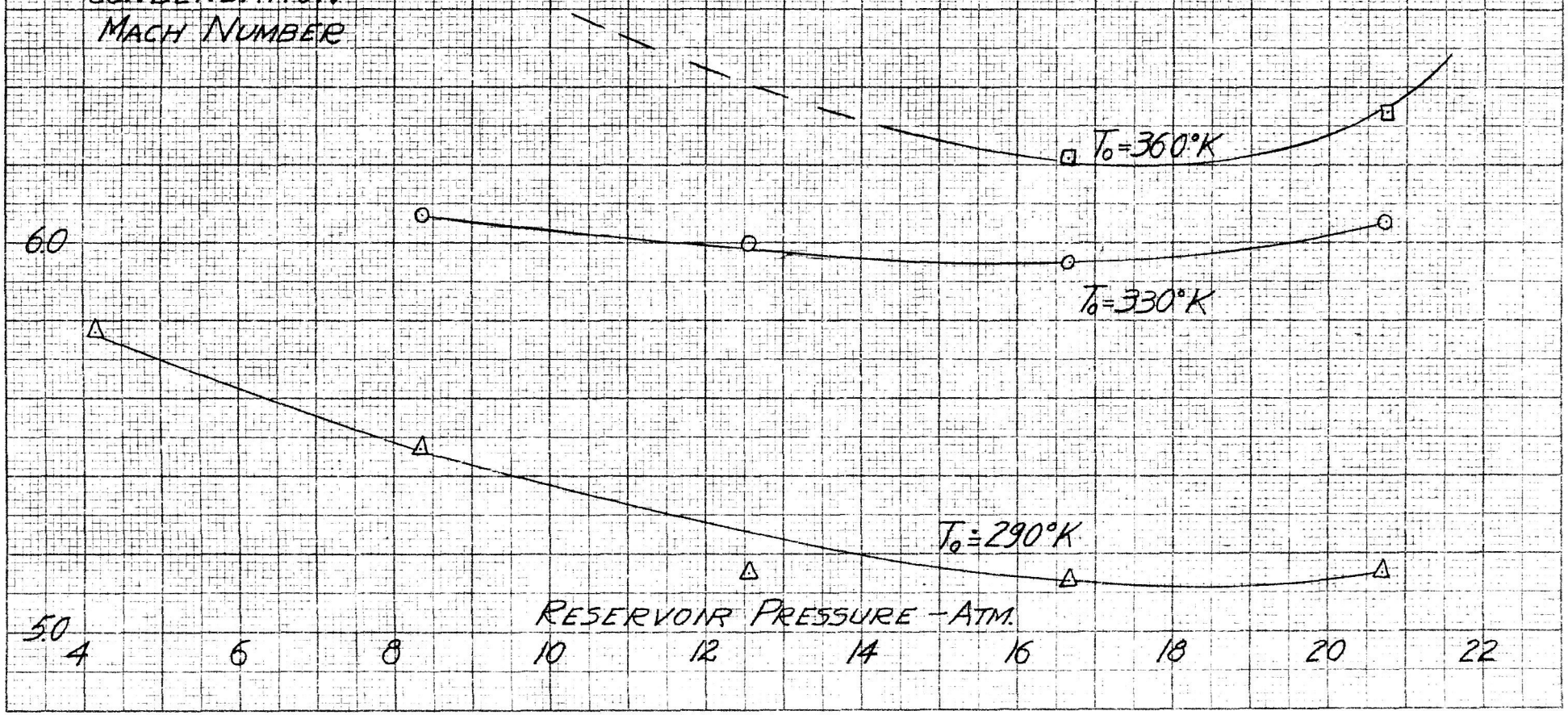

FIG. 27

EFFECTS OF RESERVOIR PRESSURE AND TEMPERATURE ON SUPERSATURATION TEMPERATURE OF NITROGEN

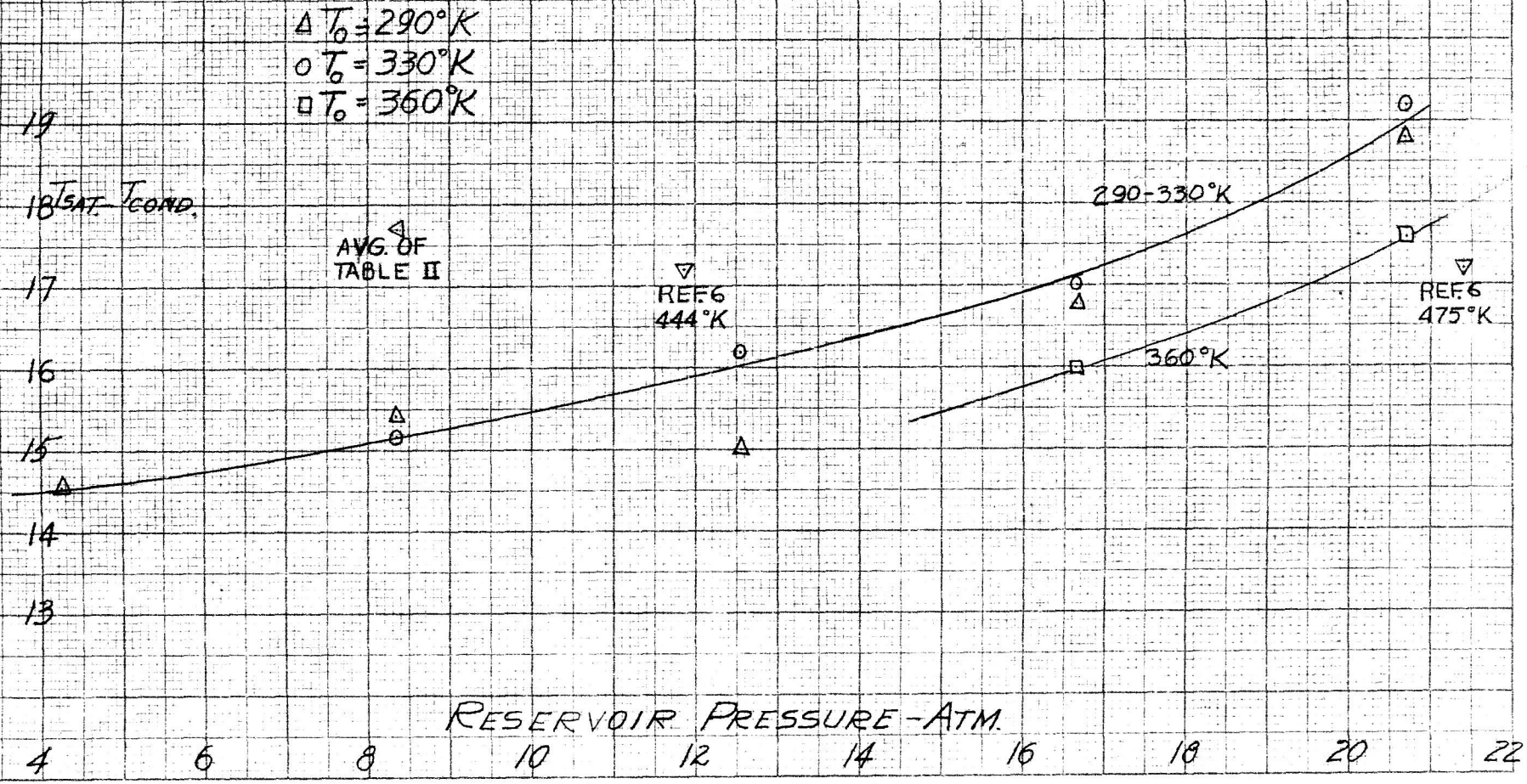

MEASURED IMPACT PRESSURE DEFICIT AS A FUNCTION OF ADDITIVE CONCENTRATION

FIG. 28

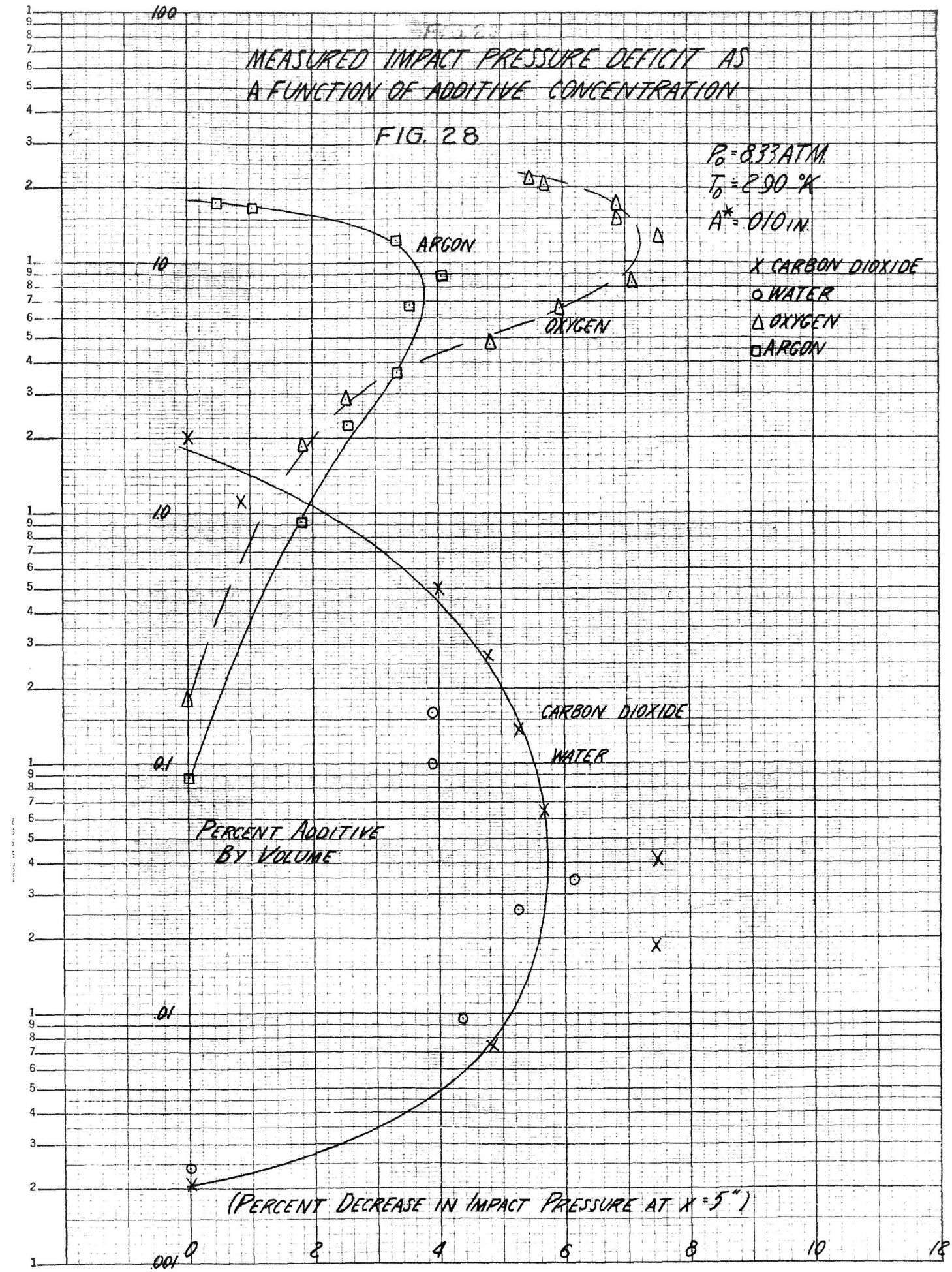

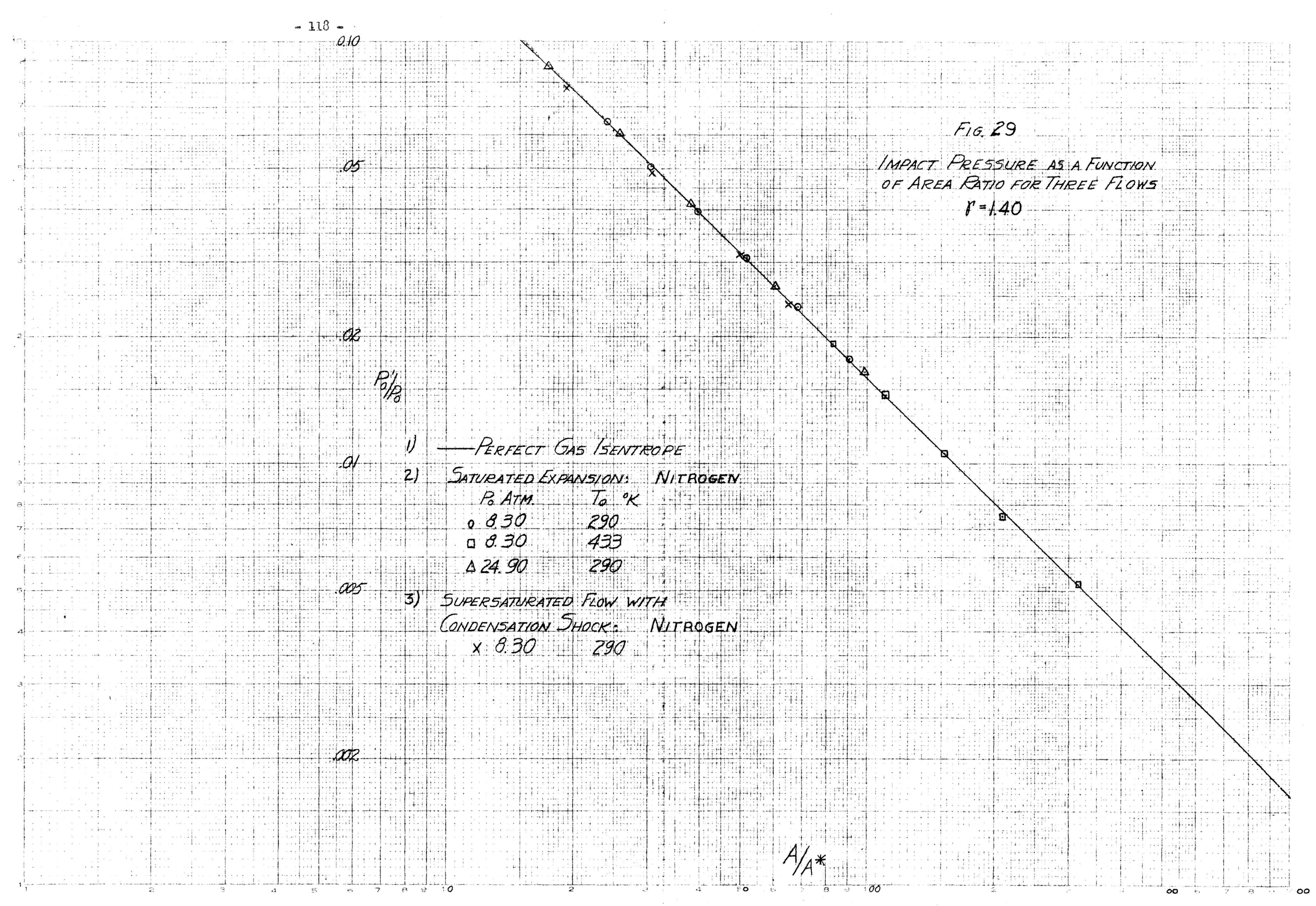

FIG. 29

IMPACT PRESSURE AS A FUNCTION OF AREA RATIO FOR THREE FLOWS

$\gamma = 1.40$

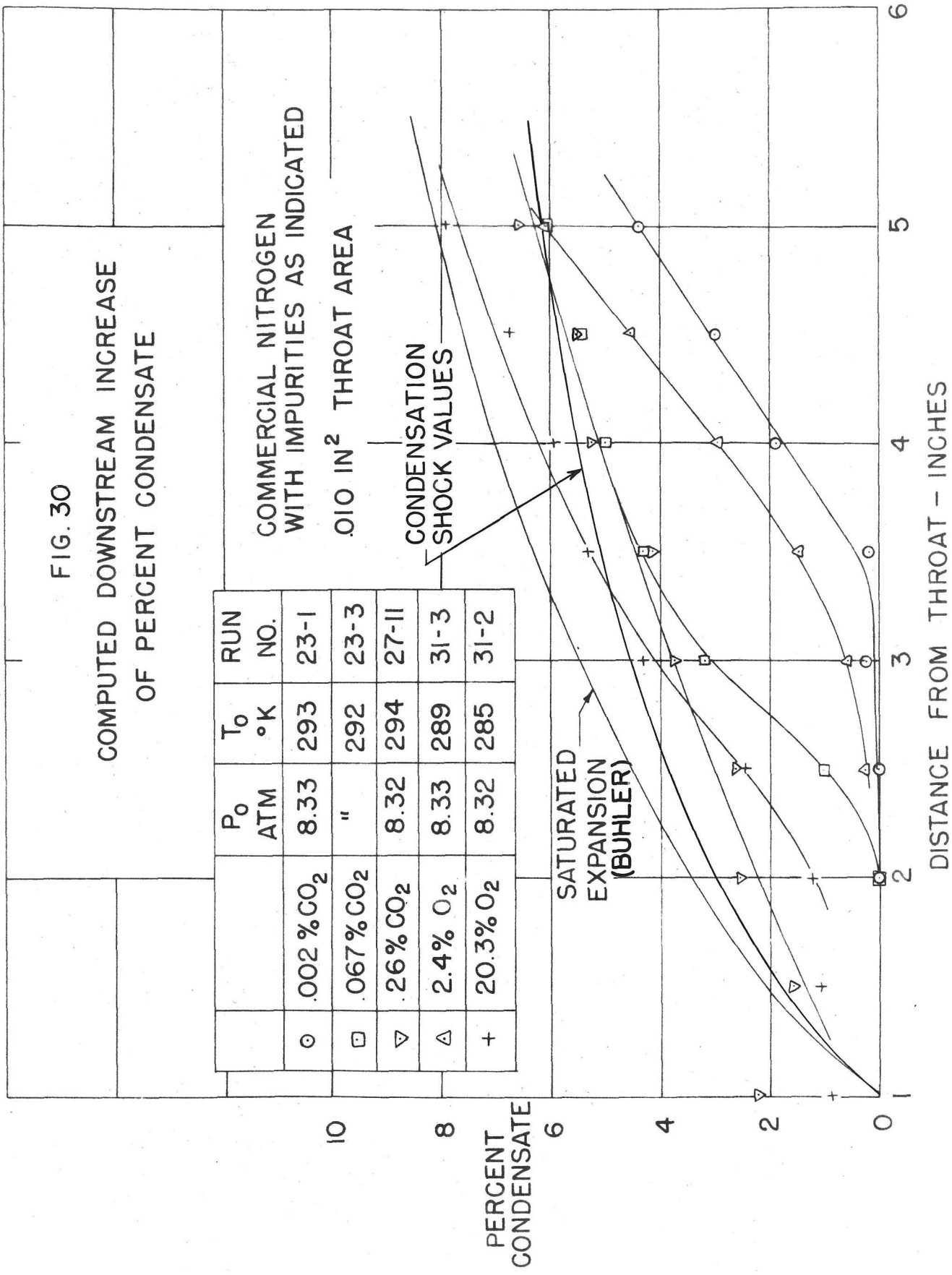

		P_o ATM	T_o °K	RUN NO.
⊙	.002 % CO_2	8.33	293	23-1
⊡	.067 % CO_2	"	292	23-3
▽	.26 % CO_2	8.32	294	27-11
△	2.4 % O_2	8.33	289	31-3
+	20.3 % O_2	8.32	285	31-2

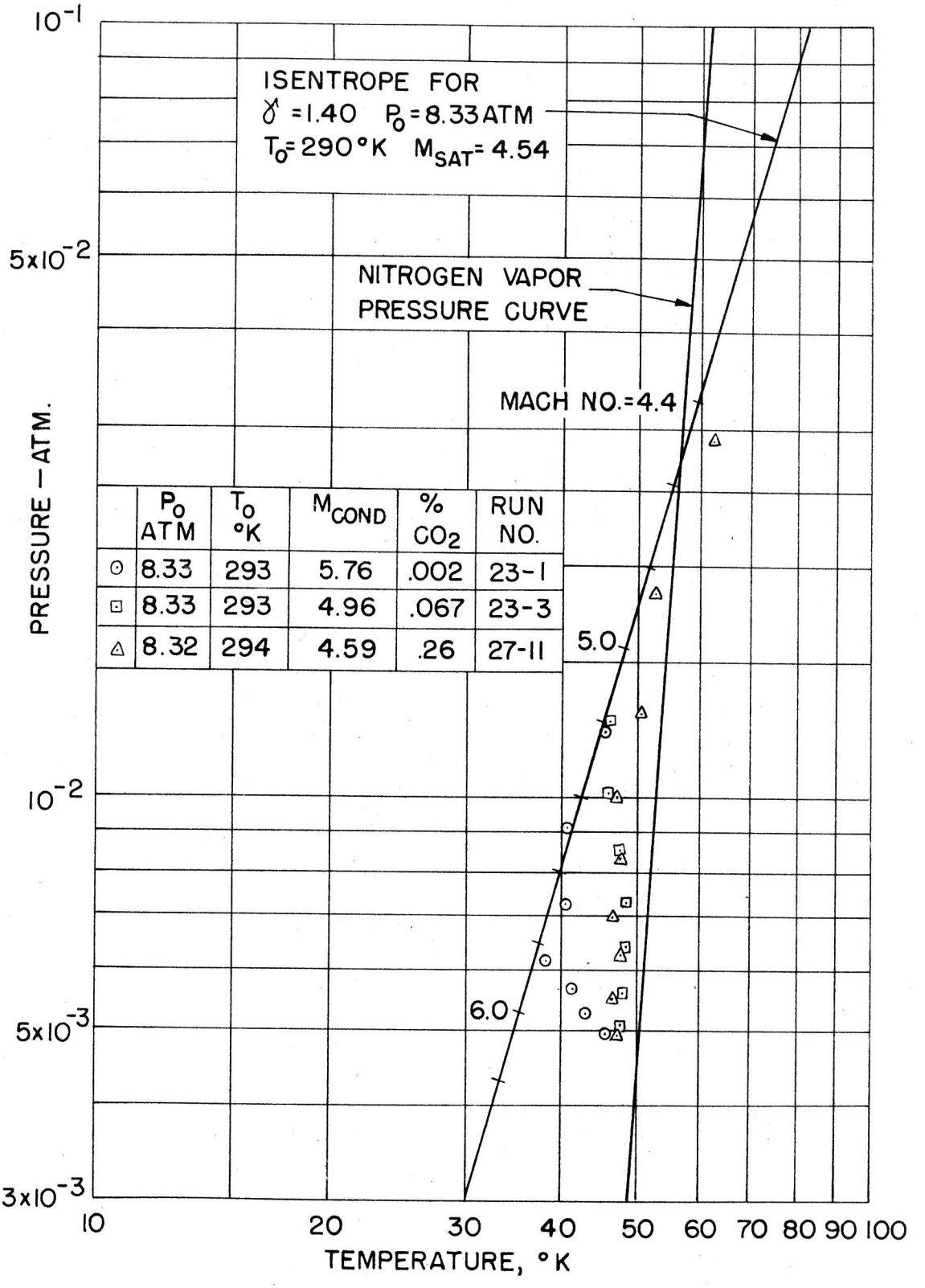

FIG. 31

EFFECT OF CARBON DIOXIDE ON MEASURED PRESSURE vs COMPUTED TEMPERATURE

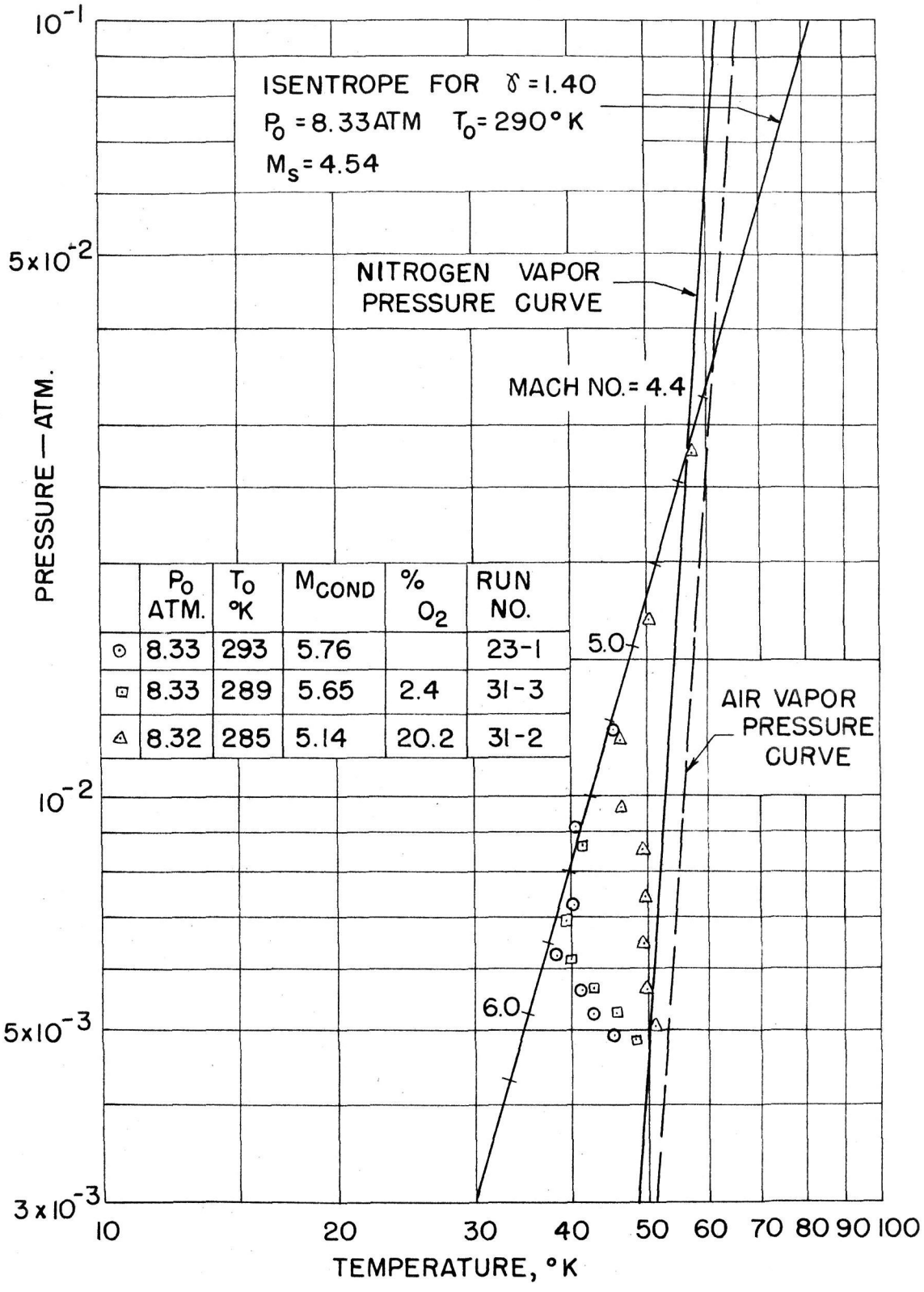

	P_0 ATM.	T_0 °K	M_{COND}	% O_2	RUN NO.
⊙	8.33	293	5.76		23-1
⊡	8.33	289	5.65	2.4	31-3
△	8.32	285	5.14	20.2	31-2

FIG. 32

EFFECT OF OXYGEN ON MEASURED PRESSURE vs COMPUTED TEMPERATURE

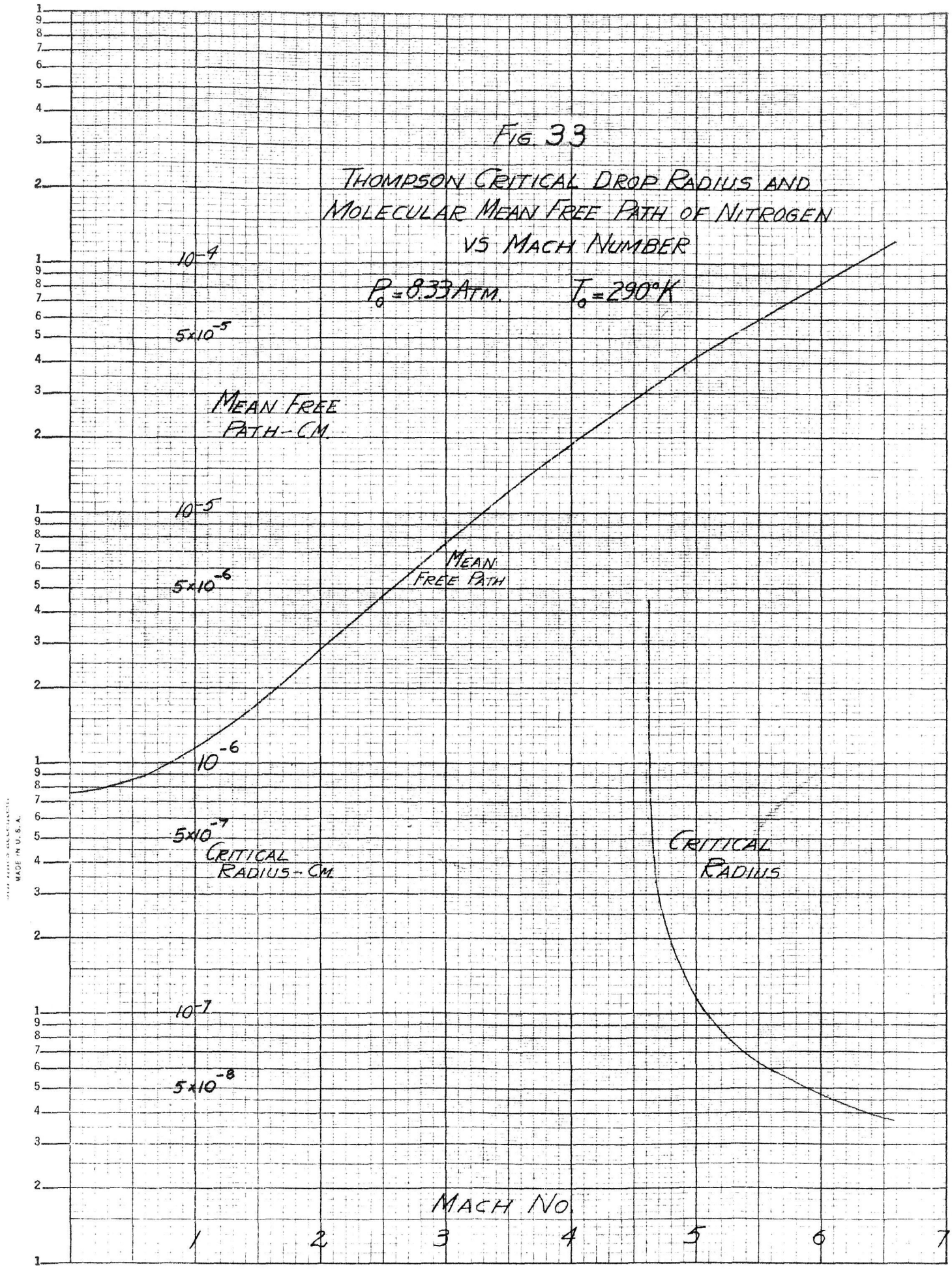
FIG. 33
THOMPSON CRITICAL DROP RADIUS AND
MOLECULAR MEAN FREE PATH OF NITROGEN
VS MACH NUMBER
P_0 = 8.33 ATM. T_0 = 290°K
10^{-4}
5×10^{-5}
MEAN FREE PATH - CM
10^{-5}
5×10^{-6}
MEAN FREE PATH
10^{-6}
5×10^{-7}
CRITICAL RADIUS - CM.
CRITICAL RADIUS
10^{-7}
5×10^{-8}
MACH NO.
1
2
3
4
5
6
7

FIG. 34

COMPUTED MACH NUMBER ALONG NOZZLE
(CF. FIG. 4)

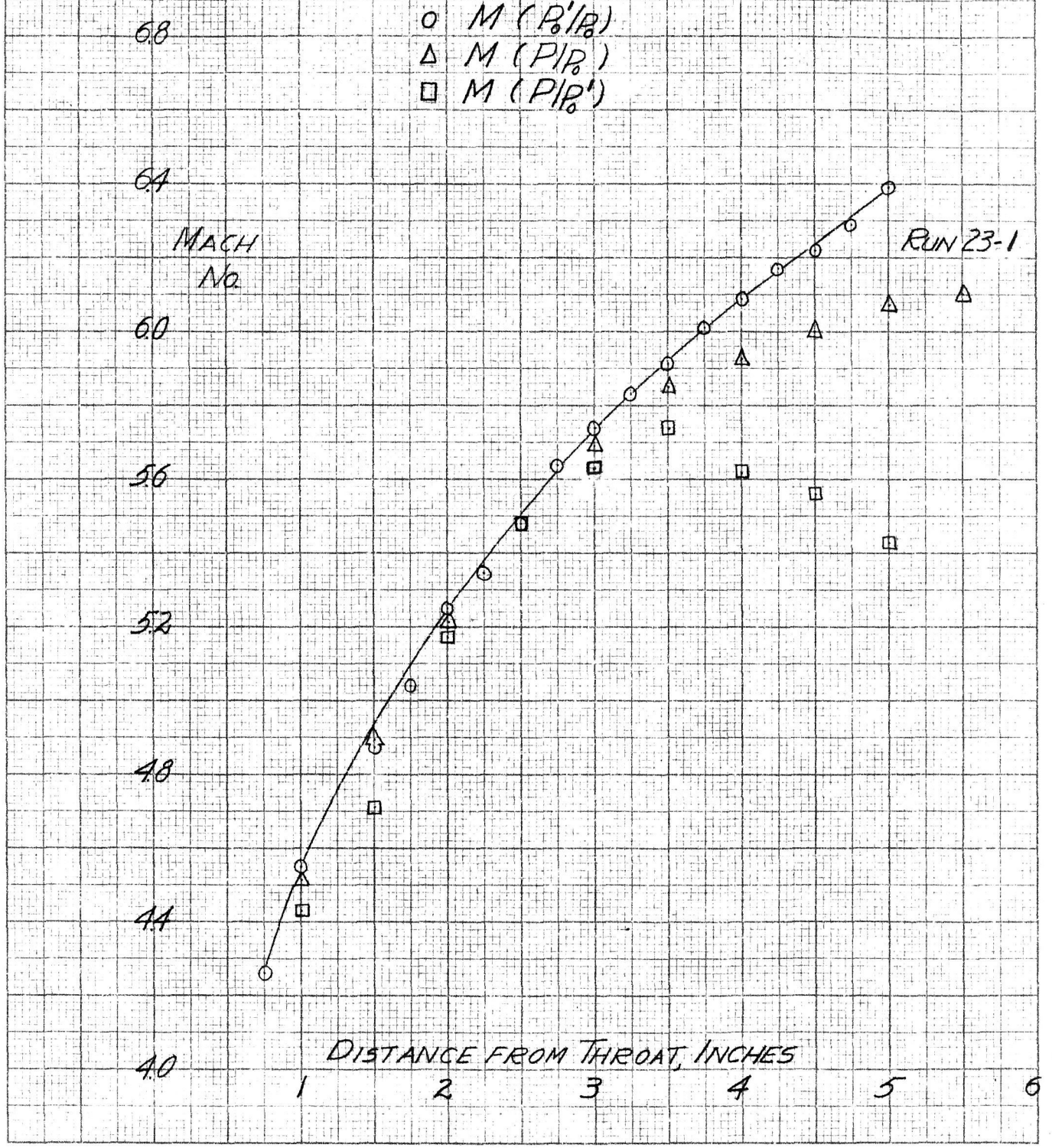

FIG. 35

TYPICAL DROP GROWTH ALONG NOZZLE

$\frac{dr}{dx}$ VS. X

$P_o = 8.33$ ATM.

$T_o = 290°K$

NITROGEN

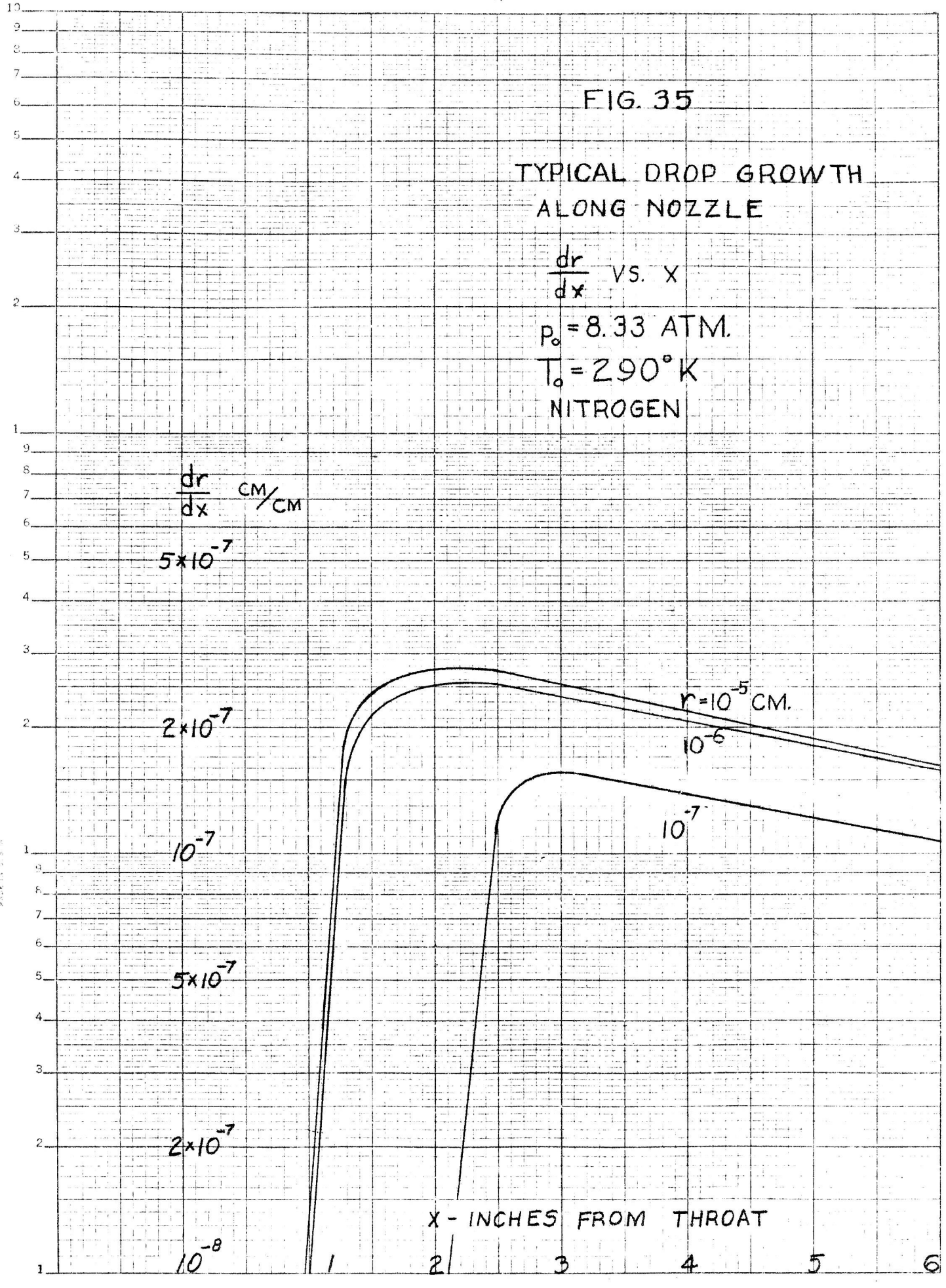

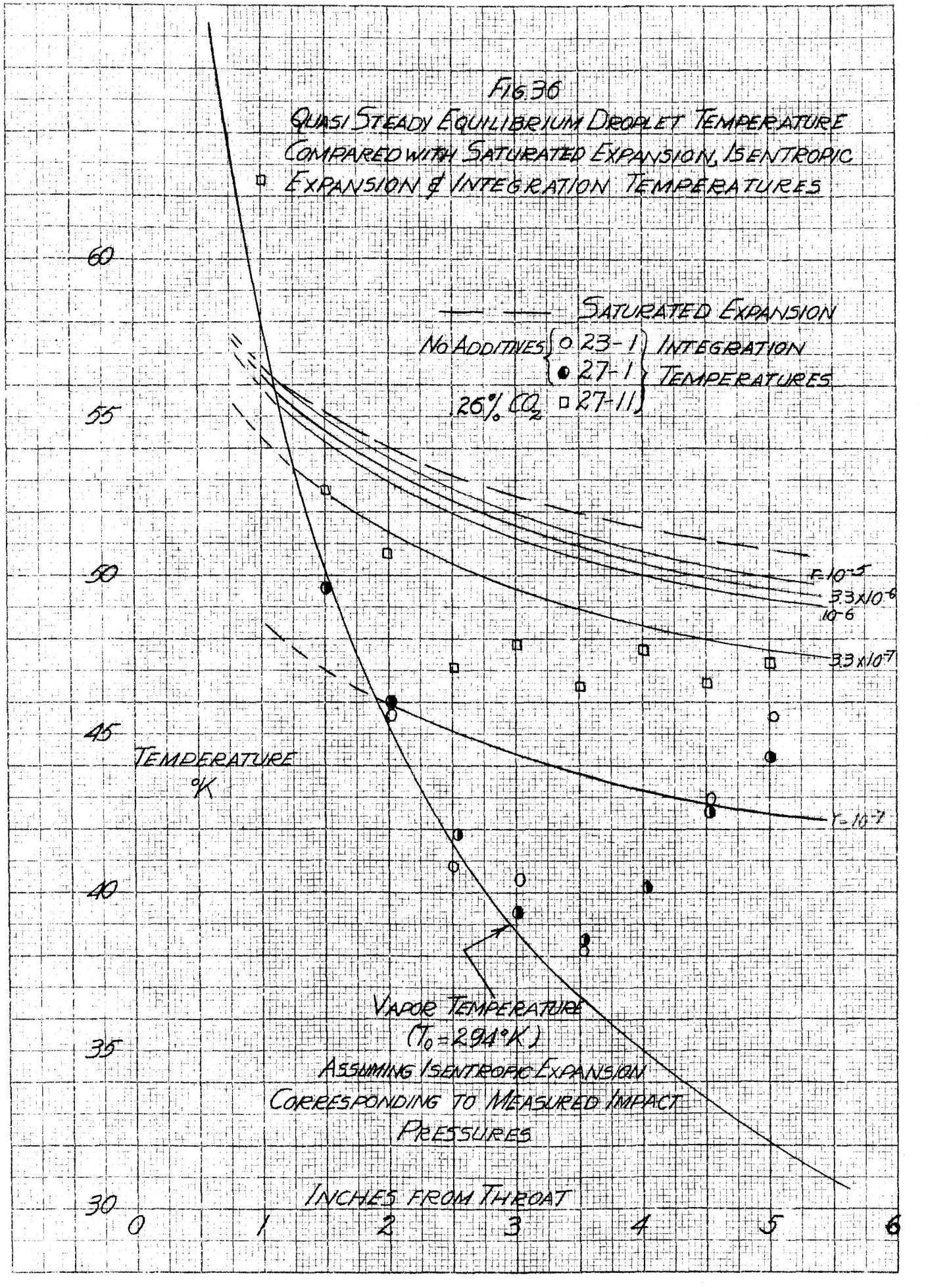

FIG. 36
QUASI STEADY EQUILIBRIUM DROPLET TEMPERATURE COMPARED WITH SATURATED EXPANSION, ISENTROPIC EXPANSION & INTEGRATION TEMPERATURES

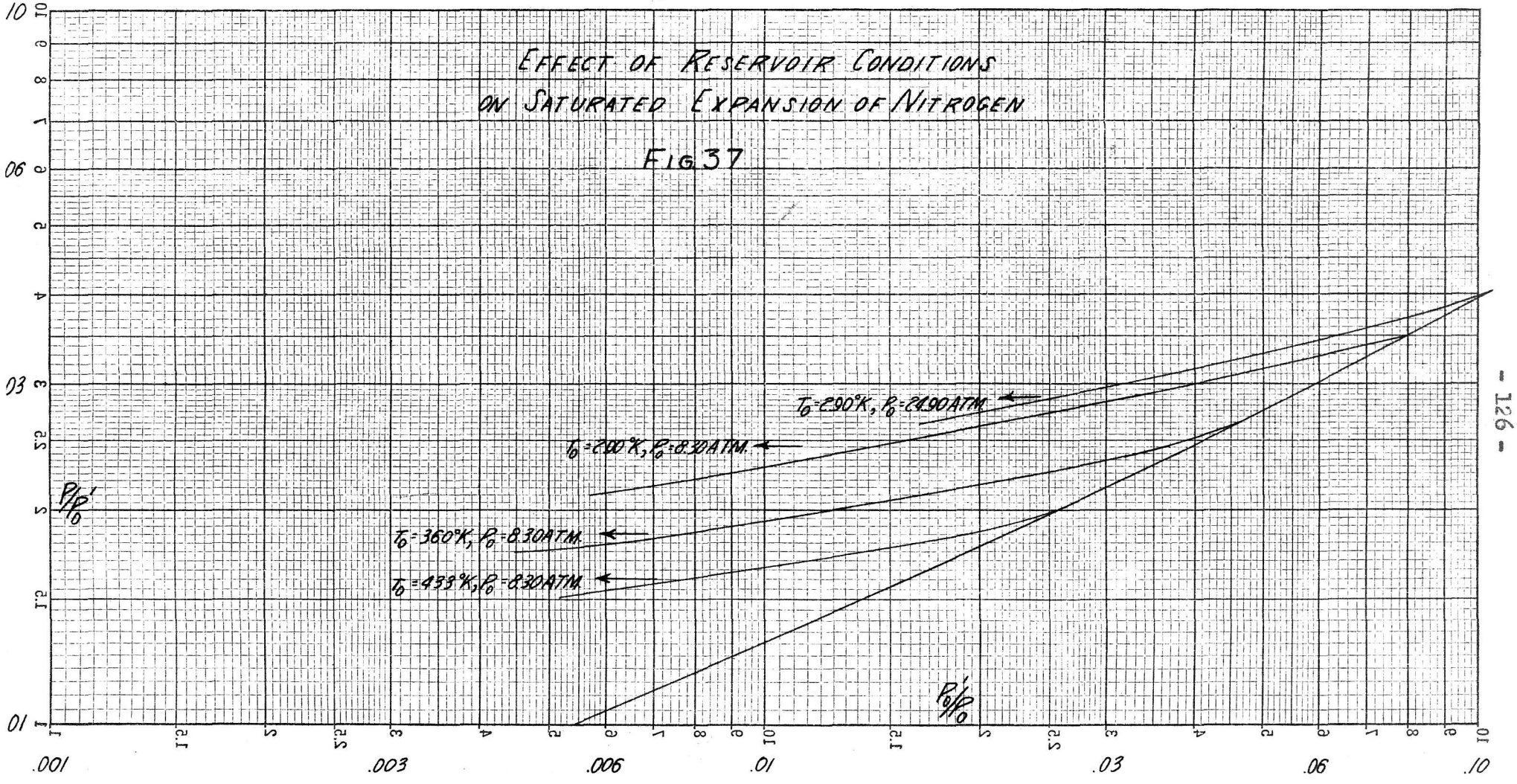
EFFECT OF RESERVOIR CONDITIONS
ON SATURATED EXPANSION OF NITROGEN
FIG 37
T_0=290°K, P_0=24.90 ATM.
T_0=290°K, P_0=8.30 ATM.
T_0=360°K, P_0=8.30 ATM.
T_0=433°K, P_0=8.30 ATM.
P/P_0'
P_0'/P_0
.001
.003
.006
.01
.03
.06
.10

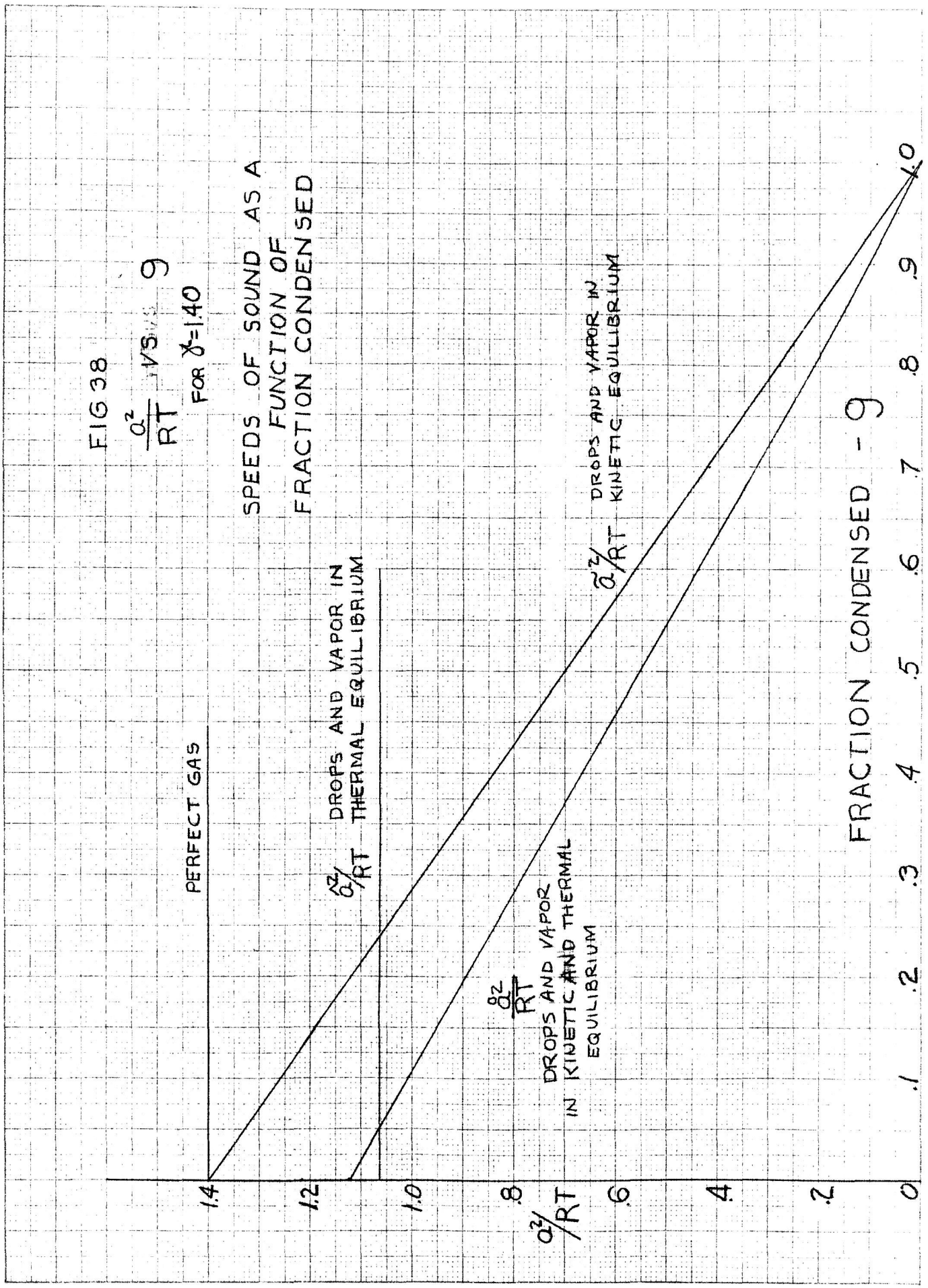
FIG 38
$\frac{a^2}{RT}$ VS $\frac{9}{}$
FOR γ=1.40
SPEEDS OF SOUND AS A FUNCTION OF FRACTION CONDENSED
PERFECT GAS
$\hat{a}^2/RT$ DROPS AND VAPOR IN THERMAL EQUILIBRIUM
$\hat{a}^2/RT$ DROPS AND VAPOR IN KINETIC EQUILIBRIUM
$\frac{a^2}{RT}$ DROPS AND VAPOR IN KINETIC AND THERMAL EQUILIBRIUM
a^2/RT
1.4
1.2
1.0
.8
.6
.4
.2
0
.1
.2
.3
.4
.5
.6
.7
.8
.9
1.0
FRACTION CONDENSED - 9

SPEEDS OF SOUND ALONG NOZZLE

FIG 39

SPEED OF SOUND / $\sqrt{RT}$

TEMPERATURE, DENSITY, AND FRACTION CONDENSED FROM STEPWISE INTEGRATION

dp, dρ: ○ 23-1 .002% CO_2; □ 23-3 .067% CO_2; △ 27-11 .26% CO_2

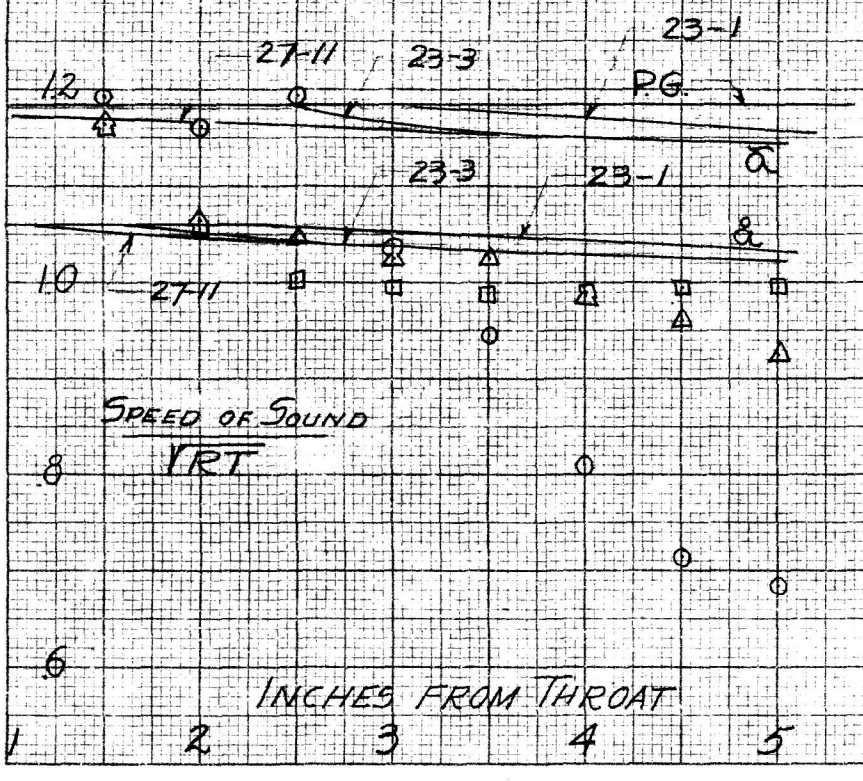

SPEED OF SOUND

dp, dρ: ○ 23-1 .002% CO_2; □ 23-3 .067% CO_2; △ 27-11 .26% CO_2

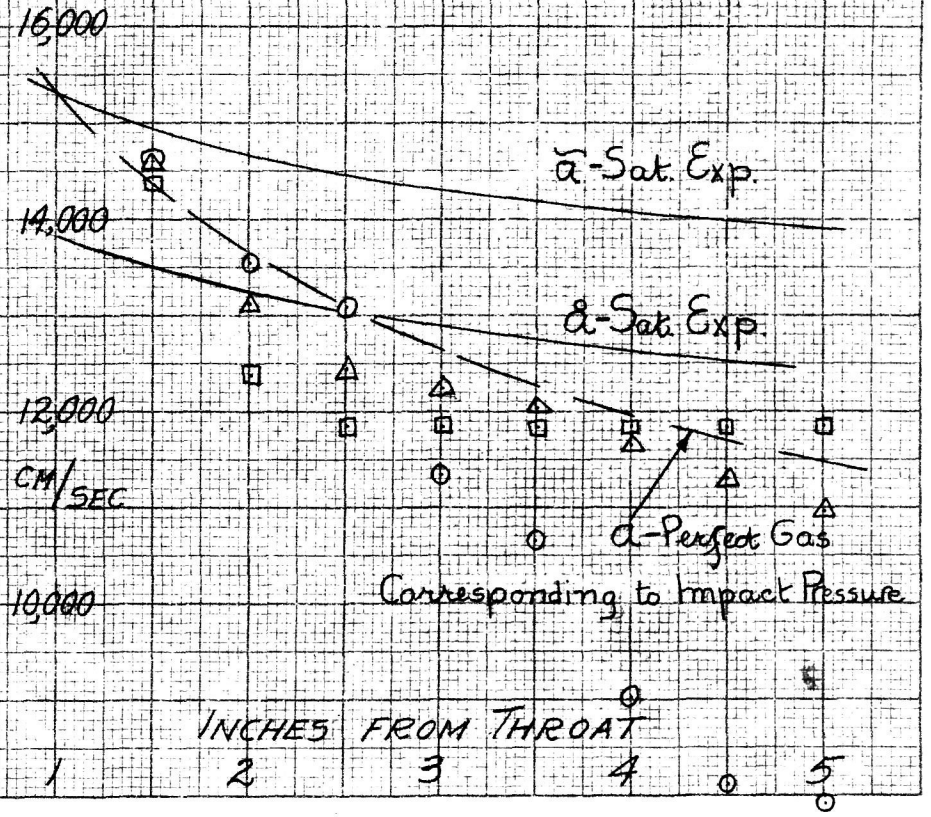

FIG 40

THEORETICAL PERCENT CONDENSED ALONG NOZZLE
(BY ISENTROPIC DROP GROWTH)
.067% CO_2 (RUN 23-3) EXC. AS NOTED
SHOWING EFFECT OF THE
EMPIRICAL PARAMETER r_0